Flow and transport in complex porous media : particle methods

Hamza Oukili

▶ **To cite this version:**

Hamza Oukili. Flow and transport in complex porous media : particle methods. Earth Sciences. Institut National Polytechnique de Toulouse - INPT, 2019. English. NNT : 2019INPT0056 . tel-04167190

HAL Id: tel-04167190
https://theses.hal.science/tel-04167190v1

Submitted on 20 Jul 2023

HAL is a multi-disciplinary open access archive for the deposit and dissemination of scientific research documents, whether they are published or not. The documents may come from teaching and research institutions in France or abroad, or from public or private research centers.

L'archive ouverte pluridisciplinaire **HAL**, est destinée au dépôt et à la diffusion de documents scientifiques de niveau recherche, publiés ou non, émanant des établissements d'enseignement et de recherche français ou étrangers, des laboratoires publics ou privés.

THÈSE

En vue de l'obtention du

DOCTORAT DE L'UNIVERSITÉ DE TOULOUSE

Délivré par :

Institut National Polytechnique de Toulouse (Toulouse INP)

Discipline ou spécialité :

Surfaces Interfaces Continentales Hydrologie

Présentée et soutenue par :

M. HAMZA OUKILI

le mercredi 10 juillet 2019

Titre :

Flow and transport in complex porous media: Particle Methods

Ecole doctorale :

Sciences de l'Univers de l'Environnement et de l'Espace (SDU2E)

Unité de recherche :

Institut de Mécanique des Fluides de Toulouse (IMFT)

Directeur(s) de Thèse :

M. RACHID ABABOU

M. GERALD DEBENEST

Rapporteurs :

M. AMVROSSIOS BAGTZOGLOU, UNIVERSITE DU CONNECTICUT

M. MARCO DENTZ, CSIC BARCELONE

M. PHILIPPE ACKERER, CNRS

Membre(s) du jury :

M. BENOÎT NOETINGER, IFPEN, Président

M. ERIC CLIMENT, TOULOUSE INP, Membre

M. GERALD DEBENEST, TOULOUSE INP, Membre

Mme ENRICA MASI, UNIVERSITE PAUL SABATIER, Membre

M. RACHID ABABOU, TOULOUSE INP, Membre

Flow and transport in complex porous media: Particle Methods

Abstract

Particle methods have been extensively used for modeling transport problems in porous soils, aquifers, and reservoirs. They reduce or avoid some of the problems of Eulerian methods, e.g. instabilities, excessive artificial diffusion, mass balance, and/or oscillations that could lead to negative concentrations. This thesis develops a new class of gridless Lagrangian particle methods for modeling flow and transport phenomena in complex porous media with heterogeneities and discontinuities. Firstly, stochastic processes are reviewed, in relation to particle positions X(t) and to the corresponding macroscopic Advection-Diffusion Equation (ADE). This review leads to the conditions required for the Probability Density Function (PDF) of X(t) to satisfy the Fokker-Planck equation (and the ADE). However, one of these conditions is the differentiability of transport coefficients: therefore, discontinuities are difficult to treat, particularly discontinuous diffusion D(x) and porosity q(x). In the literature on particle Random Walks, the methods used to handle discontinuous diffusion required excessively small time steps. These restrictions on the time step lead to inefficient algorithms. In this study, we propose a novel approach without restrictions on time step size. The novel RWPT (Random Walk Particle Tracking) algorithms proposed here are discrete in time and continuous in space (gridless). They are based on an adaptive "Stop&Go" time-stepping, combined with partial reflection/refraction schemes, and extended with three new concepts: negative mass particles; adaptive mass particles; and "homing" particles. To test the new Stop&Go RWPT schemes in infinite domains, we develop analytical and semi-analytical solutions for diffusion in the presence of multiple interfaces (discontinuous multi-layered medium) in infinite domains. The results show that the proposed Stop&Go RWPT schemes (with adaptive, negative, or homing particles) fit extremely well the semi-analytical solutions, even for very high contrasts for transport proper-

ties even in the neighborhood of the interfaces. The schemes provide a correct diffusive solution in only a few macro-steps (macroscopic time steps), with a precision that depends only on the number of particles, and not on the macro-step. The algorithms are then, extended from infinite to semi-infinite and finite domains. Dirichlet conditions are particularly difficult to implement in particle methods. Thus, in this thesis we propose different methods on how to implement Dirichlet boundary conditions with the "discontinuous" RWPT algorithm. This study proposes an algorithm to solve diffusion equations semi-analytically in heterogeneous semi-infinite and finite domains with Dirichlet boundary conditions. The RWPT Dirichlet methods are then checked analytically and verified for various configurations. Finally, the RWPT method is applied for studying diffusion at different scales in 2D composite media (grain/pore systems). A zero-flux condition is assumed locally at the grain/pore interfaces. At the macro-scale, diffusion occurs in an equivalent effective homogeneous medium with macroscopic parameters (porosity and effective diffusion coefficients) obtained from the temporal evolution of second order moments. The RWPT algorithm is then applied to more complex geometries of grains and pores. Different configurations or structures at the micro-scale level will be chosen in order to obtain composite isotropic media at the macro-scale level with different porosities. Then, by choosing elongated micro-structures, anisotropy effects emerge at the macroscopic level. Effective macro-scale properties (porosities, effective diffusion tensors, tortuosities) are calculated using the second order moment. The different methods proposed in this thesis can be used for different problems, since each has its drawbacks and advantages. The schemes proposed seem promising with a view to extensions towards more complex 3D geometries.

Résumé (Français)

Abstract

Les méthodes utilisant des particules ont été largement utilisées pour modéliser les problèmes de transport dans les sols poreux, les aquifères et les réservoirs. Ils réduisent ou évitent certains des problèmes des méthodes eulériennes, par exemple instabilités, diffusion artificielle excessive, bilan massique et / ou oscillations pouvant conduire à des concentrations négatives. Cette thèse développe de nouvelles méthodes de particules lagrangiennes pour modéliser les phénomènes d'écoulement et de transport dans des milieux poreux complexes avec des hétérogénéités. Pour ce faire, cette thèse passe d'abord en revue les processus stochastiques et leurs relations avec l'équation (EDP) macroscopique d'Advection-Diffusion ADE. Cette mise en revue permet de trouver les conditions nécessaires à un processus stochastique pour que sa densité de probabilité vérifie l'équation EDP de Fokker-Planck et donc l'ADE. Cependant, l'une de ces conditions est la différentiabilité des coefficients de transport. Il est donc difficile de traiter les discontinuités et les hétérogénéités, en particulier la diffusion et la porosité discontinues. Dans la littérature sur les marches aléatoires de particules, les méthodes précédentes utilisées pour traiter ce problème de discontinuité nécessitaient de petits pas de temps afin de converger vers la solution attendue. Ces restrictions sur le pas de temps conduisent à des algorithmes inefficaces. Dans cette étude, nous proposons une nouvelle approche sans restrictions sur la taille des pas de temps. L'algorithme RWPT (Random Walk Particle Tracking) proposé ici est discret en temps et continu en espace (sans grille). Le nouvel algorithme RWPT est basé sur un pas de temps adaptatif « Stop&Go », combiné à des schémas de réflexion partielle/réfraction, et étendu à trois nouveaux concepts : particules de masse négative ; particules de masse adaptative ; et particules à tête chercheuse ("homing"). Les algo-

rithmes en domaines infinis ont ensuite été généralisés au cas de domaines finis ou semi-infinis. Les conditions aux limites de Dirichlet (concentrations) sont particulièrement difficiles à mettre en œuvre dans les méthodes particulaires. Ainsi, cette thèse propose-t-elle différentes méthodes de mise en œuvre des conditions de Dirichlet avec l'algorithme RWPT utilisé pour traiter les discontinuités. Pour tester les nouveaux schémas RWPT Stop&Go, nous développons des solutions analytiques et semi-analytiques pour la diffusion en présence de multiples interfaces (milieu multicouche discontinu) dans des domaines infinis, semi-infinis et finis avec des conditions limites de Dirichlet. Les résultats montrent que les schémas RWPT Stop&Go proposés correspondent extrêmement bien aux solutions semi-analytiques, même pour des contrastes très forts des coefficients de diffusion et porosités, y compris au voisinage des interfaces. Ensuite, la méthode RWPT est appliquée pour étudier les processus de diffusion à différentes échelles dans des supports composites (systèmes grains/pores 2D). Une condition de flux nul est appliquée localement aux interfaces grain/pore. Au niveau macroscopique, la diffusion se produit dans un milieu homogène avec des paramètres macro-échelle (porosité et coefficients de diffusion effectifs) induits par des méthodes de montée d'échelle à l'aide des moments spatiaux d'ordre 2. L'algorithme RWPT est ensuite appliqué à des géométries plus complexes de grains et pores. Tout d'abord, différentes configurations ou structures micro-échelle sont choisies afin d'obtenir des milieux composites isotropes ayant différentes porosités. Puis, en choisissant des micro-structures allongées, des effets d'anisotropies apparaissent au niveau macroscopique. Les différentes méthodes proposées dans cette thèse pourraient être utilisées pour différents problèmes, chacune ayant ses inconvénients et ses avantages. Les schémas proposés semblent prometteurs dans la perspective d'extensions vers des géométries 3D plus complexes.

Remerciements

Aucun remerciement ne saurait exprimer ma profonde gratitude vis-à-vis de mes chers professeurs et directeurs de thèse : Rachid Ababou et Gérald Debenest. Je vous serais très reconnaissant pour l'aide et le soutien que vous m'avez apportés à travers toutes ces années. Vos conseils et votre disponibilité m'ont énormément soutenu pour réussir ce travail. J'avoue que j'ai beaucoup appris même en dehors de la mécanique des fluides.

Un grand merci au membre du comité de suivies et examinateur de cette thèse, Benoit Noetinger pour sa considération. Merci pour sa disponibilité et son intérêt scientifique pour le sujet de thèse. Je tiens également à remercier Amvrossios Bagtzoglou qui m'a accueilli dans son laboratoire lors d'une mobilité et qui a accepté de rapporter cette thèse. Je remercie aussi Philippe Ackerer et Marco Dentz, rapporteurs de cette thèse, pour avoir évalué mon travail avec beaucoup d'attention. Je remercie de même Enrica Massi et Eric Climent, examinateurs, pour l'intérêt qu'ils ont porté à ce travail et leurs remarques judicieuses.

Je tiens à remercier tous mes collègues au sein du Groupe d'Etude des Milieux Poreux et dans tout le laboratoire de mécanique des fluides. L'entraide et l'entente entre les membres de ce groupe permet de passer des moments très sympas surtout dans la salle de pause. Merci à Ruddy, Manuel, Michel, Yohan, Pauline, Nahla, Manel, Frédéric, Martin, Myriam, Ange, Mauricio, Jacques, Amy, Adlan, Maxime, Vincent, Pierre, Pierre-Yves, et à tous ceux que j'oublie probablement. J'aimerais aussi remercier mes camarades de bureau qui se sont succédés Sylvain, Romain, Maxime, Anthony et Edith, je suis très content d'avoir partagé le bureau avec eux et j'en garde de beaux souvenirs.

Je tiens également, et surtout, à exprimer mes remerciements et ma profonde gratitude envers mes amis et collègues Mostafa, Khalil, Youness, Omar,

Marwane qui, tous et sans exception, m'ont assuré soutien et encouragement. Je garde de très beaux souvenirs partagés avec vous les amis. Un remerciement spécial pour mon cher ami Tawfik que je considère comme un frère. Non seulement, nous avons commencé la thèse en même temps avec le même directeur de thèse, mais notre sincère amitié nous a permis de surmonter toutes les difficultés pour mener à bien nos travaux de recherche.

Pour finir, je tiens à remercier ma famille. Je remercie infiniment mes très chers parents de m'avoir soutenu jusqu'au bout dans la poursuite de mes études, ils ont beaucoup contribué à la réussite de cette thèse. Merci pour avoir fait de moi ce que je suis aujourd'hui. Veuillez trouver dans ce travail le fruit de votre dévouement et des efforts que vous avez dispensés.

Contents

List of Algorithms

List of Tables

Chapter 1

General Introduction

1.1 General Introduction (English)

1.1.1 Context

The concept of diffusion has a wide range of applications: physics, mathematics, biology, economics, finance, etc. In physics, diffusion has been observed to describe several phenomena at different scales see (Table 1). Thus, diffusion can be studied using two different approaches: the first one uses flux-gradient laws, e.g. Fick's law. Such laws describe diffusion or conduction phenomena at a macroscopic level. For instance solute diffusion is driven by the gradient of concentration, a macroscopic quantity. The second approach uses Random Walk particles. This approach can be seen as local or microscopic: each particle diffuses individually and independently from other particles, at least for pure diffusion without reactions. This thesis focuses on Random Walk particle methods.

Particle methods have been much used to model, mathematically and numerically, the transport of mass, heat, and other quantities through solids, fluids, and fluid-filled porous media. The last two cases may involve both diffusive and advective transport phenomena (due to the moving fluid). Hydrodynamic dispersion due to detailed spatial variations of the velocity field has also been modeled as a Fickian diffusion-type process, e.g. in turbulent flows and in fluid-filled porous structures (see [Sahimi, 1993]).

Particle methods are based on a discrete representation of the transported quantity (solute concentration, fluid pressure, fluid saturation, heat or temperature) as discrete packets (the "particles"), each carrying a unit mass, or a unit heat, etc. The advantage of particle methods is that they avoid some of the problems of PDE (Partial Differential Equation) based Eulerian methods, such as numerical instability, artificial diffusion, mass balance errors, and/or oscillations that could lead for instance to negative concentrations or saturations.

Types of diffusion	Solute diff. in Porous Media	Porous Media flow Eq.	Thermal conduction
Quantity diffused	C: Concentration	P : Pressure	T : Temperature
Fick's 1^{st} law	$J = -D_{eff}\nabla C$	$J = -\frac{k}{\mu}\nabla P$	$J = -\lambda\nabla T$
Fick's 2^{nd} law	$\theta\frac{\partial C}{\partial t} = -\nabla J$	$C_a\frac{\partial P}{\partial t} = -\nabla J$	$C_T\frac{\partial T}{\partial t} = -\nabla J$
Diffusion Coefficient	D_{eff}: Effective Diffusivity	$\frac{k}{\mu}$: $\frac{permeability}{viscosity}$	λ : Thermal conductivity
Capacity	θ: porosity	C_a : Capacity	C_T : Heat capacity

Table 1.1: Relevance to several types of diffusion problems (phenomena)

Various types of particle methods have been devised: non-Lagrangian Particle-in-Cell methods (PIC); particles undergoing Markov processes in a PIC framework with stochastic time steps [Spiller et al., 2000]; continuous-time particles on a grid; and Lagrangian particles with discrete time-steps in continuous space (gridless). Particle methods, both continuous time and discrete-time, have been extensively used for modeling advective-diffusive solute transport problems in porous soils, aquifers, and reservoirs. But they also have the potential for solving a broader class of porous reservoir flow and transport problems, including: solute mass transport, multiphase fluid displacements, heat transport, and Darcy flow (pressure diffusion). Diffusion processes are important in these transport phenomena, either directly (solute diffusion, heat diffusion, pressure diffusion) or indirectly (when the hydrodynamic dispersion of transported quantities is modeled as a diffusion-type process).

In particle methods, the advective component is modeled by displacing the particles according to the velocity (this is relatively straightforward); on the other hand, the diffusive process is modeled by randomly displacing the particles according to a Wiener process, or Brownian Motion, or Random Walk. In gridless "Lagrangian" particle methods, space is assumed continuous, and particle positions $X(t)$ are real numbers.

In the present work, we focus on gridless Lagrangian particle tracking to solve diffusion processes by the random walk method, under the generic name RWPT (Random Walk Particle Tracking). This is relevant for electrical conduction in solid materials (*Ohm*'s law), heat conduction in solids or fluid-filled porous materials *(Fourier*'s law)[1], pressure diffusion in slightly compressible fluid-filled porous media (*Darcy*'s law)[2], and solute diffusion in partially or

[1]Thermal conductivity λ divided by heat capacity c yields the thermal diffusion coefficient D, although λ and c should be considered separately if both are spatially variable.

[2]The pressure diffusion equation is obtained by combining Darcy's law with Terzaghi or Biot poro-elasticity. The pressure diffusion coefficient D involves Darcy permeability k divided by fluid viscosity μ and by the bulk elastic compressibility of the fluid-filled medium

fully water-saturated porous media (based on *Fick*'s law)[3].

Heterogeneity and discontinuity

A specific study of the macroscopic behavior of Random Walk particles is necessary when dealing with heterogeneous or discontinuous diffusion coefficient $D(x)$. The case of discontinuous diffusion is particularly troublesome, and this is our main focus. Such discontinuities occur at "*material interfaces*" sudden changes of microstructure (composite materials, layered porous media*, etc.)*. For solute diffusion in a porous medium, an additional point of interest is the case of discontinuous porosity $\theta(x)$ (if the medium is water-saturated), or discontinuous volumetric water content $\theta(x)$ (if the medium is unsaturated). The case of heat conduction with discontinuous conductivity $\lambda(x)$ and discontinuous heat capacity $c(x)$ is similar. The capacity $c(x)$ for heat transport in a heterogeneous solid material, plays a role similar to the porosity $\theta(x)$ for solute transport in a heterogeneous water-filled porous medium.

As mentioned above, heterogeneities are difficult to treat, particularly the case of discontinuous diffusion $D(x)$ and discontinuous porosity $\theta(x)$. In the literature on particle Random Walks, the displacement schemes used for handling the discontinuity can be characterized into two classes as follows:

1. Interface coarsening, interpolation and drift velocity scheme (e.g. [Labolle et al., 1996, Spiller, 2004])

2. Partial reflection schemes (e.g. [Uffink, 1985]).

The first class ("interpolation techniques") smooth out the discontinuity: the interface is coarsened and the parameters (diffusion, porosity) are considered

(*not detailed here*).

[3]For solute diffusion in a porous medium, Fick's law is extended to account for porosity θ and tortuosity τ.

continuously variable rather than discontinuous through the coarsened interface. The second class ("partial reflection methods"), introduced by [Uffink, 1985], implements a probabilistic *reflection/transmission* of the particles across the discontinuous interface: probabilities are assigned for particle *reflection* and *transmission* across the interface[4]. One of the main drawbacks of these two approaches is that a small time step is required in order to converge to the correct solution of the discontinuous PDE, even if the number of particles is very large. This is particularly limiting in the presence of many interfaces. These time step restrictions lead to inefficient algorithms.

In Chapter 3 of this thesis, we propose a novel approach without restrictions on time step size. The RWPT algorithm proposed here is, like others in the literature, discrete in time and continuous in space (gridless). The novel aspects have to do with the treatment of discontinuities. The new RWPT algorithm is based on an adaptive "Stop and go" time-stepping, combined with partial reflection/transmission schemes, and extended with three concepts: (i) negative mass particles; (ii) adaptive mass particles; and (iii) "homing" particles. To test the new stop-and-go RWPT schemes, we develop analytical and semi-analytical solutions for diffusion in the presence of multiple interfaces (discontinuous multi-layered medium). The results show that the proposed stop-and-go RWPT schemes (with adaptive, negative, or homing particles) fits extremely well the semi-analytical solutions, even for very high contrasts and in the neighborhood of interfaces. The three schemes provide a correct diffusive solution in only a few macro-time steps, with a precision that depends only on the number of particles, and not on the macro-time step. These schemes seem promising, with a view to extensions towards more complex 3D geometries. In the next chapters, the RWPT algorithms are extended to treat Dirichlet

[4]The "transmission" step is sometimes loosely called "refraction" by analogy with ray optics.

conditions in Chapter 4, and zero flux conditions in Chapter 5 (Application grain/pore systems), see subsection 1.1.3 "Scope of this thesis" below.

1.1.2 Literature review on RWPT with discontinuities

[Noetinger et al., 2016] extensively reviewed several particle methods for diffusive or advective-diffusive transport, including the (classical) discrete time, continuous space, gridless Random Walk Particle Tracking (RWPT) method [Labolle et al., 1996], and other variants like the continuous time random walk (CTRW) [Kang et al., 2015], and the time-domain random walk (TDRW) [Delay & Bodin, 2001, Bodin, 2015]. In comparison, the present study focuses on an extension of the gridless RWPT scheme for the case of multiple discontinuities, leading to an adaptive "stop-and-go" macro-time step scheme coupled with various new types of "adaptive" particles (*more on this later*). We now present, below, a brief review of two types of "asynchronous" particle tracking schemes, applied to Brownian Motion particles, in the case of a porous medium with discontinuous $D(x)$ and/or $\theta(x)$ coefficients. The two types of schemes that have been used in the literature to treat such discontinuities are, essentially: (1) Partial reflection schemes (e.g. [Uffink, 1985]); and (2) Interface coarsening, interpolation and drift velocity scheme (e.g. [Labolle et al., 1996, Spiller, 2004]).

However, these methods present stringent restrictions on the time step. [Ackerer & Mose, 2000, Bechtold et al., 2011] showed that the above methods are only valid for $\Delta t \to 0$. A small time step must be used in order to avoid the overshoot of heterogeneous and discontinuous regions of space by the particles. In addition, as particles may have to cross the same interface multiple times (with small time step), another problem emerges: [Bechtold et al., 2011], showed that each reflection introduces numerical error. Hence, restrictions on the time step still persist, and so does the error with the scheme proposed by

[Bechtold et al., 2011]. In addition, specific literature reviews are presented in each chapter (Chapter 2, 3, 4, 5).

1.1.3 Scope of this thesis

Discontinuities of material properties have always been difficult to deal with for diffusive transport phenomena, both at the macroscopic level (considering the diffusion PDE with discontinuous diffusion parameter) and at the microscopic level of random walk "particles" (which represent discrete packets of heat or mass).

In previous particle methods proposed in the literature, the precision of the solution depends on the time step. The solution is an approximation, which becomes more precise as the number of time steps is increased for a given fixed number of particles (issues of post-processing from particles to concentrations will be discussed later in Chapter 3). The novel model proposed in this article does not depend on time step constraints, i.e., its precision is not limited by a priori choice of time step size. The precision of the solution will depend solely on the number of particles required to recover particle moments and mass concentration or temperature distribution. The idea behind this new algorithm is inspired, as in some of the previously reviewed particle methods, from the analytical solution of the diffusion PDE for an initial Dirac source in an infinite domain, with an interface where the diffusion coefficient is discontinuous. As mentioned earlier, the corresponding quantity transported by diffusion could either be mass (solute concentration), heat energy (temperature), or mechanical work (pore pressure). The new proposed scheme (and its variants) have several innovating features. One is that the time-steps, for each given particle, are adapted in such a way that the particle crosses each material element between interfaces in a single "micro time-step". The scheme is therefore asyn-

chronous (during a "macro time-step") across the ensemble of particles, and it also remains gridless (the only "grid" being the material grid of elements generated by the discontinuous interfaces). Other novel features involve adaptation of the particles as they cross the interfaces (including for instance the creation of negative mass particles).

Dirichlet conditions[5] are difficult to implement in particle methods. This thesis proposes new methods to implement Dirichlet conditions with no restriction on the time step. The methods are induced from novel analytical and semi-analytical solutions developed in this thesis. The Dirichlet conditions are then, combined with RWPT algorithms, that treat discontinuities.

The RWPT algorithm is used for a multi-scale study of diffusion in grain-pore systems. The RWPT algorithm proposed is based on 2D/3D analytical solutions in finite and semi-infinite domains with zero flux boundary conditions. The RWPT algorithm is then applied to more complex geometries of grains and pores (that are difficult to solve analytically). Different configurations of a composite media at the micro-scale level (grains and pores in a porous media). We study the impact of porosity, then the effect of local anisotropy on macro-scale properties. Effective properties at the macro-scale are calculated using spatial moments of particles positions.

1.1.4 Summary

This thesis is organized as follows. The next chapter, Chapter 2, presents a review on the theory behind stochastic processes, and the corresponding macroscopic PDE, particularly for advective-diffusive problems. Chapter 3 presents novel particle-based Random Walk Particle Tracking (RWPT) methods and algorithms for solving heterogeneous and discontinuous transport problems with

[5] In this thesis, the term Dirichlet conditions is used in relation to both: the PDE problem based on concentration $C(x,t)$, and the corresponding RWPT implementation of such BC's.

more precision and less restrictions on the time step. This chapter, develops also new analytical and semi-analytical solutions for discontinuous diffusion and porosity in multi-layered infinite domains. The schemes proposed fit extremely well the analytical solutions. Chapter 4 proposes new implementations of Dirichlet boundary conditions for the RWPT algorithms of Chapter 3, with no restrictions on the time step. To test these algorithms, we extend the semi-analytical solutions of Chapter 3, to solve discontinuous diffusion and porosity in multi-layered finite and semi-infinite domains. The results obtained for single or multiple interfaces are presented and discussed based on the proposed Dirichlet methods. In Chapter 5, we apply a RWPT based on multi-dimensional analytical solutions on a 2D grain/pore system. A zero-flux condition is assumed locally at the grain/pore interfaces. At the macro-scale level, macroscopic parameters (porosities, tortuosities and effective diffusion tensors) are induced from moments upscaling methods. By choosing different sizes and elongated grains, porosity and anisotropy effects emerge at the macroscopic level. The conclusive chapter, Chapter 6, recapitulates results and discusses extensions.

1.2 Introduction générale (Français)

1.2.1 Contexte

Le concept de diffusion s'applique à de nombreuses disciplines : physique, mathématiques, biologie, économie, finance, etc. En physique, on a observé que la diffusion décrivait plusieurs phénomènes et à différentes échelles, voir le tableau 1. On peut donc étudier la diffusion en utilisant deux approches différentes : la première utilise les lois des gradients des flux (par exemple la loi de Fick). Ces lois expliquent la diffusion ou la conduction à un niveau macroscopique. Par exemple, la diffusion d'un soluté étant entraînée par des gradients de concentrations, des macro-quantités. La deuxième approche utilise des particules

Random Walk. Cette approche peut être considérée comme locale ou microscopique: chaque particule diffuse individuellement et indépendamment des autres particules, dans le cas de la diffusion pure sans réactions. Cette thèse porte sur les méthodes de particules Random Walk.

Les méthodes utilisant des particules ont été les plus utilisées pour modéliser, mathématiquement et numériquement, le transport de masse, de chaleur et d'autres quantités à travers les solides, les fluides et les milieux poreux remplis de fluides. Les deux derniers cas peuvent impliquer des phénomènes de transport diffusif et advectif (dus au fluide en mouvement). La dispersion hydrodynamique due aux variations spatiales détaillées du champ de vitesse a également été modélisée comme un processus de type diffusion fickienne, par exemple dans des écoulements turbulents ou dans des structures poreuses remplies de fluide (voir [Sahimi, 1993]). Les méthodes particulaires sont basées sur une représentation discrète de la quantité transportée (concentration de soluté, pression de fluide, saturation de fluide, chaleur ou température) sous forme de paquets discrets (les «particules»), chacun transportant une unité de masse, ou une unité de chaleur, etc. L'avantage des méthodes particulaires est qu'elles évitent certains des problèmes posés par les méthodes eulériennes basées sur les équations différentielles partielles (EDP), telles que l'instabilité numérique, la diffusion artificielle, les erreurs de bilan massique et / ou les oscillations pouvant conduire par exemple à des concentrations négatives ou à des saturations. Différents types de méthodes particulaires ont été mis au point : méthodes non Lagrangiennes des particules dans des cellules (PIC) ; particules régies par des processus de Markov dans un cadre PIC avec des pas de temps stochastiques [Spiller et al., 2000] ; particules à temps continu sur une grille ; et des particules lagrangiennes avec des pas de temps discrets dans un espace continu (sans grille). Les méthodes utilisant des particules, à

Types of diffusion	Solute diff. in Porous Media	Porous Media flow Eq.	Thermal conduction
Quantity diffused	C: Concentration	P : Pressure	T : Temperature
Fick's 1^{st} law	$J = -D_{eff}\nabla C$	$J = -\frac{k}{\mu}\nabla P$	$J = -\lambda\nabla T$
Fick's 2^{nd} law	$\theta\frac{\partial C}{\partial t} = -\nabla J$	$C_a\frac{\partial P}{\partial t} = -\nabla J$	$C_T\frac{\partial T}{\partial t} = -\nabla J$
Diffusion Coefficient	D_{eff}: Effective Diffusivity	$\frac{k}{\mu}$: $\frac{permeability}{viscosity}$	λ : Thermal conductivity
Capacity	θ: porosity	C_a : Capacity	C_T : Heat capacity

Table 1.2: Relevance to several types of diffusion problems (phenomena)

la fois en temps continu et en temps discret, ont été largement utilisées pour modéliser les problèmes de transport de soluté par la convection et la diffusion dans les sols poreux, les aquifères et les réservoirs. Mais ils ont également le potentiel de résoudre une classe plus large de problèmes de transport et de flux de réservoir poreux, notamment : le transport de masse de soluté, les déplacements de fluide multiphasique, le transport de chaleur et le flux de Darcy (diffusion de pression). Les processus de diffusion sont importants dans ces phénomènes de transport, soit directement (diffusion de solutés, diffusion de chaleur, diffusion de pression), soit indirectement (lorsque la dispersion hydrodynamique des quantités transportées est modélisée comme un processus de type diffusion). Dans les méthodes particulaires, la composante advective est modélisée en déplaçant les particules en fonction de la vitesse (ceci est relativement simple); d'autre part, le processus diffusif est modélisé en déplaçant les particules de manière aléatoire selon un processus de Wiener, ou mouvement brownien, ou une marche aléatoire. Dans les méthodes de particules Lagrangiennes sans grille, l'espace est supposé continu et les positions des particules sont des nombres réels. Dans le présent travail, nous nous concentrons sur le suivi de particules Lagrangien sans grille pour résoudre les processus de diffusion par la méthode de la marche aléatoire, sous le nom générique RWPT (Random Walk Particle Tracking). Ceci est pertinent pour la conduction électrique dans les matériaux solides (loi d'Ohm), la conduction thermique dans les solides ou les matériaux poreux remplis de fluide (loi de Fourier), diffusion de pression dans des milieux poreux légèrement compressibles saturés en fluide (loi de Darcy) et diffusion de solutés dans des milieux poreux partiellement ou totalement saturés d'eau (d'après la loi de Fick).

Hétérogénéité et discontinuité

Une étude spécifique du comportement macroscopique des particules Random Walk est nécessaire s'agissant du coefficient de diffusion hétérogène ou discontinu. Le cas de la diffusion discontinue est particulièrement gênant, et c'est notre objectif principal. De telles discontinuités se produisent aux «interfaces matérielles», des changements soudains de la microstructure (matériaux composites, supports poreux stratifiés, etc.). Pour la diffusion de soluté dans un milieu poreux, un autre point d'intérêt est le cas de la porosité discontinue (si le milieu est saturé d'eau) ou de la teneur en eau volumétrique discontinue (si le milieu est insaturé). Le cas de la conduction thermique avec une conductivité discontinue et une capacité thermique discontinue est similaire. La capacité de transfert de chaleur dans un matériau solide hétérogène joue un rôle similaire à celui de la porosité pour le transport de soluté dans un milieu poreux hétérogène rempli d'eau. Comme il est mentionné ci-dessus, les hétérogénéités sont difficiles à traiter, en particulier dans le cas d'une diffusion discontinue et d'une porosité discontinue. Dans la littérature sur les marches aléatoires de particules, les schémas de déplacement utilisés pour traiter la discontinuité peuvent être divisés en deux classes :

1. Schéma de grossissement d'interface, d'interpolation et de vitesse de dérive (par exemple [Labolle et al., 1996, Spiller, 2004])

2. Schémas de réflexion partielle (par exemple [Uffink, 1985]).

La première classe (« techniques d'interpolation ») atténue la discontinuité : l'interface est grossie ou élargie et les paramètres (diffusion, porosité) sont considérés comme continuellement variables plutôt que discontinus à travers l'interface grossie. La deuxième classe (« méthodes de réflexion partielle »), introduite par [Uffink, 1985], met en œuvre une réflexion / transmission prob-

abiliste des particules à travers l'interface discontinue : des probabilités sont attribuées pour la réflexion et la transmission de particules à travers l'interface. L'un des principaux inconvénients de ces deux approches est qu'il faut un petit pas de temps pour converger vers la solution correcte de la EDP discontinue, même si le nombre de particules est très grand. Ceci est particulièrement limitant en présence de nombreuses interfaces. Ces restrictions de pas de temps conduisent à des algorithmes inefficaces.

Dans le Chapitre 3 de cette thèse, nous proposons une nouvelle approche sans restrictions sur la taille des pas de temps. L'algorithme RWPT proposé ici est, comme d'autres dans la littérature, discret dans le temps et continu dans l'espace (sans grille). Les aspects nouveaux concernent le traitement des discontinuités. Le nouvel algorithme RWPT est basé sur un pas de temps adaptatif «Stop and Go», combiné à des schémas de réflexion / transmission partielle et étendu à trois concepts: (i) particules de masse négative; (ii) particules de masse adaptative; et (iii) les particules de "homing". Pour tester les nouveaux schémas RWPT stop-and-go, nous développons des solutions analytiques et semi-analytiques pour la diffusion en présence de multiples interfaces (milieu multicouche discontinu). Les résultats montrent que les schémas RWPT stop-and-go proposés (avec des particules adaptatives, négatives ou homing) correspondent extrêmement bien aux solutions semi-analytiques, même pour des contrastes très forts et au voisinage des interfaces. Les trois schémas fournissent une solution de diffusion correcte en quelques incréments de macro-temps, avec une précision qui ne dépend que du nombre de particules et non du pas de macro-temps. Ces schémas semblent prometteurs, dans la perspective d'extensions vers des géométries 3D plus complexes. Dans les chapitres suivant, les algorithmes RWPT sont étendus pour traiter des conditions de Dirichlet dans le Chapitre 4 et les conditions de flux nuls dans le Chapitre 5

(Voir plus bas sous-section 1.3 « Cadre de cette thèse »).

1.2.2 Revue de la littérature sur les méthodes RWPT avec discontinuités

[Noetinger et al., 2016] ont examiné de manière approfondie plusieurs méthodes de particules pour le transport diffusif ou advectif-diffusif, y compris la méthode de traçage par particule à temps discret (classique), à espace continu, sans grille [RWPT] [Labolle et al., 1996], et d'autres variantes telles que la marche aléatoire à temps continu (CTRW) [Kang et al., 2015] et la marche aléatoire à domaine temporel (TDRW) [Delay et Bodin, 2001, Bodin, 2015]. En comparaison, la présente étude se concentre sur une extension du schéma RWPT sans grille dans le cas de discontinuités multiples, conduisant à un schéma de pas de temps adaptatif «stop-and-go» couplé à divers nouveaux types de particules «adaptatives» (voir CH III pour plus de détails). Nous présentons maintenant, ci-dessous, un bref aperçu de deux types de systèmes de suivi de particules «asynchrones», appliqués aux particules de mouvement brownien, dans le cas d'un milieu poreux à discontinu et / ou à coefficients. Les deux types de schémas utilisés dans la littérature pour traiter de telles discontinuités sont essentiellement : (1) Schéma de vitesse de dérive, d'interpolation et de dérive d'interface (par exemple [Labolle et al., 1996, Spiller, 2004]) ; et (2) les schémas de réflexion partielle (par exemple [Uffink, 1985]). Cependant, ces méthodes présentent des restrictions strictes sur le pas de temps. [Ackerer & Mose, 2000, Bechtold et al., 2011] ont montré que les méthodes ci-dessus ne sont valables que pour Δ t $\rightarrow$ 0. Un petit pas de temps doit être utilisé afin d'éviter le dépassement des régions hétérogènes et discontinues de l'espace par les particules. De plus, comme les particules doivent parfois traverser la même interface plusieurs fois (avec un petit pas de temps), un autre problème

se pose : [Bechtold et al., 2011] ont montré que chaque réflexion introduisait une erreur numérique. Par conséquent, les restrictions sur le pas de temps persistent, de même que l'erreur avec le schéma proposé par [Bechtold et al., 2011]. En plus, une revue de la littérature plus spécifique est présentée dans l'introduction des chapitre 4 (Conditions de Dirichlet) et chapitre 5 (flux nul et systèmes grain/pore).

1.2.3 Cadre de cette thèse

Les discontinuités des propriétés des matériaux ont toujours été difficiles à traiter pour les phénomènes de transport diffusif, tant au niveau macroscopique (considérant la EDP de diffusion avec paramètre de diffusion discontinue) qu'au niveau microscopique de «particules» de chemin aléatoire (qui représentent des paquets de chaleur Masse). Dans les méthodes de particules précédentes proposées dans la littérature, la précision de la solution dépend du pas de temps. La solution est une approximation, qui devient plus précise lorsque le nombre de pas de temps augmente pour un nombre donné de particules (les problèmes de post-traitement des particules aux concentrations seront discutés plus loin au Chapitre 3). Le nouveau modèle proposé dans cet article ne dépend pas des contraintes de pas de temps, c'est-à-dire que sa précision n'est pas limitée par un choix a priori de la taille du pas de temps. La précision de la solution dépendra uniquement du nombre de particules nécessaires pour récupérer les moments et la concentration en masse ou la distribution de la température des particules. Comme dans certaines des méthodes de particules examinées précédemment, ce nouvel algorithme est inspiré de la solution analytique de la diffusion EDP pour une source de Dirac initiale dans un domaine infini, avec une interface où le coefficient de diffusion est discontinu. Comme mentionné précédemment, la quantité correspondante transportée par diffusion pourrait

être soit la masse (concentration de soluté), l'énergie thermique (température) ou le travail mécanique (pression interstitielle). Le nouveau schéma proposé (et ses variantes) présentent plusieurs caractéristiques innovantes. La première est que les pas de temps, pour chaque particule donnée, sont adaptés de telle sorte que la particule traverse chaque élément matériel entre les interfaces en un seul «micro-pas de temps». Le schéma est donc asynchrone (pendant un «pas de temps macro») sur l'ensemble des particules, et il reste également sans grille (la seule «grille» étant la grille matérielle d'éléments générée par les interfaces discontinues). D'autres caractéristiques innovantes impliquent une adaptation des particules lorsqu'elles traversent les interfaces (y compris par exemple la création de particules de masse négative). Les Conditions de Dirichlet 5 sont difficiles à mettre en œuvre dans les méthodes particulaires. Cette thèse propose donc de nouvelles méthodes pour implémenter les conditions de Dirichlet sans restriction sur le pas de temps. Les méthodes sont induites de nouvelles solutions analytiques et semi-analytiques développées dans cette thèse. Les conditions de Dirichlet sont ensuite associées aux algorithmes RWPT pour traiter les discontinuités. L'algorithme RWPT est utilisé pour une étude multi-échelle de la diffusion dans des systèmes à grains et pores. L'algorithme RWPT proposé est basé sur des solutions analytiques 2D / 3D dans des domaines finis et semi-infinis avec des conditions aux limites de flux nul. L'algorithme RWPT est ensuite appliqué à des géométries plus complexes de grains et de pores (difficiles à résoudre analytiquement). Différentes configurations d'un support composite à l'échelle micro (grains et pores dans un support poreux). Nous étudions l'impact de la porosité, puis l'effet de l'anisotropie locale sur les propriétés à l'échelle macro. Les propriétés effectives à l'échelle macro sont calculées en utilisant les moments spatiaux des positions des particules.

1.2.4 Récapitulatif

Cette thèse est organisée comme suit. Le chapitre suivant, le Chapitre 2, présente une analyse de la théorie sous-jacente aux processus stochastiques et de l'EDP macroscopique correspondante, en particulier pour les problèmes convectifs-diffusifs. Le Chapitre 3 présente de nouvelles méthodes et algorithmes de suivi de particules aléatoires à base de particules (RWPT) permettant de résoudre les problèmes de transport hétérogènes et discontinus avec plus de précision et moins de restrictions sur le pas de temps. Ce chapitre développe également de nouvelles solutions analytiques et semi-analytiques pour la diffusion en discontinu et la porosité dans des domaines infinis multicouches. Les schémas proposés s'adaptent parfaitement aux solutions analytiques. Le Chapitre 4 propose de nouvelles implémentations des conditions limites de Dirichlet pour les algorithmes RWPT du Chapitre 3, sans restrictions sur le pas de temps. Pour tester ces algorithmes, nous étendons les solutions semi-analytiques du Chapitre 3, afin de résoudre la diffusion discontinue et la porosité dans les domaines finis et semi-infinis multicouches. Les résultats obtenus pour une ou plusieurs interfaces sont présentés et discutés en fonction des méthodes de Dirichlet proposées. Au Chapitre 5, nous appliquons un algorithme RWPT, basé sur des solutions analytiques multidimensionnels, sur un système de grains / pores 2D. Une condition de flux nul est supposée localement aux interfaces grain / pore. Au niveau macro, les paramètres macroscopiques (porosités, tortuosités et tenseurs de diffusion effectifs) sont induits par les méthodes de mise à l'échelle des moments. En choisissant différentes tailles et grains allongés, des effets de porosité et d'anisotropie apparaissent au niveau macroscopique. Le chapitre concluant, le Chapitre 6, récapitule les résultats et discute des extensions.

Chapter 2

Stochastic processes, Probability Theory and Advection-Diffusion Equation

2.1 Introduction

This study reviews the relation between the Probability Density Function PDF of a Markovian stochastic process and the macroscopic Advection-Diffusion Equation ADE (Fick), using the following books [Arnold, 1974, Gardiner, 1985, Papoulis, 1991, Gillespie, 1992, Risken, 1996, Van Kampen, 2007, Gillespie & Seitaridou, 2013]. The aim of this review is to pinpoint the exact assumptions required for the PDF of a stochastic process to follow the ADE. This chapter is organized as follow: The next section, defines all functions (and properties) used in the following sections in this chapter. Section 3 is a proof of the Chapman-Kolmogorov equation. Starting from this last equation, section 4 gives Kramers-Moyal developments, both forward and backward. Section 5 shows the conditions for a PDF to satisfy the Fokker-Planck equation, then it links this equation to the ADE. Section 6 links Stochastic Processes to PDF's. Finally, section 7 states the main conclusions of this chapter.

2.2 Definitions

A real stochastic process $(X_t)_{t\epsilon \mathrm{T}}$ with $\mathrm{T} \subset \mathbb{R}^+$ is defined by, for every $t\epsilon \mathrm{T}$; X_t is a Random Variable (RV) from the probability space $(\Omega, \mathcal{F}, \mathbb{P})$ into $\mathbb{R}$.

For $t\epsilon \mathrm{T}$; X_t is a RV with distribution $\forall x \epsilon \mathbb{R}; F(x;t) = \mathbb{P}(X_t \leq x)$

We suppose that there exists an integrable function $P(x;t) \geq 0$ such that $F(x,t) = \int_{-\infty}^{x} P(y;t)\, dy$, P is called density of X_t. The probability to find the random variable X_t in the interval $[x, x+dx]$ is given by $P(x,t)\, dx$.

If the function $P(x;t)$ is continuous we can write $P(x;t) = \dfrac{\partial F}{\partial x}(x;t)$

Generally, let$(t_1, t_2, ..., t_n)$ be n times and $(X_{t_1}, X_{t_2}, ..., X_{t_n})$ be n-RV's.

We define the joint distribution function as : $\forall (x_1, ..., x_n) \epsilon \mathbb{R}^n$

$$F(x_1, x_2, ..., x_n; t_1, t_2, ..., t_n) = \mathbb{P}(X_{t_1} \leq x_1, X_{t_2} \leq x_2, ..., X_{t_n} \leq x_n) \quad (2.2.1)$$

The joint distribution function F verifies: For every permutation $(j_1, ..., j_n)$ of $(1, ..., n)$;

$$F(x_{j_1}, x_{j_2}, ..., x_{j_n}; t_{j_1}, t_{j_2}, ..., t_{j_n}) = F(x_1, x_2, ..., x_n; t_1, t_2, ..., t_n) \tag{2.2.2}$$

And for $m < n$;

$$F(x_1, x_2, ..., x_m, \infty, ..., \infty; t_1, t_2, ..., t_m, t_{m+1}, ..., t_n) = F(x_1, x_2, ..., x_m; t_1, t_2, ..., t_m) \tag{2.2.3}$$

We suppose that there exists an integrable function $P(x;t) \geq 0$ such that:

$$F(x_1, x_2, ..., x_n; t_1, t_2, ..., t_n) = \int_{-\infty}^{x_1} ... \int_{-\infty}^{x_n} P(y_1, ..., y_n; t_1, ..., t_n)\, dy_1 ... dy_n \tag{2.2.4}$$

P is called the probability density function or the PDF of $(X_{t_1}, X_{t_2}, ..., X_{t_n})$.

The probability to find the random variables X_{t_i} in the intervals $[x_i, x_i + dx_i]$ for all $i = 1, 2, ..., n$ is $P(x_1, x_2, ..., x_n; t_1, t_2, ..., t_n)\, dx_1 dx_2 ... dx_n$.

If the function P is continuous we can write

$$P(x_1, x_2, ..., x_n; t_1, t_2, ..., t_n) = \frac{\partial^n F}{\partial x_1 \partial x_2 ... \partial x_n}(x_1, x_2, ..., x_n; t_1, t_2, ..., t_n) \tag{2.2.5}$$

The PDF $P(x;t)$ satisfies the property:

1. $P(x;t)$ is positive.

2. $$\int_{\mathbb{R}} ... \int_{\mathbb{R}} P(x_1, x_2, ..., x_n; t_1, t_2, ..., t_n)\, dx_1 dx_2 ... dx_n = 1 \tag{2.2.6}$$

For all $i \in [\![1; n]\!]$ we have:

$$P(x_1, ..., x_{i-1}, x_{i+1}, ..., x_n; ; t_1, ..., t_{i-1}, t_{i+1}, ..., t_n) = \int_{\mathbb{R}} P(x_1, ..., x_n; t_1, ..., t_n)\, dx_i \tag{2.2.7}$$

Let us now define the conditional transition probability, let $t_1$and t_2 be two times and $x_1$and x_2 in $\mathbb{R}$.

For $P(x_1;t_1) \neq 0$ we define:

$$P(x_2;t_2|x_1;t_1) = \frac{P(x_1,x_2;t_1,t_2)}{P(x_1;t_1)} \tag{2.2.8}$$

and

$$\lim_{t_2 \to t_1} P(x_2;t_2|x_1;t_1) = \delta(x_2 - x_1) \tag{2.2.9}$$

If the time difference is infinitesimally small, the conditional probability will have the sharp value $\delta(x_2 - x_1)$, where the distribution $\delta(x)$ (e.g. Schwartz [Schwartz, 1951]) Dirac verifies:

$$\int_{\mathbb{R}} \delta(x - x_0) f(x)\, dx = f(x_0) \tag{2.2.10}$$

Using Eq.2.2.7 and Eq.2.2.8 we have:

$$\int_{-\infty}^{+\infty} P(x_3;t_3|x_1;t_1)\, dx_3 = \frac{1}{P(x_1;t_1)} \int_{-\infty}^{+\infty} P(x_1,x_3;t_1,t_3)\, dx_3 = \frac{P(x_1;t_1)}{P(x_1;t_1)} = 1 \tag{2.2.11}$$

We will be using this Eq.2.2.11 in the next section Kramers-Moyal equation.

For $t_0 < t$; $P(x;t|x_0;t_0)\, dx$ is the probability that the RV X_t will lie in the infinitesimal interval $[x, x + dx]$, given that $X_{t_0} = x_0$. From Eq.2.2.8 we have:

$$P(x_1,x_2;t_1,t_2) = P(x_2;t_2|x_1;t_1)\, P(x_1;t_1) \tag{2.2.12}$$

Generally, for $n \geq 2$ and we define:

$$P(x_n;t_n|x_1,x_2,...,x_{n-1};t_1,t_2,...,t_{n-1}) = \frac{P(x_1,x_2,...x_n;t_1,t_2,...,t_n)}{P(x_1,x_2,...x_{n-1};t_1,t_2,...,t_{n-1})} \tag{2.2.13}$$

For $t_1 < t_2 < ... < t_n$; The conditional transition probability density of the RV X_t at time t_n under the condition that the RV at the time $t_{n-1} < t_n$ has the sharp value x_{n-1}; at the time $t_{n-2} < t_{n-1}$ has the sharp value x_{n-2};...; at the time $t_1 < t_2$ has the sharp value x_1.

For $n = 3$ (in Eq.2.5.1) we have:

$$P(x_3;t_3|x_1,x_2;t_1,t_2) = \frac{P(x_1,x_2,x_3;t_1,t_2,t_3)}{P(x_1,x_2;t_1,t_2)}$$

$$\Rightarrow P(x_1, x_2, x_3; t_1, t_2, t_3) = P(x_3; t_3|x_1, x_2; t_1, t_2)\, P(x_1, x_2; t_1, t_2)$$

Then,

$$P(x_1, x_2, x_3; t_1, t_2, t_3) = P(x_3; t_3|x_1, x_2; t_1, t_2)\, P(x_2; t_2|x_1; t_1)\, P(x_1; t_1) \tag{2.2.14}$$

By mathematical induction we have:

$$P(x_1, ...x_n; t_1, ..., t_n) = P(x_n; t_n|x_1, ..., x_{n-1}; t_1, ..., t_{n-1}) ...P(x_2; t_2|x_1; t_1)\, P(x_1; t_1) \tag{2.2.15}$$

Definition A process is Markovian if: $\forall (t_1 < ... < t_n) \forall (x_1, ..., x_n) \epsilon \mathbb{R}^n$;

$$P(x_n; t_n|x_1, x_2, ..., x_{n-1}; t_1, t_2, ..., t_{n-1}) = P(x_n; t_n|x_{n-1}; t_{n-1}) \tag{2.2.16}$$

The conditional probability density depends only on the value $X_{t_{n-1}} = x_{n-1}$ at the next earlier time, but not on $X_{t_k} = x_k$ with $k \in [\![1; n-2]\!]$. The future depends only on the present.

So for a Markovian process Eq.2.2.15 becomes:

$$P(x_1, x_2, ...x_n; t_1, t_2, ..., t_n) = P(x_n; t_n|x_{n-1}; t_{n-1}) ...P(x_2; t_2|x_1; t_1)\, P(x_1; t_1) \tag{2.2.17}$$

2.3 Chapman-Kolmogorov equation (Proof)

For a Markovian process the Chapman-Kolmogorov equation is: $\forall (t_1 < t_2 < t_3); \forall (x_1, x_2, x_3) \epsilon \mathbb{R}^3$;

$$P(x_3; t_3|x_1; t_1) = \int_{-\infty}^{+\infty} P(x_3; t_3|x_2; t_2)\, P(x_2; t_2|x_1; t_1)\, dx_2 \tag{2.3.1}$$

Proof

In the subsection above we proved Eq.2.2.14 which is: $\forall (t_1 < t_2 < t_3); \forall (x_1, x_2, x_3) \epsilon \mathbb{R}^3$;

$$P(x_1, x_2, x_3; t_1, t_2, t_3) = P(x_3; t_3|x_1, x_2; t_1, t_2)\, P(x_2; t_2|x_1; t_1)\, P(x_1; t_1)$$

We integrate on x_2 the equation above from $-\infty$ to $+\infty$:

$$\int_{-\infty}^{+\infty} P\left(x_1, x_2, x_3; t_1, t_2, t_3\right) dx_2 = \int_{-\infty}^{+\infty} P\left(x_3; t_3 | x_1, x_2; t_1, t_2\right) P\left(x_2; t_2 | x_1; t_1\right) P\left(x_1; t_1\right) dx_2$$

Using Eq.2.2.7 for $i = 2$ and $n = 3$ we have:

$$P\left(x_1, x_3; t_1, t_3\right) = P\left(x_1; t_1\right) \int_{-\infty}^{+\infty} P\left(x_3; t_3 | x_1, x_2; t_1, t_2\right) P\left(x_2; t_2 | x_1; t_1\right) dx_2 \tag{2.3.2}$$

We divide by $P\left(x_1; t_1\right)$:

$$\frac{P\left(x_1, x_3; t_1, t_3\right)}{P\left(x_1; t_1\right)} = \int_{-\infty}^{+\infty} P\left(x_3; t_3 | x_1, x_2; t_1, t_2\right) P\left(x_2; t_2 | x_1; t_1\right) dx_2$$

Finally, the Chapman-Kolmogorov equation is:

$$P\left(x_3; t_3 | x_1; t_1\right) = \int_{-\infty}^{+\infty} P\left(x_3; t_3 | x_1, x_2; t_1, t_2\right) P\left(x_2; t_2 | x_1; t_1\right) dx_2 \tag{2.3.3}$$

And if the process (X_t) is Markovian then the Chapman-Kolmogorov equation becomes

$$P\left(x_3; t_3 | x_1; t_1\right) = \int_{-\infty}^{+\infty} P\left(x_3; t_3 | x_2; t_2\right) P\left(x_2; t_2 | x_1; t_1\right) dx_2 \tag{2.3.4}$$

The PDF of X_{t_3} conditioned on X_{t_1} is the integral of the product of the PDF of X_{t_3} conditioned on all the possible values of X_t and the PDF of all the possible values of X_t conditioned on X_{t_1}.

2.4 Kramers-Moyal equation (development & discussion)

2.4.1 Forward development

Let (X_t) be a Markovian process and $P(x; t | x_0; t_0)$ the transition probability, which is the probability for a particle to be at the position x at the time t : $(X_t = x)$ knowing that it was at the position x_0 at the time t_0 :$(X_{t_0} = x_0)$ with $t_0 \leq t$.

From the Chapman Kolmogorov equation (Eq.2.3.4) for a Markovian process we have:

$$P\left(x;t+dt|x_0;t_0\right)=\int_{-\infty}^{+\infty}P\left(x;t+dt|y;t\right)P\left(y;t|x_0;t_0\right)dy \tag{2.4.1}$$

Let $y=x-\zeta$, then we have:

$$P(x;t+dt|x_0;t_0)=\int_{-\infty}^{+\infty}P(x;t+dt|x-\zeta;t)P(x-\zeta;t|x_0;t_0)d\zeta \tag{2.4.2}$$

Let $f\left(z\right)$ be the function defined for all $z\epsilon\mathbb{R}$:

$$f(z)=P(z+\zeta;t+dt|z;t)P(z;t|x_0;t_0)$$

We assume that f verifies the following Taylor expansion around x:

$$f(x-\zeta)=f(x)+\sum_{n=1}^{+\infty}(-\zeta)^n\frac{1}{n!}\frac{d^nf}{dx^n}(x) \tag{2.4.3}$$

Then we have:

$$P(x;t+dt|x-\zeta;t)P(x-\zeta;t|x_0;t_0)=P(x+\zeta;t+dt|x;t)P(x;t|x_0;t_0)$$
$$+\sum_{n=1}^{+\infty}(-\zeta)^n\frac{1}{n!}\frac{\partial^n}{\partial x^n}(P(x+\zeta;t+dt|x;t)P(x;t|x_0;t_0)) \tag{2.4.4}$$

By using Eq.2.4.4 and assuming that the integral in Eq.2.4.2 is linear (Fubini), so that we can permute the integral and the sum, Eq.2.4.2 becomes:

$$P(x;t+dt|x_0;t_0)=\int_{-\infty}^{+\infty}P(x+\zeta;t+dt|x;t)P(x;t|x_0;t_0)d\zeta$$
$$+\sum_{n=1}^{+\infty}\int_{-\infty}^{+\infty}(-\zeta)^n\frac{1}{n!}\frac{\partial^n}{\partial x^n}(P(x+\zeta;t+dt|x;t)P(x;t|x_0;t_0))d\zeta$$
$$P(x;t+dt|x_0;t_0)=P(x;t|x_0;t_0)\int_{-\infty}^{+\infty}P(x+\zeta;t+dt|x;t)d\zeta$$
$$+\sum_{n=1}^{+\infty}\int_{-\infty}^{+\infty}(-\zeta)^n\frac{1}{n!}\frac{\partial^n}{\partial x^n}(P(x+\zeta;t+dt|x;t)P(x;t|x_0;t_0))d\zeta \tag{2.4.5}$$

By using Eq.2.2.11 with a change of variable we have:

$$P(x;t+dt|x_0;t_0)-P(x;t|x_0;t_0)=\sum_{n=1}^{+\infty}\int_{-\infty}^{+\infty}(-\zeta)^n\frac{1}{n!}\frac{\partial^n}{\partial x^n}(P(x+\zeta;t+dt|x;t)P(x;t|x_0;t_0))d\zeta \tag{2.4.6}$$

We divide Eq.2.4.6 by dt on both sides, then we have:

$$\frac{P(x;t+dt|x_0;t_0)-P(x;t|x_0;t_0)}{dt}=\sum_{n=1}^{+\infty}\frac{(-1)^n}{n!dt}\int_{-\infty}^{+\infty}\zeta^n\frac{\partial^n}{\partial x^n}(P(x+\zeta;t+dt|x;t)P(x;t|x_0;t_0))d\zeta \tag{2.4.7}$$

Letting dt go to zero in Eq.2.4.7, we obtain:

$$\frac{\partial P}{\partial t}(x;t|x_0;t_0)=\sum_{n=1}^{+\infty}\frac{(-1)^n}{n!}lim_{dt\to 0}\frac{1}{dt}\int_{-\infty}^{+\infty}\zeta^n\frac{\partial^n}{\partial x^n}(P(x+\zeta;t+dt|x;t)P(x;t|x_0;t_0))d\zeta \tag{2.4.8}$$

Then we assume that we can invert the umpteenth derivative and the integral of Eq.2.4.8, and we obtain the Forward Kramers-Moyal equation:

$$\frac{\partial P}{\partial t}(x;t|x_0;t_0)=\sum_{n=1}^{+\infty}\frac{(-1)^n}{n!}\frac{\partial^n}{\partial x^n}(P_n(x;t)P(x;t|x_0;t_0)) \tag{2.4.9}$$

where

$$P_n(x;t)=lim_{dt\to 0}\frac{1}{dt}\int_{-\infty}^{+\infty}\zeta^n P(x+\zeta;t+dt|x;t)d\zeta \tag{2.4.10}$$

Eq.2.4.21 is called the Forward Kramers-Moyal equation. This equation shows that the time evolution of the conditional probability $P(x;t|x_0;t_0)$, at $(x;t)$ given the initial state $(x_0;t_0)$, is fully determined by the set of functions $\left(P_n\left(x;t\right)\right)_{n\in\mathbb{N}^*}$. Later in section 2.5 we will show that for $n=1$ and $n=2$, $P_n(x;t)$ is equivalent to a velocity and a diffusivity respectively. The unit of $P_n(x;t)$ is a length unit power n per time unit.

If we replace $P\left(x;t|x_0;t_0\right)=\dfrac{P\left(x,x_0;t,t_0\right)}{P\left(x_0,t_0\right)}$ in Eq.2.4.21 we find that:

$$\frac{\partial}{\partial t}\left(\frac{P\left(x,x_0;t,t_0\right)}{P\left(x_0;t_0\right)}\right)=\sum_{n=1}^{+\infty}\frac{(-1)^n}{n!}\frac{\partial^n}{\partial x^n}\left(P_n(x;t)\frac{P\left(x,x_0;t,t_0\right)}{P\left(x_0;t_0\right)}\right)$$

$$\frac{1}{P\left(x_0;t_0\right)}\frac{\partial P}{\partial t}\left(x,x_0;t,t_0\right)=\frac{1}{P\left(x_0;t_0\right)}\sum_{n=1}^{+\infty}\frac{(-1)^n}{n!}\frac{\partial^n}{\partial x^n}\left(P_n(x;t)P\left(x,x_0;t,t_0\right)\right)$$

$$\frac{\partial P}{\partial t}(x, x_0; t, t_0) = \sum_{n=1}^{+\infty} \frac{(-1)^n}{n!} \frac{\partial^n}{\partial x^n} \left(P_n(x;t) P(x, x_0; t, t_0)\right) \tag{2.4.11}$$

By integrating Eq.2.4.11 on x_0 from $-\infty$ to $+\infty$ we find:

$$\frac{\partial P}{\partial t}(x;t) = \sum_{n=1}^{+\infty} \frac{(-1)^n}{n!} \frac{\partial^n}{\partial x^n} \left(P_n(x;t) P(x;t)\right) \tag{2.4.12}$$

Eq.2.4.12 is called the Forward Kramers-Moyal equation of the PDF $P(x;t)$. The PDF $P(x;t)$ of all Markovian processes verifies the Kramers-Moyal equation. This equation is used in section 2.5 in order to prove that the PDF $P(x;t)$ of a Markovian process verifies, under certain conditions, the Fokker-Planck equation and hence the Advection Diffusion PDE.

2.4.2 Backward development

Let (X_t) be a Markovian process and $P(x_0;t_0|x;t)$ the transition probability, which is the probability for a particle to be at the position x at the time $t : (X_t = x)$ knowing that it will be at the position x_0 at the time t_0 $(X_{t_0} = x_0)$ with $t \leq t_0$.

The Chapman-Kolmogorov Eq.2.3.4 for a Markovian process with a transition probability $P(x_0;t_0|x;t)$ is:

$$P(x_0;t_0|x;t) = \int_{-\infty}^{+\infty} P(x_0;t_0|x';t') P(x';t'|x;t) dx' \tag{2.4.13}$$

with $0 \leq t \leq t' \leq t_0$.

By changing the variable of integration in Eq.2.4.13, it becomes:

$$P(x_0;t_0|x;t) = \int_{-\infty}^{+\infty} P(x_0;t_0|x+\zeta;t+dt) P(x+\zeta;t+dt|x;t) d\zeta \tag{2.4.14}$$

with $0 \leq t \leq t+dt \leq t_0$.

Let $h(z)$ be the function defined for all $z \epsilon \mathbb{R}$:

$$h(z) = P(x_0;t_0|z;t+dt) \tag{2.4.15}$$

We assume that h verifies the following Taylor expansion around x:

$$h\left(x+\zeta\right)=h(x)+\sum_{n=1}^{+\infty}\zeta^{n}\frac{1}{n!}\frac{d^{n}h}{dx^{n}}(x) \tag{2.4.16}$$

By inserting $h\left(x+\zeta\right)$ in Eq.2.4.14 we obtain:

$$P(x_0;t_0|x;t)=\int_{-\infty}^{+\infty}h\left(x+\zeta\right)P(x+\zeta;t+dt|x;t)d\zeta \tag{2.4.17}$$

By inserting the Taylor development of h in Eq.2.4.17 we obtain:

$$P(x_0;t_0|x;t)=\int_{-\infty}^{+\infty}P(x_0;t_0|x;t+dt)P(x+\zeta;t+dt|x;t)d\zeta$$

$$+\int_{-\infty}^{+\infty}\sum_{n=1}^{+\infty}\zeta^{n}\frac{1}{n!}\frac{\partial^{n}P}{\partial x^{n}}\left(x_0;t_0|x;t+dt\right)P(x+\zeta;t+dt|x;t)d\zeta \tag{2.4.18}$$

We assume that the integral in Eq.2.4.18 is linear (Fubini), so that we can permute the integral and the sum, and by using Eq.2.2.11, we obtain:

$$P\left(x_0;t_0|x;t\right)-P\left(x_0;t_0|x;t+dt\right)=$$

$$+\sum_{n=1}^{+\infty}\int_{-\infty}^{+\infty}\zeta^{n}\frac{1}{n!}\frac{\partial^{n}P}{\partial x^{n}}\left(x_0;t_0|x;t+dt\right)P(x+\zeta;t+dt|x;t)d\zeta \tag{2.4.19}$$

We divide Eq.2.4.19 by dt then we have:

$$\frac{P\left(x_0;t_0|x;t\right)-P\left(x_0;t_0|x;t+dt\right)}{dt}=\sum_{n=1}^{+\infty}\frac{1}{n!}\frac{\partial^{n}P}{\partial x^{n}}\left(x_0;t_0|x;t+dt\right)\frac{1}{dt}\int_{-\infty}^{+\infty}\zeta^{n}.P(x+\zeta;t+dt|x;t)d\zeta \tag{2.4.20}$$

We let dt go to zero in Eq.2.4.20, we obtain the Backward Kramers-Moyal equation:

$$-\frac{\partial P}{\partial t}\left(x_0;t_0|x;t\right)=\sum_{n=1}^{+\infty}\frac{1}{n!}P_{n}\left(x;t\right)\frac{\partial^{n}P}{\partial x^{n}}\left(x_0;t_0|x;t\right) \tag{2.4.21}$$

where

$$P_{n}(x;t)=lim_{dt\rightarrow0}\frac{1}{dt}\int_{-\infty}^{+\infty}\zeta^{n}P(x+\zeta;t+dt|x;t)d\zeta \tag{2.4.22}$$

Which is the same definition of $P_{n}\left(x;t\right)$ found in Eq.2.4.10.

This backward version of the Kramers-Moyal equation is sometimes used in the literature to analyze inverse and source identification problems. Recall that $P(x_0;t_0|x;t)$ is the conditional probability density of being at initial state $(x_0;t_0)$ given the final state $(x;t)$. In this work, we will not use directly this backward version.

2.5 Fokker-Planck and Advection-Diffusion Equations

2.5.1 ADE with variable coefficients

The Advection-Diffusion Equation (ADE) for a deterministic space-time function $P(x;t)$ with a variable diffusion coefficient $D(x;t)$ and velocity $V(x;t)$ is the following PDE (Partial Differential Equation):

$$\frac{\partial P}{\partial t}(x;t) = -\frac{\partial}{\partial x}(VP)(x;t) + \frac{\partial}{\partial x}\left(D\frac{\partial P}{\partial x}\right)(x;t) \tag{2.5.1}$$

where $P(x;t)$ could represent concentration, temperature, etc. (see Chapter 1)

Eq.2.5.1 is the "conservative" formulation of the ADE.

By developing Eq.2.5.1 (ADE) we obtain:

$$\frac{\partial P}{\partial t}(x;t) = -\left(V\frac{\partial P}{\partial x}\right)(x;t) - \left(P\frac{\partial V}{\partial x}\right)(x;t) + \left(\frac{\partial D}{\partial x}\frac{\partial P}{\partial x}\right)(x;t) + \left(D\frac{\partial^2 P}{\partial x^2}\right)(x;t)$$

$$\frac{\partial P}{\partial t} = -\left(\frac{\partial V}{\partial x}P\right)(x;t) + \left(\left(-V + \frac{\partial D}{\partial x}\right)\frac{\partial P}{\partial x}\right)(x;t) + \left(D\frac{\partial^2 P}{\partial x^2}\right)(x;t) \tag{2.5.2}$$

Eq.2.5.2 can be viewed as the developed form of the ADE.

2.5.2 The Fokker-Planck equation

Let us go back to the Forward Krames-Moyal equation (Eq.2.4.12) obtained in the subsection 2.4.1 for a Markov process (X_t):

$$\frac{\partial P}{\partial t}(x;t) = \sum_{n=1}^{+\infty} \frac{(-1)^n}{n!}\frac{\partial^n}{\partial x^n}(P_n(x;t)P(x;t)) \tag{2.5.3}$$

With $P_n(x;t) = lim_{dt\to 0}\frac{1}{dt}\int_{-\infty}^{+\infty}\zeta^n P(x+\zeta;t+dt|x;t)d\zeta$.

First, let us assume that:

$$\exists k \geq 2; P_{2k} = 0 \tag{2.5.4}$$

By Pawula's theorem (see Appendix A), under hypothesis Eq.2.5.4:

$$\forall n \geq 3; P_n = 0 \tag{2.5.5}$$

As a consequence, from theorem Eq.2.5.5, Eq.2.4.12 becomes the Fokker-Planck equation:

$$\frac{\partial P}{\partial t}(x;t) = -\frac{\partial}{\partial x}(P_1(x;t)P(x;t)) + \frac{1}{2}\frac{\partial^2}{\partial x^2}(P_2(x;t)P(x;t)) \tag{2.5.6}$$

2.5.3 Equivalence between Fokker-Planck equation and ADE

We will now develop the resulting Fokker-Planck Eq.2.7.12 in order to identify it with the ADE Eq.2.5.2.

By developing Eq.2.7.12 we obtain:

$$\frac{\partial P}{\partial t}(x;t) = -\left(P\frac{\partial P_1}{\partial x}\right)(x;t) - \left(P_1\frac{\partial P}{\partial x}\right)(x;t) + \frac{1}{2}\frac{\partial}{\partial x}\left(\left(P\frac{\partial P_2}{\partial x}\right) + \left(P_2\frac{\partial P}{\partial x}\right)\right)(x;t)$$

$$\frac{\partial P}{\partial t}(x;t) = \left(-\frac{\partial P_1}{\partial x} + \frac{1}{2}\frac{\partial^2 P_2}{\partial x^2}\right)(x;t)\,P(x;t) + \left(-P_1 + \frac{\partial P_2}{\partial x}\right)(x;t)\frac{\partial P}{\partial x}(x;t) + \frac{1}{2}P_2(x;t)\frac{\partial^2 P}{\partial x^2}(x;t) \tag{2.5.7}$$

Therefore, to find equivalence between the Fokker-Planck Eq.2.5.7 and the ADE Eq.2.5.2, the probability function of the Markov process $P(x;t)$ should verify the following conditions:

$$-\frac{\partial V}{\partial x}(x;t) = \left(-\frac{\partial P_1}{\partial x} + \frac{1}{2}\frac{\partial^2 P_2}{\partial x^2}\right)(x;t) \tag{2.5.8a}$$

$$\left(-V + \frac{\partial D}{\partial x}\right)(x;t) = \left(-P_1 + \frac{\partial P_2}{\partial x}\right)(x;t) \tag{2.5.8b}$$

$$D\left(x;t\right)=\frac{1}{2}P_2\left(x;t\right) \tag{2.5.8c}$$

By inserting Eq.2.5.8c in Eq.2.5.8a and Eq.2.5.8b we obtain:

$$-\frac{\partial V}{\partial x}\left(x;t\right)=\left(-\frac{\partial P_1}{\partial x}+\frac{\partial^2 D}{\partial x^2}\right)\left(x;t\right) \tag{2.5.9a}$$

$$\left(-V+\frac{\partial D}{\partial x}\right)\left(x;t\right)=\left(-P_1+2\frac{\partial D}{\partial x}\right)\left(x;t\right) \tag{2.5.9b}$$

$$P_2\left(x;t\right)=2D\left(x;t\right) \tag{2.5.9c}$$

Then by replacing $P_1\left(x;t\right)$ in Eq.2.5.9a by its expression in Eq.2.5.9b we have:

$$-\frac{\partial V}{\partial x}\left(x;t\right)=\left(-\frac{\partial V}{\partial x}-\frac{\partial^2 D}{\partial x^2}+\frac{\partial^2 D}{\partial x^2}\right)\left(x;t\right) \tag{2.5.10a}$$

$$P_1\left(x;t\right)=\left(V+\frac{\partial D}{\partial x}\right)\left(x;t\right) \tag{2.5.10b}$$

$$P_2\left(x;t\right)=2D\left(x;t\right) \tag{2.5.10c}$$

Eq.2.5.10a is trivial (always satisfied), therefore we obtain finally the following system of relations on the coefficients $P_1\left(x;t\right)$ and $P_2\left(x;t\right)$:

$$P_1\left(x;t\right)=\left(V+\frac{\partial D}{\partial x}\right)\left(x;t\right)=lim_{dt\to 0}\frac{1}{dt}\int_{-\infty}^{+\infty}\zeta P(x+\zeta;t+dt|x;t)d\zeta \tag{2.5.11a}$$

$$P_2\left(x;t\right)=2D\left(x;t\right)=lim_{dt\to 0}\frac{1}{dt}\int_{-\infty}^{+\infty}\zeta^2 P(x+\zeta;t+dt|x;t)d\zeta \tag{2.5.11b}$$

Conclusion If the PDF $P\left(x;t\right)$ of a Markovian stochastic process verifies the conditions of Eq.2.5.15 (???) and Pawula's condition Eq.2.5.4, then $P\left(x;t\right)$ is the solution of the ADE Eq.2.5.1 with variable coefficients $V\left(x;t\right)$ and $D\left(x;t\right)$.

2.5.4 ADE with constant coefficients

This subsection analyzes the particular case of ADE with constant coefficients and in an infinite domains (the theory of Stochastic processes in this chapter is in infinite domains).

For constant coefficients D and V the ADE Eq.2.5.1 becomes:

$$\frac{\partial P}{\partial t}(x;t) = -V\frac{\partial P}{\partial x}(x;t) + D\frac{\partial^2 P}{\partial x^2}(x;t) \tag{2.5.12}$$

For an infinite domain with no boundaries and with the condition:

$$\lim_{x\to\pm\infty} P(x;t) = 0 \tag{2.5.13}$$

The solution, for this Eq.2.5.12 with the boundary condition 2.5.13, is a Gaussian with a mean equal to Vt and a variance equal to $2Dt$:

$$P(x;t) = \frac{1}{\sqrt{4\pi Dt}} exp\left(-\frac{(x-Vt)^2}{4Dt}\right) \tag{2.5.14}$$

Now Let us verify if this solution $P(x;t)$ satisfies the system of equations Eq.2.5.15

The system of equations 2.5.15 becomes :

$$P_1(x;t) = V = lim_{dt\to 0}\frac{1}{dt}\int_{-\infty}^{+\infty} \zeta P(x+\zeta; t+dt|x;t)d\zeta \tag{2.5.15a}$$

$$P_2(x;t) = 2D = lim_{dt\to 0}\frac{1}{dt}\int_{-\infty}^{+\infty} \zeta^2 P(x+\zeta; t+dt|x;t)d\zeta \tag{2.5.15b}$$

In addition to Eq.2.5.15 the PDF $P(x;t)$ should verify also the previous Pawula's hypothesis:

$$\exists k \geq 2; P_{2k} = 0 \tag{2.5.16}$$

Let us now calculate $P_n(x;t)$ for this Gaussian process:

$$P_n(x;t) = lim_{dt\to 0}\frac{1}{dt}\int_{-\infty}^{+\infty} \zeta^n \frac{1}{\sqrt{2\pi 2Ddt}} exp\left(-\frac{(\zeta - Vdt)^2}{4Ddt}\right) d\zeta \tag{2.5.17}$$

$P_n(x;t)$ of Eq.2.5.17 could also be written as:

$$P_n(x;t) = lim_{dt\to 0}\frac{1}{dt}E\left((dX_t)^n\right)$$

with (dX_t) is a Gaussian process with a mean equal to Vdt and a variance equal to $2Ddt$. And $E(dX_t)$ is the expected value of (dX_t) it can be noted as $E(dX_t) = \langle dX_t \rangle$ see more details in the next section.

The moments of the Gaussian process are: for $n = 1$; we have $E(dX_t) = Vdt$.

For $k \geq 1$, for $n = 2k+1$; $E\left(dX_t^{2k+1}\right) = 0$.

Therefore for $k \geq 1$ if $n = 2k+1$; $P_{2k+1}(x;t) = 0$.

And if $n = 2k$;

$$E\left(dX_t^{2k}\right) = \frac{(2k)!}{2^k k!}\left(\sqrt{2Ddt}\right)^{2k}$$

So for $n = 2k$; with $k > 1$:

$$P_{2k}(x;t) = lim_{dt\to 0}\frac{1}{dt}\frac{(2k)!}{2^k k!}\left(\sqrt{2Ddt}\right)^{2k} = lim_{dt\to 0}\frac{(2k)!}{2^k k!}(2D)^k dt^{k-1}$$

$$P_{2k}(x;t) = lim_{dt\to 0}\frac{(2k)!}{k!}D^k dt^{k-1} = 0$$

For $n = 2$ which means $k = 1$, we have:

$$P_2(x;t) = lim_{dt\to 0}\frac{(2)!}{1!}D = 2D$$

And for $n = 1$ we have

$$P_1(x;t) = lim_{dt\to 0}\frac{1}{dt}Vdt = V$$

And for $n \geq 3$ we have

$$P_n(x;t) = 0$$

By inserting the previous expressions of $P_n(x;t)$ in the Forward Kramers-Moyal equation Eq.2.4.12 we obtain:

$$\frac{\partial P}{\partial t}(x;t) = \frac{(-1)^1}{1!}\frac{\partial}{\partial x}(P_1(x;t)P(x;t)) + \frac{(-1)^2}{2!}\frac{\partial^2}{\partial x^2}(P_2(x;t)P(x;t))$$

$$\frac{\partial P}{\partial t}(x;t) = -V\frac{\partial P}{\partial x}(x;t) + D\frac{\partial^2 P}{\partial x^2}(x;t)$$

Which is the ADE for constant velocity and diffusive coefficient.

2.6 From Stochastic Processes to PDF's

The previous section, showed that under certain conditions the PDF of a stochastic process verifies the ADE. Hence, the ADE could be solved using stochastic processes then induce the PDF of the stochastic process which is the deterministic solution of the ADE. This section gives a different approach to the PDF from the one given in section 2.2. It shows how to induce the PDF from its stochastic process using the Dirac function. This relation between the PDF and its stochastic process X_t can be used in post-processing, to calculate the PDF at the end of particles simulation.

The PDF $P_{X_t}(x;t)$ of the random variable X_t is the derivative of $\mathbb{P}$ with respect to x.

$$P_{X_t}(x;t) = \frac{d}{dx}\mathbb{P}(X_t \leq x) \tag{2.6.1}$$

with $(X_t \leq x) = \{\omega \epsilon \Omega / X_t(\omega) \leq x\}$. Hence Eq.2.6.1 implies:

$$\mathbb{P}(X_t \leq x) = \int_{-\infty}^{x} P_{X_t}(y;t)\, dy \tag{2.6.2}$$

Let us define the Heaviside function:

$$\Theta(x) = \begin{cases} 1 & if\ x \geq 0 \\ 0 & if\ x < 0 \end{cases} \tag{2.6.3}$$

And the derivation of Θ in a distribution sense is the Dirac function:

$$\langle D\Theta, \varphi \rangle = -\langle \Theta, \varphi' \rangle = -\int_0^{+\infty} \varphi'(t)\, dt = \varphi(0) = \langle \delta, \varphi \rangle \tag{2.6.4}$$

with $\varphi \in C^{\infty}$ and compactly supported, φ is a Bump function. Hence:

$$D\Theta = \Theta' = \delta \tag{2.6.5}$$

Eq.2.6.5 can also be expressed as:

$$\frac{d}{dx}\Theta = \delta \tag{2.6.6}$$

On the other hand, using Θ definition Eq.2.6.3:

$$\Theta\left(x - X_t\right) = \begin{cases} 1 & if\ X_t \leq x \\ \\ 0 & if\ X_t > x \end{cases} \tag{2.6.7}$$

$$\left\langle \Theta\left(x - X_t\right) \right\rangle = \int_{\omega \epsilon \Omega} \Theta\left(x - X_t\left(\omega\right)\right) dP\left(\omega\right) = \mathbb{P}\left(X_t \leq x\right) \tag{2.6.8}$$

By combining Eq.2.6.1 and 2.6.8 we obtain:

$$P_{X_t}\left(x;t\right) = \frac{d}{dx}\mathbb{P}\left(X_t \leq x\right) = \frac{d}{dx} < \Theta\left(x - X_t\right) > \tag{2.6.9}$$

On the other hand, the Transfer theorem states that for a RV $\Omega \xrightarrow{\xi} \mathbb{R}$ and a real function $\mathbb{R} \xrightarrow{h} \mathbb{R}$:

$$\int_{\omega \epsilon \Omega} h \circ \xi\left(\omega\right) dP\left(\omega\right) = \int_{\mathbb{R}} h\left(y\right) P_{\xi}\left(y\right) dy \tag{2.6.10}$$

Thus,

$$\begin{aligned} < \delta\left(x - X_t\right) > &= \int_{\omega \epsilon \Omega} \delta\left(x - X_t\left(\omega\right)\right) dP\left(\omega\right) \\ &= \int_{\mathbb{R}} \delta\left(x - y\right) P_{X_t}\left(y;t\right) dy = P_{X_t}\left(x;t\right) \end{aligned} \tag{2.6.11}$$

Using Eq.2.6.11, Eq.2.6.6:

$$P_{X_t}\left(x;t\right) = < \delta\left(x - X_t\right) > = \left\langle \frac{d}{dx}\Theta\left(x - X_t\right) \right\rangle \tag{2.6.12}$$

For two Stochastic processes $\left(X_t, Y_t\right)$ we find that:

$$< \delta\left(x - X_t\right)\delta\left(y - Y_t\right) > = \int_{\omega \epsilon \Omega} \delta\left(x - X_t\left(\omega\right)\right)\delta\left(y - Y_t\left(\omega\right)\right) dP\left(\omega\right) \tag{2.6.13}$$

Using the Transfer theorem we have:

$$= \int_{\mathbb{R}^2} \delta(x - x') \, \delta(y - y') \, P_{X_t,Y_t}(x', y'; t) \, dx' dy' \tag{2.6.14}$$

Using Fubini's theorem:

$$= \int_{\mathbb{R}} \delta(y - y') \left(\int_{\mathbb{R}} \delta(x - x') \, P_{X_t,Y_t}(x', y'; t) \, dx' \right) dy' = \int_{\mathbb{R}} \delta(y - y') \, P_{X_t,Y_t}(x, y'; t) \, dy' \tag{2.6.15}$$

Hence:

$$P_{X_t,Y_t}(x, y; t) =< \delta(x - X_t) \, \delta(y - Y_t) > \tag{2.6.16}$$

Similarly we introduce the n-dimensional distribution function:

$$P_{X_1,...,X_n}(x_1, ..., x_n) = P(x_1, ..., x_n) = \langle \delta(x_1 - X_1) ... \delta(x_n - X_n) \rangle \tag{2.6.17}$$

Eq.2.6.17 gives a different approach to calculate the PDF of n-RV's $(X_1, ..., X_n)$.

Calculus of the expected value $\langle f(X_t) \rangle$

Using the definition of the Dirac function Eq.2.2.10 applied to X_t instead of x_0:

$$f(X_t) = \int_{\mathbb{R}} f(x) \, \delta(x - X_t) \, dx \tag{2.6.18}$$

Hence, the expected value $\langle f(X_t) \rangle$:

$$\langle f(X_t) \rangle = \left\langle \int_{\mathbb{R}} f(x) \, \delta(x - X_t) \, dx \right\rangle = \int_{\omega \epsilon \Omega} \left[\int_{\mathbb{R}} f(x) \, \delta(x - X_t(\omega)) \, dx \right] dP(\omega)$$

By Fubini's theorem we inverse the integrals and we obtain:

$$\langle f(X_t) \rangle = \int_{\mathbb{R}} f(x) \, \langle \delta(x - X_t) \rangle \, dx$$

Using Eq.2.6.12, we have:

$$\langle f(X_t) \rangle = \int_{\mathbb{R}} f(x) \, P(x; t) \, dx \tag{2.6.19}$$

Eq.2.6.19 is the general case to calculate the expected value $\langle f(X_t)\rangle$, if $f(x)$ is taken as x^n, then $\langle f(X_t)\rangle$ becomes the n^{th} order moment of X_t (e.g. moments were calculated in subsection 2.5.4).

2.7 From Langevin to Fokker-Planck equation

The general Langevin equation has the form:

$$\frac{dX_t}{dt} = h(X_t;t) + g(X_t;t)\,\Gamma(t) \tag{2.7.1}$$

The Langevin force (stochastic force) $\Gamma(t)$ is assumed to be a Gaussian random variable with zero mean and $\delta - correlation$ function:

$$\langle\Gamma(t)\rangle = 0; \langle\Gamma(t)\,\Gamma(t')\rangle = q\delta(t-t') \tag{2.7.2}$$

The parameter q will be determined by the physics of the problem (when $q=1$, $\Gamma(t)$ is labeled in literature as "White noise").

We assume $g(x;t)=1$, Eq.2.7.1 becomes:

$$\frac{dX_t}{dt} = h(X_t;t) + \Gamma(t) \tag{2.7.3}$$

Let us consider the finite difference scheme of Eq.2.7.3:

$$dX_t = X_{t+dt} - X_t = h(X_t;t)\,dt + \sqrt{q}dW_t \tag{2.7.4}$$

where $dW_t = W_{t+dt} - W_t$ and W_t is the Wiener process and $\sqrt{q}\frac{dW_t}{dt} \underset{dt\to 0}{\to} \Gamma(t)$.

The increments dW_t are independent and verify the following properties:

$$E(dW_t) = 0; E\left((dW_t)^2\right) = dt \tag{2.7.5}$$

Let us now determine the drift terms P_1 and the diffusion term P_2:

$$P_n(x;t) = lim_{dt\to 0}\frac{1}{dt}\int_{-\infty}^{+\infty}\zeta^n P(x+\zeta;t+dt|x;t)d\zeta \tag{2.7.6}$$

$$P_n(x;t) = lim_{dt\to 0}\frac{1}{dt}E\left\{(X_{t+dt}-X_t)^n\,|X_t = x\right\} \tag{2.7.7}$$

with $E\left\{dX_t^n | X_t = x\right\}$ is the conditional expectation.

By using properties of the conditional expectation and dW_t properties Eq.2.7.5, the drift terms P_1 and the diffusion term P_2 of Eq.2.7.7 become:

$$E\left\{dX_t | X_t = x\right\} = h\left(x;t\right) dt \tag{2.7.8}$$

$$E\left\{\left(dX_t\right)^2 | X_t = x\right\} = \Gamma\left(t\right) dt + O\left(dt^2\right) \tag{2.7.9}$$

Hence,

$$P_1\left(x;t\right) = lim_{dt\to 0}\frac{1}{dt} E\left\{dX_t | X_t = x\right\} = h\left(x;t\right) \tag{2.7.10}$$

$$P_2\left(x;t\right) = lim_{dt\to 0}\frac{1}{dt} E\left\{\left(dX_t\right)^2 | X_t = x\right\} = q \tag{2.7.11}$$

And for $n \geq 3$; $P_n\left(x;t\right) = 0$. Whence, using the expressions of $P_n\left(x;t\right)$ in the Forward Kramers-Moyal equation we obtain the corresponding Fokker-Planck equation:

$$\frac{\partial P}{\partial t}\left(x;t|x_0;t_0\right) = -\frac{\partial}{\partial x}(h(x;t)P(x;t|x_0;t_0)) + \frac{q}{2}\frac{\partial^2}{\partial x^2}(P(x;t|x_0;t_0)) \tag{2.7.12}$$

Therefore, to solve the ADE Eq.2.7.12, we can start by solving the Langevin Eq.2.7.3, by first integrating (e.g. Itô's or Stratonovich's integral) the Langevin equation. Then use, for example, Random Walk Particle Tracking methods as in Chapter 3, 4, 5. Finally, we calculate the PDF from the stochastic process using section 2.6. The PDF P will be the solution of the Advection Diffusion PDE, when the PDF is multiplied by mass we obtain the mass concentration.

2.8 Conclusion and recapitulation

In conclusion, the conditions for the PDF of a stochastic process (X_t) to follow the Fokker Planck and hence the ADE with variable coefficients are:

1. (X_t) is required to be a Markovian process.

2. The PDF $P(x;t)$ of (X_t) must verify:

$$\exists k \geq 2; P_{2k}(x;t) = lim_{dt\to 0}\frac{1}{dt}\int_{-\infty}^{+\infty}\zeta^{2k}P(x+\zeta;t+dt|x;t)d\zeta = 0 \tag{2.8.1}$$

   In addition, if the coefficients of the ADE are spatially variable, they must be differentiable. The next chapter (Chapter 3) studies ADE's with discontinuities, in this case the ADE's coefficients are not differentiable.

The second condition is difficult to be verified unless the PDF $P(x;t)$ is known explicitly. It has been shown [Gillespie & Seitaridou, 2013, Risken, 1996] that Eq.2.8.1 is satisfied, if (X_t) is a continuous Markovian process (a Markov process is continuous if it satisfies the continuity condition $X_{t+dt} \to X_t$ as $dt \to 0$)
.

When the coefficients of the ADE are constant then the PDF $P(x;t)$ is the Gaussian function and it verifies all the above conditions. This implies that for a fixed time t, X_t becomes the Gaussian RV.

The next chapter proposes to solve ADE's with discontinuous coefficients with no restrictions on the time step.

Chapter 3

Efficient random walk algorithm with discontinuous diffusion and porosity (negative, adaptive and homing particles)

3.1 Introduction

3.1.1 Preamble

One of the methods described in this chapter (subsection 3.3.5.3) has been published in a paper in the Journal of Computational Physics [Oukili et al., 2019].

3.1.2 Overview

Particle methods have been much used to model the transport of mass, heat, and other quantities through solids, fluids, and fluid-filled porous media. The last two cases involve both diffusive and advective transport phenomena (due to the moving fluid). Hydrodynamic dispersion due to detailed spatial variations of the velocity field has also been modeled as a Fickian diffusion-type process, e.g. in fluid-filled porous structures (see [Sahimi, 1993]). Other purely diffuse processes include heat diffusion in materials (*Fourier*'s law), and pressure diffusion (compressible Darcy flow in a fluid-filled porous medium).

Particle methods are based on a discrete representation of the transported quantity (solute concentration, fluid pressure, fluid saturation, heat or temperature) as discrete packets (the "particles"), each carrying a unit mass, or a unit heat, etc. The advantage of particle methods is that they avoid some of the problems of Eulerian methods based on Partial Differential Equations (PDE's), such as numerical instability, artificial diffusion, mass balance errors, and/or oscillations that could lead to negative concentrations or saturations. Various types of particle methods have been devised: non-Lagrangian Particle-in-Cell methods (PIC); implementing Markov processes in a PIC framework with stochastic times [Spiller et al., 2000]; continuous-time particles on a grid [Kang et al., 2015]; the time-domain random walk (TDRW) [Delay & Bodin, 2001, Bodin, 2015]; and Lagrangian particles with discrete time-steps in continuous

space (gridless). Such particle methods have been extensively used for modeling advective-diffusive solute transport in porous soils, aquifers, and reservoirs [Noetinger et al., 2016, Sbai, 2018].

In "Lagrangian" methods, space is assumed continuous, and particle positions $X(t)$ are real numbers (the method is then "gridless"). In the present work, we focus on Lagrangian particle tracking to solve diffusion processes by random walk (Wiener process), under the generic name RWPT (Random Walk Particle Tracking).

A specific study of the macroscopic behavior of Random Walk particles is necessary when dealing with a heterogeneous or discontinuous diffusion coefficient $D(x)$. The case of discontinuous diffusion is particularly troublesome, and this is our main focus. Such discontinuities occur at "*material interfaces*", with sudden changes of microstructure (composite materials, layered porous media*, etc.)*. For solute diffusion in a porous medium, an additional point of interest is the case of discontinuous porosity $\theta(x)$ (if the medium is water-saturated), or discontinuous volumetric water content $\theta(x)$ (if the medium is unsaturated).

In the literature on particle Random Walks, the displacement schemes used for handling the discontinuity can be characterized into two classes: (1) Interface coarsening, interpolation, and drift velocity scheme (e.g. [Labolle et al., 1996, Spiller et al., 2002]); (2) Partial reflection schemes (e.g. [Uffink, 1985]). The first class ("interpolation techniques") smooth out the discontinuity[Bagtzoglou et al., 1992]: the interface is coarsened and the parameters (diffusion, porosity) are considered continuous through the coarsened interface. The second class ("partial reflection methods"), introduced by Uffink [Uffink, 1985], implements a probabilistic *reflection/transmission* of the particles across the discontinuous interface: probabilities are assigned for particle *reflection* and *transmission* across the interface. Other similar partial reflection/ transmission schemes

were investigated by [Labolle et al., 1998, Ackerer, 1985, Cordes et al., 1991, Semra et al., 1993, Hoteit et al., 2002, Lim, 2006, Bechtold et al., 2011].

Lejay & Pichot [Lejay & Pichot, 2012] proposed a "two-step algorithm" (their Algo.2), equivalent to a Stop&Go procedure: the particle is stopped at the interface, and then undergoes a "Skewed Brownian Motion"(SBM) for the next step, which may lead the particle to cross the interface. Their two-step algorithm was presented for a 1D finite domain with zero flux boundary conditions. On the other hand, they also presented a "one-step algorithm" (their Algo.3) where, it seems, they use a type of acceptance-rejection method to obtain the displacement in the neighborhood of the interface (this method is different from ours). More recently, Lejay & Pichot [Lejay & Pichot, 2016] tested their approaches [Lejay & Pichot, 2012] by implementing 1D benchmark tests, involving comparisons between their SBM and two Random Walks approaches in the literature [Uffink, 1985, Hoteit et al., 2002].

One of the drawbacks of these approaches is that a small time step is required in order to converge to the correct solution of the discontinuous PDE, even if the number of particles is very large. This is particularly limiting in the presence of many interfaces. This limitation becomes even more drastic for very large diffusion contrasts, e.g., two orders of magnitude or more. Thus, [Ackerer & Mose, 2000, Bechtold et al., 2011] showed that the above methods are only valid for infinitesimal time steps. A small time step must be used in order to avoid the overshoot of heterogeneous and discontinuous subregions of space by the particles.

In this study, we propose a novel approach in the framework of "partial reflection methods" but without restrictions on time step size. The new RWPT algorithm is discrete in time and continuous in space (gridless), and the novel aspects have to do with the treatment of discontinuities. The new

algorithm is based on adaptive "Stop&Go" time-stepping, combined with partial reflection/transmission schemes similar to [Hoteit et al., 2002, Lim, 2006, Bechtold et al., 2011, Lejay & Pichot, 2012], and extended with the concept of negative mass particles.

This chapter is organized as follows. The next section, 3.2, presents the theory behind Random Walk Particle Tracking methods (RWPT), and the corresponding macroscopic diffusion PDE. Section 3.3 presents a novel particle-based method for solving heterogeneous and discontinuous transport problems using RWPT with "negative mass particles". Section 3.4 compares analytical solutions to our RWPT results. Section 3.5 recapitulates the method and discusses extensions of this work.

3.2 Theory

This section presents the theory of advective-diffusive transport :

- The partial differential equations (PDE's) (concentration based) at macroscopic scale.
- The related theory of stochastic differential equations (SDE's), driven by white noise governing particles at the microscopic scale (packets/quanta of concentration).

3.2.1 Concentration based, the partial differential equations (PDE's)

3.2.1.1 The Gaussian function

Let us define the Gaussian function G, with a mean μ and a variance σ^2. It is convenient to define the Gaussian Probability Density Function (PDF) of particle positions (x) at any given time (t); and as a macroscopic concentration

solution of the diffusion PDE for a particular case of initial sources (homogeneous advective-diffusive transport, heterogeneous diffusion).

$$\forall x \epsilon \mathbb{R}; G\left(\mu, \sigma^2, x\right) = \frac{1}{\sigma\sqrt{2\pi}} exp\left(-\frac{\left(x-\mu\right)^2}{2\sigma^2}\right) \tag{3.2.1}$$

A Gaussian random variable (RV) with mean μ and variance σ^2 is denoted $N\left(\mu, \sigma^2\right)$ and has the Probability Density Function (PDF) $G\left(\mu, \sigma^2, x\right)$. Letting $\sigma^2 = 2D_0 t$, this Gaussian PDF represents the macroscopic concentration solution $C\left(x,t\right)$ of the diffusion PDE with spatially constant diffusion coefficient D_0, for an initial point source condition $C\left(x,t\right) = M_0\delta\left(x-\mu\right)$, with unit mass $M_0 = 1$, in an infinite domain.

3.2.1.2 The advection-diffusion transport PDE for concentration

The equation governing the transport of solute concentration (C) in a heterogeneous medium with variable parameters $\mathbf{D}$ (diffusion coefficient), θ (porosity) and $\mathbf{V}$ (velocity) is (see for instance [Labolle et al., 1998]):

$$\frac{\partial\left(\theta C\right)}{\partial t} = -\nabla \cdot \left(\theta \mathbf{V} C\right) + \nabla \cdot \left(\theta \mathbf{D} \cdot \nabla C\right) \tag{3.2.2}$$

Note that in this chapter we do not distinguish between vectors and second rank tensors ($D_{ij} = D\delta_{ij}$ in the case of scalar diffusion).
Eq.3.2.2 could also be written as follow :

$$\begin{aligned} \frac{\partial\left(\theta C\right)}{\partial t} &= \nabla\cdot\left(-\theta C\mathbf{V} + \mathbf{D}\cdot\nabla\left(\theta C\right)\right) \\ &= -\nabla\cdot\left\{\theta C\left(\mathbf{V} + \nabla\cdot\mathbf{D} + \mathbf{D}\cdot\nabla\left(ln\theta\right)\right)\right\} + \frac{1}{2}\nabla\cdot\nabla\cdot\left(2\theta C\mathbf{D}\right) \end{aligned} \tag{3.2.3}$$

The first equality corresponds to the conservative (divergence) form of the PDE, while the second equality corresponds to its decomposed form (from which apparent "drift velocity" terms emerge due to spatially variable diffusion and porosity coefficients).

For a 1D problem with scalar diffusion D, the transport PDE for an initial source at $x = x_0$ in a homogeneous medium with constant parameters D, θ and V is:

$$\begin{cases} \forall t > 0; \forall x \epsilon \mathbb{R}; & \frac{\partial C}{\partial t}(x,t) = -V \frac{\partial C}{\partial x}(x,t) + D \frac{\partial^2 C}{\partial x^2}(x,t) \\ \forall t > 0; & lim_{x \to \pm\infty} C(x,t) = 0 \\ \forall x \epsilon \mathbb{R}; & C(x,0) = \frac{M_0}{\theta} \delta(x - x_0) \end{cases} \tag{3.2.4}$$

The last equation represents an initial point source located at $x = x_0$ with mass M_0, and $\delta(x)$ represents the Dirac pseudo-function (δ distribution)(e.g. Schwartz [Schwartz, 1951]).

This PDE will be later formulated for purely diffusive discontinuous diffusion coefficients and water contents in section 3.2.3.

The analytical solution of Eq.3.2.4, is

$$\forall t > 0; \forall x \epsilon \mathbb{R};\ C(x,t) = \frac{M_0}{\theta} G(x_0 + Vt, 2Dt, x) \tag{3.2.5}$$

where G is the Gaussian PDF defined in Eq.3.2.1

3.2.1.3 From concentration to particle positions

Let us consider now a particle based method to solve Eq.3.2.4, and the concentration will be determined from the particles positions distribution PDF.

$$C(x,t) = \int_{\mathbb{R}} C(X_t, t)\, \delta(X_t - x)\, dX_t \tag{3.2.6}$$

$$C(x,t) = \int_{\mathbb{R}} \delta(X_t - x)\, dm_t \tag{3.2.7}$$

To solve Eq.3.2.4 using particle methods. For a time t. We need to generate particles with a PDF equivalent to Eq.3.2.5. Thus, these particles must follow the RV $N(x_0 + Vt, 2Dt)$, hence

$$X_t = N(x_0 + Vt, 2Dt) \tag{3.2.8}$$

Using simple Gaussian RV operations, we obtain :

$$X_t = x_0 + V\,t + \sqrt{2\,D\,t}\,N\,(0,1) \tag{3.2.9}$$

where $N\,(0,1)$ is a Gaussian RV, with 0 mean and unit variance.

In conclusion, the PDF of RV X_t is identical to the concentration solution in Eq.3.2.5 multiplied by the porosity θ and divided by M_0.

3.2.2 Discrete time SDE algorithms for diffusion for constant or continuously variable parameters

Let (X_t) be a continuous Markovian process of particles positions[1]. The Kramers-Moyal forward development of the PDF of(X_t) [Risken, 1996]:

$$\frac{\partial P}{\partial t}\,(x;t) = \sum_{n=1}^{+\infty} \frac{(-1)^n}{n!} \frac{\partial^n}{\partial x^n}\,(F_n(x;t)P\,(x;t)) \tag{3.2.10}$$

where

$$F_n(x;t) = \lim_{dt\to 0^+} \frac{1}{dt} \int_{-\infty}^{+\infty} \zeta^n P(x+\zeta;t+dt|x;t)d\zeta = \lim_{dt\to 0^+} \frac{1}{dt}\,\langle dX\,(dt,t)^n\rangle \tag{3.2.11}$$

F_n is the n^{th} moment of the random variable $dX\,(dt,t) = X_{t+dt} - X_t$

If (X_t) is a continuous Markovian process ([Gillespie & Seitaridou, 2013] p157,173) then :

$$\forall n \geq 3; F_n = 0 \tag{3.2.12}$$

And Eq.3.2.10 becomes the Fokker-Planck equation:

$$\frac{\partial P}{\partial t}\,(x;t) = -\frac{\partial}{\partial x}(F_1(x;t)P(x;t)) + \frac{1}{2}\frac{\partial^2}{\partial x^2}(F_2(x;t)P(x;t)) \tag{3.2.13}$$

Therefore, by identification of Eq.3.2.3 with Eq.3.2.13, we can model advective-diffusive transport problems using Markovian processes,

[1]Briefly, (X_t) is a continuous Markovian process if : (a) its future depends only on its present ; and (b) it satisfies the continuity condition $X_{t+dt} \to X_t$ as $dt \to 0$.

$$\begin{cases} F_1 = V + \nabla D + D.\nabla\left(ln\theta\right) \\ F_2 = 2D \\ P = \frac{\theta C}{M(t)} \end{cases} \tag{3.2.14}$$

The stochastic equation equivalent to Eq.3.2.13, under the condition that dX is a smooth and self-consistent[2] function ([Gillespie & Seitaridou, 2013], p.153-154)

$$dX\left(dt,t\right) =$$

$$N\left(\left(V\left(X_t\right) + div\left(D\left(X_t\right)\right) + D\left(X_t\right) div\left(ln\theta\left(X_t\right)\right)\right)dt, 2D\left(X_t\right)dt\right) \tag{3.2.15}$$

Eq.3.2.15 shows that infinitesimal displacements of particles $dX\left(dt,t\right)$, from time t to $t+dt$, follow a Gaussian PDF. Whence, by using the properties of Gaussian RV, Eq.3.2.15 becomes:

$$X_{t+dt} = X_t + \left(V\left(X_t\right) + div\left(D\left(X_t\right)\right) + D\left(X_t\right) div\left(ln\theta\left(X_t\right)\right)\right)dt +$$

$$+\sqrt{2D\left(X_t\right)dt}\, N\left(0,1\right) \tag{3.2.16}$$

Remark : Eq.3.2.15 is exact for infinitesimal time step dt, however further below we will use it with finite Δt. In addition, $D\left(x\right)$ and $\theta\left(x\right)$ must be differentiable.

To solve the transport problem of Eq.3.2.2 stochastically, we need to find the PDF of the continuous Markovian process $\left(X_t\right)$. Thus, one needs a discretization of time of Eq.3.2.16 (and a random number generator). We choose here, like many authors ([Uffink, 1985, Tompson & Gelhar, 1990, Labolle et al., 1996, Labolle et al., 1998, Hoteit et al., 2002, Lim, 2006, Bechtold et al., 2011], an explicit time-stepping scheme, which is compatible with the Itô integration of

[2] If the infinitesimal interval $[t, t+dt)$ is divided into two subintervals $[t, t+\alpha dt)$ and $[t+\alpha dt, t+dt)$, where $\alpha \epsilon [0,1]$, then the increment incurred over the full interval $[t, t+dt)$ should be the sum of the successive increments incurred over those two subintervals.

SDE. We obtain:

$$X_i^{(p)}(t_n + \Delta t_n) = X_i^{(p)}(t_n) + \\ +\Delta t_n \left(U_i^{(p)}(t_n) + \frac{\partial D_{ij}^{(p)}}{\partial x_j} + D_{ij}^{p} \frac{\partial ln\theta^{(p)}}{\partial x_j} \right) + \\ +\sqrt{\Delta t_n} \left(B_{ij}^{(p)} Z_j^{(p)}(t_n) \right) \tag{3.2.17}$$

In this equation, the variable quantities are all Lagrangian quantities, and they should be computed at the spatial position $x = X(t)$ for each particle "p": Lagrangian velocity vector U, scalar porosity θ, diffusion tensor D and its square-root matrix B, $div(D)$, and $grad(ln\theta)$. More precisely, the different terms are defined as follows:

- (p) : particle label (a positive integer number), or equivalently, replicate number (p) of the trajectory $X_i(t_n)$
- $i = 1, 2, 3$: coordinate index (three coordinate axes if 3D space)
- $X_i^{(p)}(t_n)$ is the position of the Lagrangian particle at time t_n
- $Z_j^{(p)}(t_n)$ is a purely Gaussian random process or sequence $N(0, 1)$
- $\mathbf{B}$: "Matrix square root" of the $\mathbf{BB} = 2\mathbf{D}$ matrix
- $U_i^{(p)}(t_n)$: particle's Lagrangian velocity
- $\theta\left(\mathbf{X}^{(p)}(t_n)\right)$: porosity or water content, taken at particle position $\mathbf{X}^{(p)}(t_n)$.

The second and third terms in equation ***3.2.17*** can be interpreted as follows:

- The second term, proportional to Δt, is equivalent to a velocity term containing the actual advective velocity of the fluid (if any) plus two drift velocities due to the spatial variability of D and of θ.

- The third term, proportional to $\sqrt{\Delta t}$, is the random walk term based on the Itô representation of the diffusive Wiener process for a tensorial diffusion coefficient D_{ij} (let $D_{ij} = D\delta_{ij}$ for scalar diffusion).

The spatial variability of D_{ij} intervenes in both the second term (as drift velocity) and in the third term (as a random white noise process with spatially variable intensity). However, this is correct only if $div\,(\mathbf{D})$ is well defined. For scalar diffusion in 1D space, the requirement would be that $D(x)$ must be differentiable; otherwise equation ***3.2.17*** does not hold.

3.2.3 Prototype problem: 1D diffusive PDE with a single initial source and a single discontinuity

In this section, we will define a purely diffusive problem, with an initial Dirac source, in an infinite composite porous medium made up of two sub-domains Ω_1 and Ω_2 separated by a single discontinuity, or "material interface". The interface between the two media is located at $X_{Interface} = 0$, and the initial point source is located at $X_{Source} = x_0 < 0$. The subdomains Ω_1 and Ω_2 have different diffusion coefficients D_1 and D_2, and different water contents or porosities θ_1 and θ_2 (or equivalently, different heat capacities c_1 and c_2, as explained in the introduction). Such discontinuous media can be found in porous soils; porous and fractured rocks; and many other materials at various scales, from geologic scales to sub-micron scales. For instance, at small scales, [Spiller, 2004] studied oxygen diffusion through a discontinuous grains/joints system in a sub-micron scale layer of Nickel Oxide. Here, to illustrate our random walk particle methods, and without loss of generality, we focus on solute diffusion in a porous medium. In that case, the diffusion coefficient $D(x)$ describes the diffusion phenomenon at the mesoscale of a *Representative Elementary Volume (REV)* containing many pores, which is different from the

molecular diffusion coefficient D_{Mol} in free water. Thus, in a porous medium, the solute diffusion coefficient $D(x)$ could be discontinuous because of the difference in tortuosity of the porous medium, while the discontinuity of the water contents comes from the difference on porosity of the medium.

$$\begin{cases} \forall t > 0; \forall x \leq x_{1-2}; & \frac{\partial(\theta_1 C_1)}{\partial t} = \frac{\partial}{\partial x}\left(\theta_1 D_1 \frac{\partial C_1}{\partial x}\right) \\ \forall t > 0; \forall x \geq x_{1-2}; & \frac{\partial(\theta_2 C_2)}{\partial t} = \frac{\partial}{\partial x}\left(\theta_2 D_2 \frac{\partial C_2}{\partial x}\right) \end{cases} \tag{3.2.18a}$$

$$\begin{cases} \forall t \geq 0; & \lim_{x \to -\infty} C_1(x,t) = 0 \\ \forall t \geq 0; & \lim_{x \to +\infty} C_2(x,t) = 0 \end{cases} \tag{3.2.18b}$$

$$\begin{cases} \forall t \geq 0; & C_1(x_{1-2},t) = C_2(x_{1-2},t) \\ \forall t \geq 0; & \theta_1 D_1 \frac{\partial C_1}{\partial x}(x_{1-2},t) = \theta_2 D_2 \frac{\partial C_2}{\partial x}(x_{1-2},t) \end{cases} \tag{3.2.18c}$$

$$\begin{cases} \forall x \leq x_{1-2}; & C_1(x,0) = \frac{M_0}{\theta_1}\delta(x - x_0) \\ \forall x \geq x_{1-2}; & C_2(x,0) = 0 \end{cases} \tag{3.2.18d}$$

In the system of PDE's formulated above (***3.2.18a***), each PDE represents a mass conservation equation for the solute per volume of space (and not per volume of solvent). Nevertheless, in this particular case, the porosities θ_1 and θ_2 are constant in each sub-domain and could be factored out from each PDE. [3] The system of equations 3.2.18c enforces the continuity of solute concentration (mass per volume of solvent) and of solute flux density (mass per unit time per unit sectional area of porous medium). In all these equations, Fick's law is used for the diffusive flux.

The exact analytical solution of problem 3.2.18 is given the following system of equations:

[3] They should not be factored out in the more general case of spatially variable and discontinuous porosity, with two subdomains $\theta_1(x)$ and $\theta_2(x)$.

$$\forall t \geq 0; \forall x \leq x_{1-2}; C_1(x,t) = C_1^S(x,t) + C_1^R(x,t) \tag{3.2.19a}$$

$$\forall t \geq 0; \forall x \leq x_{1-2};$$
$$C_1^S(x,t) = \frac{M_0}{\theta_1}\left(\frac{1}{\sqrt{2\pi}\sqrt{2D_1 t}} exp\left(-\frac{(x - x_{1-2} - (x_0 - x_{1-2}))^2}{4D_1 t}\right)\right) \tag{3.2.19b}$$

$$\forall t \geq 0; \forall x \leq x_{1-2};$$
$$C_1^R(x,t) = \frac{M_0}{\theta_1}\left(\frac{R_{1-2}}{\sqrt{2\pi}\sqrt{2D_1 t}} exp\left(-\frac{(x - x_{1-2} + (x_0 - x_{1-2}))^2}{4D_1 t}\right)\right) \tag{3.2.19c}$$

$$\forall t \geq 0; \forall x \geq x_{1-2}; C_2(x,t) =$$
$$\frac{M_0}{\theta_2}\left(\frac{1 - R_{1-2}}{\sqrt{2\pi}\sqrt{2D_2 t}} exp\left(-\frac{(x - x_{1-2} - \beta_{1-2}(x_0 - x_{1-2}))^2}{4D_2 t}\right)\right) \tag{3.2.19d}$$

$$R_{1-2} = \frac{\theta_1\sqrt{D_1} - \theta_2\sqrt{D_2}}{\theta_1\sqrt{D_1} + \theta_2\sqrt{D_2}} \; and \; \beta_{1-2} = \frac{\sqrt{D_2}}{\sqrt{D_1}} \tag{3.2.19e}$$

Eq.3.2.19 could also be written using the function G defined by Eq.3.2.1:

$$\forall t \geq 0; \forall x \leq x_{1-2}; C_1(x,t) = C_1^S(x,t) + C_1^R(x,t) \tag{3.2.20a}$$

$$\forall t \geq 0; \forall x \leq x_{1-2}; C_1^S(x,t) = \frac{M_0}{\theta_1} G(x_{1-2} + (x_0 - x_{1-2}), 2D_1 t, x) \tag{3.2.20b}$$

$$\forall t \geq 0; \forall x \leq x_{1-2};$$
$$C_1^R(x,t) = \frac{M_0}{\theta_1} R_{1-2} G(x_{1-2} - (x_0 - x_{1-2}), 2D_1 t, x) \tag{3.2.20c}$$

$$\forall t \geq 0; \forall x \geq x_{1-2};$$
$$C_2(x,t) = \frac{M_0}{\theta_2}(1 - R_{1-2}) G(x_{1-2} + \beta_{1-2}(x_0 - x_{1-2}), 2D_2 t, x) \tag{3.2.20d}$$

$$R_{1-2} = \frac{\theta_1\sqrt{D_1} - \theta_2\sqrt{D_2}}{\theta_1\sqrt{D_1} + \theta_2\sqrt{D_2}} \; and \; \beta_{1-2} = \frac{\sqrt{D_2}}{\sqrt{D_1}} \tag{3.2.20e}$$

- C_1^S ("S" for "Source") is the solution of this same diffusion problem if there were no interface (constant parameters with no discontinuities).
- C_1^R is the symmetric of C_1^S relative to the interface $x = x_{1-2}$, multiplied by a coefficient R_{1-2}(R for Reflection).

- C_2 is the solution of a diffusion problem with an initial mass $(1 - R_{1-2})$ located at $x_{1-2} + \beta_{1-2}(x_0 - x_{1-2})$, as illustrated in Figure 3.2.1

3.3 Methods and algorithms

In this section, we will first start by explaining the reason behind the need of a new algorithm. Then we will be discussing previous proposed methods used to fill this need. Finally, we will be presenting the new methods proposed in this chapter and their advantages compared to the previous ones.

3.3.1 Discontinuity problem

The most straightforward test of an algorithm concerning the diffusion problem with discontinuous $D(x)$ is the uniform concentration test, where the exact theoretical solution of the transient diffusion PDE is a constant concentration $C(x,t) = C_0$ at all times (t) and all positions (x). This is obtained simply by imposing a constant initial concentration profile $C(x,0) = C_0$, and imposing ***either*** zero flux conditions $\partial C/\partial x = 0$, *or else* Dirichlet conditions $C = C_0$ at both boundaries. In Figure 3.3.1 we chose zero flux conditions.

The random walk equation can be written as follows for diffusion in 1D space:

$$X^{(p)}(t_n + \Delta t_n) = X^{(p)}(t_n) + \Delta t_n \frac{\partial D}{\partial x}\left(X^{(p)}(t_n)\right) + \sqrt{2D\left(X^{(p)}(t_n)\right)\Delta t_n}\, Z^{(p)}(t_n) \tag{3.3.1}$$

However, this equation is limited to the case of continuously variable diffusion coefficient. We now focus on the case of discontinuous $D(x)$. If we naively insert the discontinuous $D(x)$ in the above equation, a deficit of concentration appears near the interface of discontinuity, as illustrated in Figure 3.3.1 (where

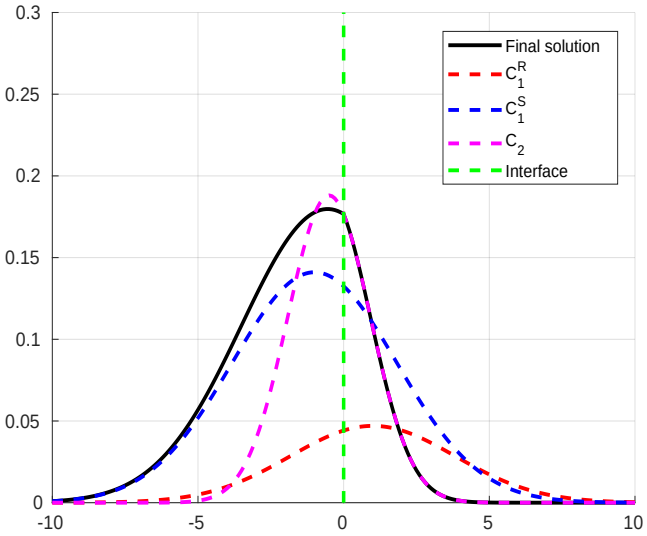

(a)

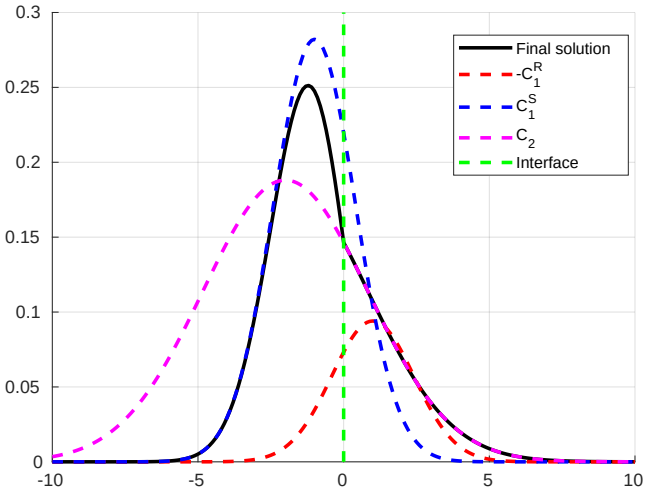

(b)

Figure 3.2.1: Component parts (bold dashed lines) of analytical solution given in (a) Eq.3.2.19 for $D_1 > D_2$ and (b) equivalent form of Eq.3.2.19 for $D_1 < D_2$ are summed to form final solution (bold curve) about an interface.

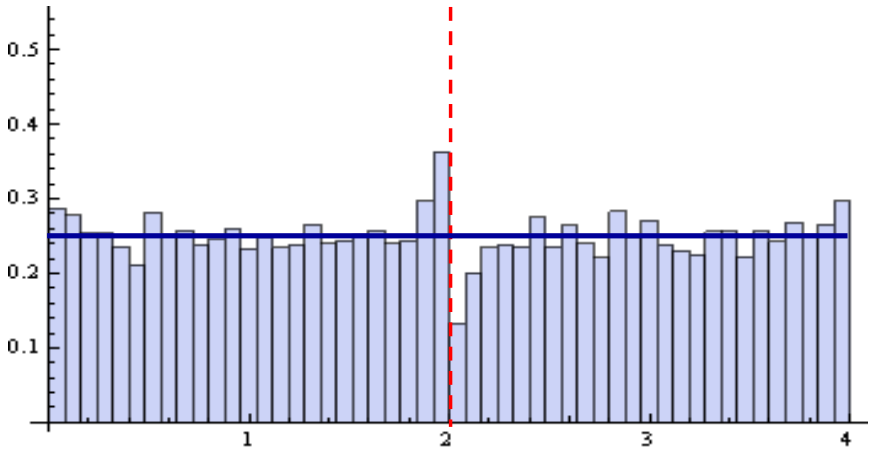

Figure 3.3.1: Kalia 2013 : Comparison of Probability density / or particle concentration profile (distribution) (Concentration kg/m) .

D1 < D2). We can deal with this deficit of concentration using two different schemes (reflection, smoothing)...

One can deal with this deficit of concentrations around the interface using two different types of approaches, reflection or smoothing, as mentioned earlier in the introduction section. For this purpose, a Stop&Go algorithm is necessary; it is described in the following section.

3.3.2 Stop and go algorithm

This subsection 3.3.2 discusses the concept of time step splitting. This concept has been mainly used in partial reflection techniques [Ackerer, 1985, Semra et al., 1993, Hoteit et al., 2002, Lim, 2006, Bechtold et al., 2011] around one discontinuity. The stop and go algorithm proposed here has been generalized into multi interfaces. This scheme is essential for particles to explore all heterogeneities of the medium during a time step, without over shooting.

Most of the previous "Stop and Go" algorithms used the following scheme for time-step splitting : $\triangle t = \triangle t_1 + \triangle t_2$, where $\triangle t$ is the overall time step used to do calculations and post-processing, $\triangle t_1$ is the time required by the particle to reach the first interface that it crosses, $\triangle t_2$ is calculated by subtracting $\triangle t_1$ from $\triangle t$ and is used to calculate the new step chosen by the algorithm from the interface to its final position. However [Bechtold et al., 2011] have shown, in their paper, that this algorithm is wrong, because it fails to pass the "first test", defined by these authors as follows: diffusion in the presence of a "transparent" interface separating two half-domains (D_1, D_2) while setting $D_1 = D_2 = D$ for the purposes of the test. The results show that the method is inconsistent. Indeed, the random walk displacement ΔX of a particle that crosses the "interface" with $D_1 = D_2 = D$ is calculated using the time step splitting RWPT scheme as:

$$\triangle X = \xi\sqrt{2D\triangle t_1} + \xi\sqrt{2D\triangle t_2} = \xi\sqrt{2D}\left(\sqrt{\triangle t_1} + \sqrt{\triangle t_2}\right) \tag{3.3.2}$$

On the other hand, since we know that with $D_1 = D_2 = D$, we can compare this to the classical calculation of the random walk displacement ΔX of a particle in a homogeneous medium with constant diffusion coefficient D:

$$\triangle X = \xi\sqrt{2D\triangle t} \tag{3.3.3}$$

Combining the two previous displacement schemes leads to:

$$\sqrt{\triangle t} = \sqrt{\triangle t_1} + \sqrt{\triangle t_2} \tag{3.3.4}$$

to be compared to the time-step splitting scheme:

$$\triangle t = \triangle t_1 + \triangle t_2 \tag{3.3.5}$$

This is a contradiction, and we conclude (along with [Bechtold et al., 2011]) that the proposed scheme **(with** $\triangle t = \triangle t_1 + \triangle t_2$**)** is indeed inconsistent.

Another scheme that may come to mind, as an alternative to the previous scheme reviewed by [Bechtold et al., 2011], is to generate a new Random Variable (RV) each time a particle reaches an interface, as follows:

$$\triangle X = \xi_1 \sqrt{2D_1 \triangle t_1} + \xi_2 \sqrt{2D_2 \triangle t_2} \tag{3.3.6}$$

where $\triangle X$ is the displacement from time (t) to $(t + \triangle t)$. Hence, generating a new RV allows the algorithm to maintain the original time splitting : $\triangle t = \triangle t_1 + \triangle t_2$, while apparently satisfying the correct rule $\triangle X \sim \xi \sqrt{2D \triangle t}$ in the case of a homogeneous domain. Indeed, if $D_1 = D_2$, then 3.3.6 leads to:

$$\triangle X = \sqrt{2D} \left(\xi_1 \sqrt{\triangle t_1} + \xi_2 \sqrt{\triangle t_2} \right) \tag{3.3.7}$$

Furthermore, because ξ_1 and ξ_2 are independent Gaussian RV's, both with 0-mean and unit variance, the previous $\triangle X$ can be expressed equivalently as:

$$\triangle X \sim \xi \sqrt{2D} \sqrt{\triangle t_1 + \triangle t_2} \sim \xi \sqrt{2D \triangle t} \tag{3.3.8}$$

where ξ is again a unit variance zero-mean Gaussian RV. Note that the mean and variance of $\triangle X$ remains the same in the last two equations. However, even though this scheme seems to be correct, it will be biasing the ensemble mean distribution of random displacements $\triangle X^{(p)}$ over all particles or replicates (p). This is due to the fact that particles (p) that are most likely to reach an interface have a higher displacement value$\triangle X^{(p)}$ than those far from the interface. This will lead to alter preferentially the highest values of the random $\triangle X$. A bias is thus introduced, and the PDF will not be Gaussian anymore, even in the case of diffusion in a homogeneous medium (see Figure 3.3.2). In fact, we conclude that the displacement $\triangle X$ should not be generated with two different RV's. Another reason for this will be given later on, while discussing our proposed methods to deal with discontinuities.

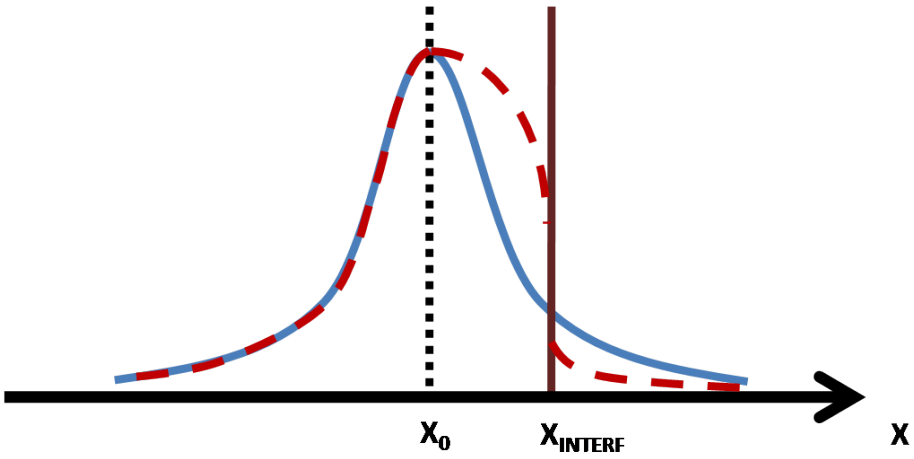

Figure 3.3.2: Schematic comparison between a Gaussian distribution of concentration (bold blue curve), and a hypothetical result of the algorithm described by Eq.3.3.6 (dashed red bold curve).

Let us now propose a new generalized version of the Stop and Go algorithm. With this algorithm there will not be any restriction on the maximum step that a particle does. This means that there will not be any restriction on (1) the value of the random variables, and (2) on the time step :

1. The algorithm allows the use of a Gaussian random variable, while most, if not all, previous algorithms use uniform random variables. Which needs many steps to approach the Gaussian random variable.

2. In previous algorithms (e.g. Uffink1985, Labolle2000, Bechtold2011) there was a restriction on the time step. So that the particles do not overshoot many cells (without taking into account the heterogeneity of intermediate cells). In the new proposed algorithm there will be no restrictions on the time step,(In case there are no other restriction on the time step, then the time step can be put equal to the final simulation time).

For all methods (reflection, refraction and smoothing)...there are local re-

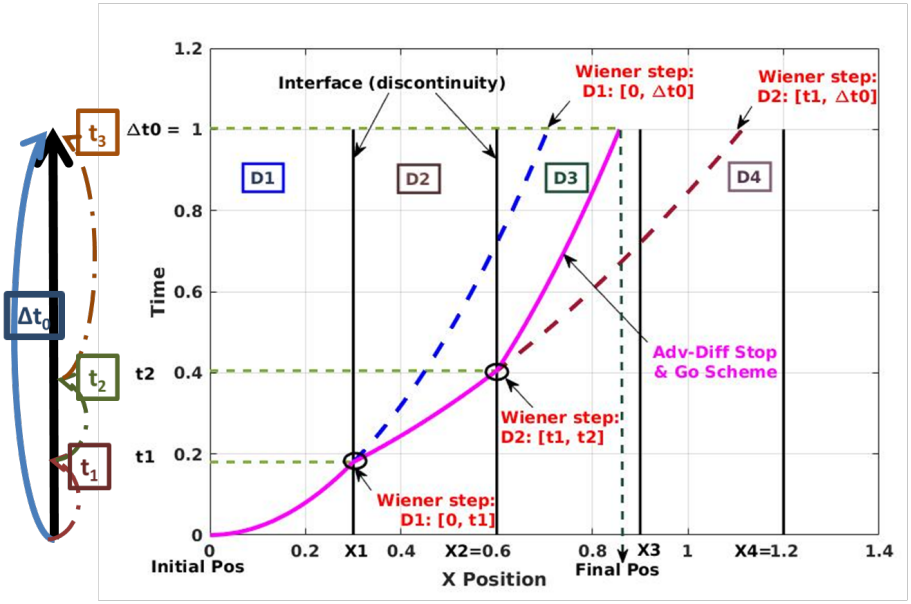

Figure 3.3.3: Time step splitting scheme: Left (vertically): macro-time step Δt_0, and intermediate steps t_1, t_2, t_3. Right: schematic space-time graph illustration of the position of a particle, in one macro-time step Δt_0, that crosses many interfaces in a domain with different diffusion coefficients.

strictions on time steps. Hence, the necessity of a new Asynchronous Stop & Go time-stepping scheme with no restrictions on time steps (shown here for heterogeneous advection+diffusion):

$$\Delta X_n^{j+1} = \sqrt{2D^j}\left(\sqrt{t_n^{j+1}} - \sqrt{t_n^j}\right) Z\left(t_n\right) + \left(t_n^{j+1} - t_n^j\right) U^j \tag{3.3.9}$$

Figure3.3.3 shows the algorithm used to split the time step for a multi-interface problem. Each time a particle crosses an interface, it stops at the interface, and a new step is calculated with the new parameters. This allows particles to avoid overshooting, and thus, explore all heterogeneities of the medium in one time step.

3.3.3 Reflection technique

The new random walk particle schemes proposed in this chapter consist basically in a combination of the previous "Stop and go" algorithm, combined with a new partial reflection scheme and in some cases, three extensions of the nature of the discrete particles: negative mass particles; adaptive mass particles; and homing particles. The resulting new schemes solve two problems in the presence of discontinuities (material interfaces): (1) the particles do not overshoot, i.e., they explore all the heterogeneities and discontinuities of the medium; and (2) the particles do not need to be reflected multiple times across each material interface (unlike previous methods in the literature). One consequence of properties (1) and (2) is that there are no stringent restrictions on the time step. In fact, the time step can be set equal to the final simulation time, or else, it can be set to coincide with any desired sequence of discrete output times. Figure 3.3.4 presents a flow-chart summarizing the new particle schemes that are developed and tested in the sequel of this chapter for dealing with diffusion in the presence of discontinuous material interfaces.

3.3.4 Partial reflection and extensions: the proposed algorithms

3.3.4.1 Methods to deal with discontinuous coefficients in the literature

Both Uffink's and Semra's methods are inspired from the analytical solution Eq.3.2.19 of the Problem Eq.3.2.18. To deal with parameter discontinuities in a medium, Uffink changes the transition probabilities of the particles near the interface using the analytical solution Eq.3.2.19. Semra on the other hand, splits particles step that crosses the interface into two steps. Once the par-

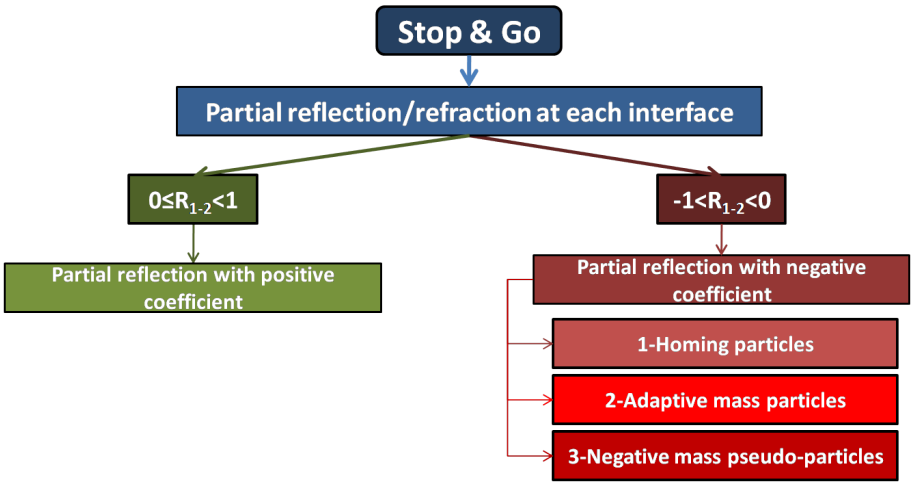

Figure 3.3.4: Flow-chart illustrating the new particle schemes in this work, for modeling diffusion via random walks in the presence of discontinuous material interfaces. The "stop & go" is a basic asynchronous time step splitting scheme, used each time a particle encounters an interface during the macro-time step Δt_0. Partial reflection is used at each interface. Several new methods are implemented, based on extensions of the concept of "particle", to deal with the case where the calculated partial reflection coefficient R_{1-2} is negative, as explained in the text.

ticles arrive at the interface, the transition probability is altered to deal with parameter discontinuities.

As with the previous methods in the literature, the novel model proposed in this chapter is also inspired from the analytical solution Eq.3.2.19. As shown in sub-section 3.2.3, in the case of a single interface, this analytical solution can be split into three Gaussian's. The sum of the first two Gaussian's is the concentration field inside the sub-domain where the initial source is located. The third Gaussian is the concentration field in the other sub-domain (where the initial source is *not* located). Each of the three Gaussian components of the analytical solution has two parameters (mean μ and variance σ^2) and a multiplicative factor which represents the intensity of the Gaussian.

The previous methods used in the literature avoided a direct utilization of

the partial reflection coefficients R_{1-2} and $1 - R_{1-2}$ appearing in Eq.3.2.20 because they could not handle negative reflection coefficients for particles. Instead, these previous methods tried to approach the solution by using other coefficients that are positive. In these methods, the distribution of particle positions approaches the analytical solution *only* after the particles cross the interface many times.

3.3.4.2 New schemes to deal with both positive and negative R

The novel idea proposed in this chapter is that both positive and negative partial reflection coefficients "R" can be used, and that the particle positions may converge to the exact analytical solution in just a single crossing of the discontinuous interface. In section3.2.3, we have presented the analytical solution of Eq.3.2.20 for a pure diffusion problem with one discontinuous interface. In this subsection, we will analyze this analytical solution; the analysis will lead to the idea behind the new algorithm (three variants, or "schemes") proposed in this chapter.

3.3.4.3 Analysis of reflection and transmission coefficients at an interface from the exact solution

First, let us analyze separately the different terms of Eq.3.2.20 :

- $C_1^S(x,t)$ is the concentration field that would obtain for a pure diffusion problem with an initial source at x_0, with no discontinuous interface (spatially constant diffusion and porosity parameters). That is why it is called the "Source" concentration solution, and labeled with an "S".

- $C_1^R(x,t)$ is the symmetric of C_1^S relative to the interface $x = x_{1-2}$, and multiplied by a coefficient R_{1-2}. Note that fields C_1^S and C_1^R are restricted to the sub-domain $x \leq x_{1-2}$. In addition, C_1^R is the symmetric

of the field C_1^S is restricted to sub-domain $x \geq x_{1-2}$. That is why C_1^R is interpreted as if the restricted part of C_1^S to sub-domain $x \geq x_{1-2}$ has been partially reflected. It is noted with an R, which refers to reflection, and R_{1-2} is the reflection coefficient.

- $C_2(x,t)$ is similar to the solution of a pure diffusion problem with an initial source located at $x_{1-2} + \beta_{1-2}(x_0 - x_{1-2})$ and multiplied by a coefficient $(1 - R_{1-2})$. This component of the solution is constructed from a new apparent source that appears to be moved (reflected) to the other side of the interface. It appears here, from the coefficients R_{1-2} and $(1 - R_{1-2})$ in C_1^R and C_2, that these two solutions components are complementary, since we have $R_{1-2} + (1 - R_{1-2}) = 1$. We notice here that the euclidean distance $(x_0 - x_{1-2})$ relative to the interface $x = x_{1-2}$ is multiplied by $\beta_{1-2} = \sqrt{\frac{D_2}{D_1}}$. This could be interpreted by the fact that this distance (from the position of the initial Dirac source to the interface) belongs to sub-domain 1 and has diffusion coefficient D_1 (instead of the coefficient D_2 used in C_2).

Based on these analyses, we now propose the following algorithm ("equivalent" to Eq.3.2.20) to solve the diffusion problem Eq.3.2.18 using RWPT:

Let X_i be the position of particles labeled "i" ; and let x_0 the position at time $t_0 = 0$ and X_1 the position at time t.

The PDF of the first displacement would have to follow $C_1^S(x,t)$. Thus:

$$X_1(t) = x_{1-2} + N(x_0 - x_{1-2}, 2D_1 t) = x_0 + \sqrt{2D_1 t} N(0,1) \tag{3.3.10}$$

Then, we test if $X_1(t)$ has crossed an interface. If it has, we alter the algorithm as follows :

- The PDF of a fraction$|R_{1-2}|$ of the particles that have crossed the interface would have to follow the distribution C_1^R, and they are reflected.

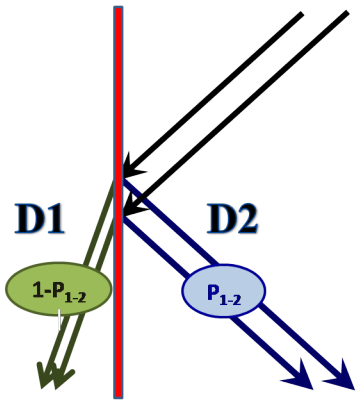

Figure 3.3.5: Partial reflection scheme in a domain with one interface and discontinuous diffusion coefficient. The interface between subdomains (D1,D2) is represented as the yellow band. Particles at the interface are either reflected and stay in the same subdomain, or refracted and cross the interface into the other subdomain.

- The PDF of the remaining fraction $(1 - |R_{1-2}|)$ of the particles that have crossed the interface would have to follow $C_2(x,t)$, and they are refracted.

3.3.4.4 The partial reflection scheme (for the case $R_{1-2} \geq 0$)

The general principle of this partial reflection scheme, so far, is illustrated schematically in Figure 3.3.5, and is similar to the one previously used in literature [Hoteit et al., 2002, Lim, 2006, Bechtold et al., 2011]

The fractions$|R_{1-2}|$ and$(1 - |R_{1-2}|)$ are interpreted as probabilities, and the issue of "negative probabilities" will be tackled later below and in the next section3.3.5.

Thus X_1 becomes :

$$\begin{cases} if \ [\![R_{1-2}]\!] = 1; \quad X_1 = x_{1-2} - N\left(x_0 - x_{1-2}, 2D_1 t\right) \\ if \ [\![R_{1-2}]\!] = 0; \quad X_1 = x_{1-2} + \sqrt{\frac{D_2}{D_1}}\, N\left(x_0 - x_{1-2}, 2D_1 t\right) \end{cases} \tag{3.3.11}$$

where $[\![R_{1-2}]\!]$ designates a Bernoulli RV that is equal to 1 with probability $|R_{1-2}|$ and equal to 0 with probability $(1 - |R_{1-2}|)$, x_0 is the initial particle

position $X(0)$, and x_{1-2} is the interface position.

Using Eq.3.3.10, Eq.3.3.11 becomes :

$$\begin{cases} if \ [\![R_{1-2}]\!] = 1; \quad X_1 = 2x_{1-2} - X_1 \\ if \ [\![R_{1-2}]\!] = 0; \quad X_1 = x_{1-2} + \sqrt{\frac{D_2}{D_1}} \ (X_1 - x_{1-2}) \end{cases} \tag{3.3.12}$$

Eq.3.3.12 could also be written as follows

$$X_1 = (1 - [\![R_{1-2}]\!]) \left(x_{1-2} + \sqrt{\frac{D_2}{D_1}} \ (X_1 - x_{1-2}) \right) + [\![R_{1-2}]\!] \left(x_{1-2} - (X_1 - x_{1-2}) \right) \tag{3.3.13}$$

And using Gaussian RV properties Eq.3.3.13 becomes

$$X_1 = x_{1-2} + (X_1 - x_{1-2}) \left(- [\![R_{1-2}]\!] + \sqrt{\frac{D_2}{D_1}} \ (1 - [\![R_{1-2}]\!]) \right) \tag{3.3.14}$$

However, until now we have considered only the absolute value of R_{1-2}. Thus, the previous algorithm is sufficient in cases where R_{1-2} is positive. And the final solution of the problem would be equivalent to the PDF of all the particles.

A negative R_{1-2} means that there was a subtraction in the analytical solution. Yet, subtractions at specific positions are more difficult to model in RWPT than additions (adding particles). The next subsections will discuss three new methods to deal with the case where R_{1-2} is negative.

3.3.4.5 Reflection/Refraction method for $R_{1-2} < 0$ with restrictions on the time step

Here we propose, in the case $R_{1-2} < 0$, to use the value of R_{1-2} instead of the Bernoulli RV $[\![R_{1-2}]\!]$ in Eq.3.3.14. Replacing the Bernoulli RV $[\![R_{1-2}]\!]$ by the value of R_{1-2} can be seen as some form of averaging, hence this method requires several steps to converge toward the solution (restrictions on time step).

Eq.3.3.14 becomes similar to a refraction (transmission) algorithm with no reflections.

$$X_1 = x_{1-2} + (X_1 - x_{1-2})\, T_{1-2} \tag{3.3.15}$$

with the Refraction/Transmission coefficient T_{1-2} :

$$T_{1-2} = -R_{1-2} + \sqrt{\frac{D_2}{D_1}}\,(1 - R_{1-2}) \tag{3.3.16}$$

T_{1-2} is positive because here $R_{1-2} < 0$.

This method is similar to the one used by Bechtold [Bechtold et al., 2011], it is a one sided partial reflection method. The difference between the two, is that Bechtold's coefficients are based on analytical solutions of equilibrium problems (concentration constant in a steady-state bounded discontinuous domain with two zero flux BC's). While the method proposed here, is based on the solution of the initial value problem in a discontinuous domain.

3.3.5 Three alternative schemes for negative reflection coefficient R_{1-2} with no restrictions on the time step

Seeing that R_{1-2} is the amplitude of C_1^R (representing reflected particles), and $(1 - R_{1-2})$ is the amplitude of C_2(refracted particles), one could expect that the partial reflection method would take R_{1-2} as its reflection probability threshold. But, this is not the case in most literature[Hoteit et al., 2002, Lim, 2006, Bechtold et al., 2011]. The reason why all previously reviewed methods did not take R_{1-2} as the reflection probability, is because of difficulties with the case $R_{1-2} < 0$. In that case, it does not make sense to define a negative coefficient as the reflection coefficient. Hence, to circumvent this problem, [Hoteit et al., 2002] chose a reflection coefficient $R_{1-2}^{Hoteit} = \frac{\sqrt{D_1}}{\sqrt{D_1}+\sqrt{D_2}}$, later generalized by [Lim, 2006] into $R_{1-2}^{Lim} = \frac{\theta_1\sqrt{D_1}}{\theta_1\sqrt{D_1}+\theta_2\sqrt{D_2}}$. [Bechtold et al., 2011], proposed a one sided reflection scheme with different positive coefficients. However, both schemes(Lim's and Bechtold's) need to converge toward the true

solution that uses the reflection coefficient R_{1-2}. Therefore, these methods have restrictions on the time step, which needs to be small in order to reduce the error and converge toward the solution [Ackerer & Mose, 2000]. On the other hand, small time steps make particles undergo multiple reflections, going back and forth through the interface many times. Yet, each reflection causes a numerical error [Bechtold et al., 2011]. The next subsections describe new algorithms proposed for particles that cross through an interface with R_{1-2} negative, complementary to the previous subsection 3.3.4.4 which discusses the case where R_{1-2} is positive.

3.3.5.1 Homing particles

We have previously stated that C_1^R represents the PDF of reflected particles, and C_2 of refracted ones. When R_{1-2} is negative, C_1^R is negative too, and the coefficient $(1 - R_{1-2})$ of C_2 is greater than one. We propose here that each particle reflected searches for the nearest particle to it, and takes it with it to the position as if it was refracted (see Figure 3.3.6). This algorithm models what happens when R_{1-2} is negative. This will allow us to have the final solution with no restriction on the time step, and the possibility to take the time step equal to the final simulation time for more efficiency.

3.3.5.2 Adaptive mass variation including negative as well as positive masses

Introduction to the concept of negative mass The concept of negative mass was first considered when Paul Dirac [Dirac, 1928] introduced his theory of elementary particles, where he included negative mass solutions. It was later formalized by Joaquin Luttinger in his research about gravity. He considered the existence of negative mass particles, and how they would behave under gravity and other forces[Luttinger, 1951].

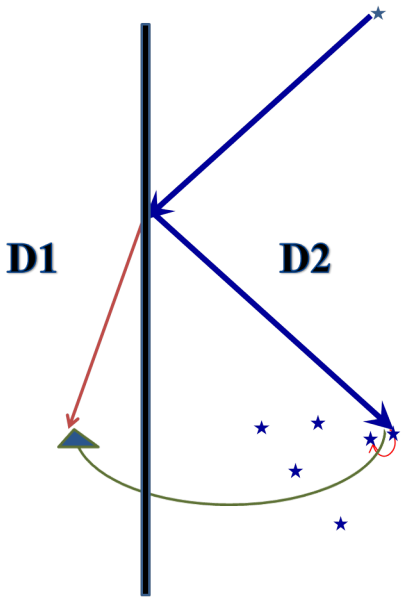

Figure 3.3.6: Homing particles scheme, in a domain with one interface between subdomains (D2<D1), it is represented here as a black band. Particle's algorithm of displacement represented here is initially in D2. When it is reflected by the interface, it searches for the nearest particle to it (red arrow), and takes it with it to the position as if it was refracted (green arrow).

More recently, Washington State University physicists have created (2017 Phys. Rev. Lett) a fluid with effective negative mass[Khamehchi et al., 2017]. The dynamic behavior of the fluid seems to be explainable as if the effective mass were negative. In addition, some theories, in quantum mechanics, are being investigated concerning the spontaneous appearance (in vacuum) of pairs of particles/antiparticles[Peskin & Schroeder, 1995].

We were inspired for this algorithm by this 2017 discovery.

In this chapter, we will be using the same concept of particles with negative mass to do more efficient and accurate predictions of diffusion in heterogeneous and discontinuous media (see Introduction section3.1).

The concept of particles with negative mass may seem absurd at first sight. In this chapter we are not discussing their real physical existence, but we will

be using the concept of particles with negative mass to solve a problem that has always been avoided to deal with a negative reflection probability.

Adaptive mass particles for R<0 For a negative R_{1-2}, the adaptive mass algorithm for the particle may lead to a particle having a different mass than the unit mass initially prescribed for all particles. The modified particle mass may be either positive or negative. The algorithm is as follows.

Each time a particle is reflected, we multiply its mass by (-1). $|R_{1-2}|$ of the particles are reflected and their mass is multiplied by $sign\,(R_{1-2})$. Thus the PDF of the reflected particles would model C_1^R which has an amplitude of R_{1-2}.

On the other hand, we know that $1-|R_{1-2}|$ are refracted, while the amplitude of C_2 is $1+|R_{1-2}|$. Thus, if a particle is refracted, we multiply its mass by $\dfrac{1+|R_{1-2}|}{1-|R_{1-2}|}$(see Figure 3.3.7).

This allow us to model C_2 with the remaining refracted particles. This algorithm gives the correct solution at every time step. Hence, the possibility to put the time step equal to the final simulation time. And the precision of the solution, in terms of the concentration field, depends solely on the number of particles.

3.3.5.3 Negative unit mass particles

Again for the case of negative R, we propose the following algorithm. Particles are always refracted. In addition, in $|R_{1-2}|\,\%$ of the cases, two particles are created : one refracted and has the same mass as the original particle, and the other is reflected with a mass of opposite sign (see Figure 3.3.8). Such algorithm allows us to model the true solution. These new particles, in a way, look like virtual particles in vacuum polarization [Dirac, 1934] in quantum field theory. (Two opposite charge theoretical particles that pop up(spontaneous produc-

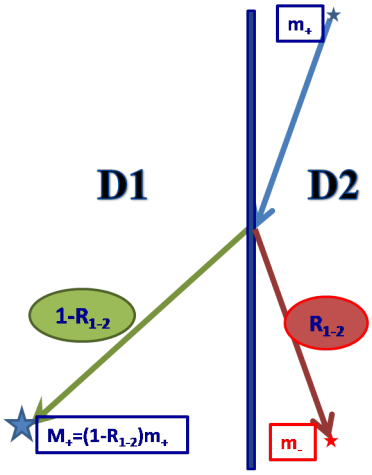

Figure 3.3.7: Adaptive mass variation scheme in a domain with discontinuous diffusion coefficient (D2<D1). When a positive particle is reflected at the interface (with probability ($|R_{1-2}|$)), its mass is multiplied by (-1) and becomes negative. If it is refracted (with probability ($1-|R_{1-2}|$)), its mass is multiplied by the positive factor $(1+|R_{1-2}|)/(1-|R_{1-2}|)$.

tion) in a vacuum, these pseudo particles allow very accurate calculations of atomic parameters). Here particles are either positive or negative with a unit absolute value.

3.3.6 Multiple interfaces

3.3.6.1 Semi-analytical solution for a pure diffusion problem with $N \geq 2$ interfaces (discontinuities)

After crossing one interface, a particle could eventually cross a second interface. The algorithm should be able to deal with any number of interfaces crossed by a given particle, in a single time step. To obtain the RWPT algorithm that deals with multiple interfaces, let us first generalize the solution Eq.3.2.19 of the problem Eq.3.2.18 for N-interfaces and (N+1) layers. The generalization

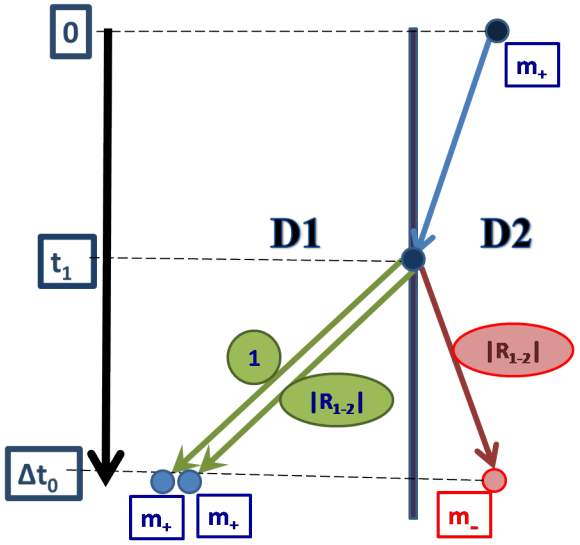

Figure 3.3.8: Partial reflection scheme for pseudo-particles, for a domain with discontinuous diffusion and porosity (e.g., here, $D_2 < D_1$). Each given particle arriving at the interface with negative R_{1-2} is refracted with probability 1. In addition, two particles with opposite masses pop up into existence with $|R_{1-2}|$ probability.

of Eq.3.2.18 for $i\epsilon\left[\!\left[1;N+1\right]\!\right]$ is:

$$\forall t>0;\forall x\epsilon\Omega_i;\frac{\partial\left(\theta_i C_i\right)}{\partial t}=\frac{\partial}{\partial x}\left(\theta_i D_i\frac{\partial C_i}{\partial x}\right) \tag{3.3.17a}$$

$$\begin{cases}\forall t\geq 0; & \lim\limits_{x\to-\infty} C_1\left(x,t\right)=0\\ \forall t\geq 0; & \lim\limits_{x\to+\infty} C_{N+1}\left(x,t\right)=0\end{cases} \tag{3.3.17b}$$

$$\begin{cases}\forall t\geq 0;\forall i\epsilon\left[\!\left[1;N\right]\!\right] & C_i\left(x_{i,i+1},t\right)=C_{i+1}\left(x_{i,i+1},t\right)\\ \forall t\geq 0;\forall i\epsilon\left[\!\left[1;N\right]\!\right] & -\theta_i D_i\frac{\partial C_i}{\partial x}\left(x_{i,i+1},t\right)=-\theta_{i+1}D_{i+1}\frac{\partial C_{i+1}}{\partial x}\left(x_{i,i+1},t\right)\end{cases} \tag{3.3.17c}$$

$$\forall x\epsilon\Omega_i;C_i\left(x,0\right)=\frac{M_0}{\theta_i}\delta\left(x-x_0\right) \tag{3.3.17d}$$

Since, the solution Eq.3.2.19 is composed of three Gaussian's, one of which $(C_1^S\left(x,t\right))$ is the solution of a pure diffusive problem. While the other two depend on the previous Gaussian and the position of the interface. Hence, we

could consider that each time a Gaussian function, in the solution, encounters a discontinuity, this Gaussian is considered as if it was a separate problem with one discontinuity. Therefore, each time a Gaussian faces one new discontinuity, we create two new Gaussian's with parameters chosen to fit the solution.

Let us define two linear operators L_{ij} and L^*_{ij}:

$$L_{ij}\left(G\left(x_0, 2D_i t, x\right)\right) = R_{ij} G\left(2x_{i-j} - x_0, 2D_i t, x\right) \tag{3.3.18}$$

$$L^*_{ij}\left(G\left(x_0, 2D_i t, x\right)\right) = \left(1 - R_{ij}\right) G\left(x_{ij} + \sqrt{\frac{D_j}{D_i}}\left(x_0 - x_{i-j}\right), 2D_j t, x\right) \tag{3.3.19}$$

Thus the solution Eq.3.2.20 could be written as follows:

$$\begin{cases} \forall t > 0; \forall x \leq x_{1-2}; \quad C_1\left(x,t\right) = C_1^S\left(x,t\right) + L_{12}\left(C_1^S\left(x,t\right)\right) \\ \forall t > 0; \forall x \geq x_{1-2}; \quad C_2\left(x,t\right) = L^*_{12}\left(C_1^S\left(x,t\right)\right) \end{cases} \tag{3.3.20}$$

The decomposition (Eq.3.3.20) can be further generalized: for each individual interface, new gaussians are generated, with parameters chosen to fit the solution. Hence, each time a gaussian function g initially in a subdomain (i) encounters an interface at position x_{i-j}, we add $L_{i,j}\left(g\right)$ to the solution in subdomain (i) and $L^*_{i,j}\left(g\right)$ to the solution in subdomain (j). See Algorithm 3.1.

For the two-interface problem ($N = 2$), the previous algorithm leads to an analytical solution for diffusion with an initial source, with discontinuous diffusion coefficients and porosities having three different values (three layers) . Thus the analytical solution for a source located at the position x_0 in subdomain $(i = 1)$, $\forall t \geq 0$:

$$\begin{cases} \forall x \leq x_{1;2}; & \frac{\theta_1}{M_0} C_1\left(x,t\right) = id + L_{12} + \sum\limits_{i=0}^{+\infty} L^*_{21}\left(L_{23}L_{21}\right)^i L_{23} L^*_{12} \\ \forall x_{1;2} \leq x \leq x_{2;3}; & \frac{\theta_2}{M_0} C_2\left(x,t\right) = \sum\limits_{i=0}^{+\infty}\left(id + L_{23}\right)\left(L_{21}L_{23}\right)^i L^*_{12} \\ \forall x \geq x_{2;3}; & \frac{\theta_3}{M_0} C_3\left(x,t\right) = L^*_{23} \sum\limits_{i=0}^{+\infty}\left(L_{21}L_{23}\right)^i L^*_{12} \end{cases} \tag{3.3.21}$$

Algorithm 3.1 Semi-analytical solution for diffusion with $N \geq 2$ interfaces

1. C_k concentration in subdomain k
2. Initialize $Ci_k = C_S$ with C_S the solution of a diffusion problem with no discontinuity.
3. $u_k = \pm 1$ the direction towards the interfaces limiting subdomain (k).
4. **while** (C_k) not converged **do**
   a) $C_k = C_k + L_{k,k+u_k}(Ci_k)$ and $C_{k+u_k} = C_{k+u_k} + L^*_{k,k+u_k}\left(C^i_k\right)$
   b) $u_{k+u_k} = u_k$ and $u_k = -u_k$
   c) $Ci_k = L_{k,k+u_k}(Ci_k)$ and $Ci_{k+u_k} = Ci_{k+u_k} + L^*_{k,k+u_k}(Ci_k)$
5. **end**

with the right side of Eq.3.3.21 is applied to $G(x_0, 2D_1t, x)$.

The analytical solution for a source located at the position x_0 in subdomain $(i = 2)$, $\forall t \geq 0$:

$$\begin{cases} \forall x \leq x_{1;2}; & \frac{\theta_1}{M_0} C_1(x,t) = L^*_{21} \sum_{i=0}^{+\infty} (L_{23}L_{21})^i (id + L_{23}) \\ \forall x_{1;2} \leq x \leq x_{2;3}; & \frac{\theta_2}{M_0} C_2(x,t) = \sum_{i=0}^{+\infty} (id + L_{21})(L_{23}L_{21})^i (id + L_{23}) \\ \forall x \geq x_{2;3}; & \frac{\theta_3}{M_0} C_3(x,t) = L^*_{23} \sum_{i=0}^{+\infty} (L_{21}L_{23})^i (id + L_{21}) \end{cases} \tag{3.3.22}$$

with the right side of Eq.3.3.21 is applied to $G(x_0, 2D_2t, x)$.

This solution is detailed in B.1, and it has been verified by substitution into the governing PDE's.

3.3.6.2 Generalization of the RWPT algorithm for $N \geq 2$ interfaces

The same idea of generalization of the analytical solution in subsection 3.3.6.1 (from one interface into a multi-interface) has been applied to the RWPT method for a problem with N interfaces. If a particle crosses an interface, then (step 1) its position is altered according to previous algorithms that deal with discontinuities (see subsection 3.3.4, Eq.3.3.11 for $R \geq 0$ and Eq.3.3.12

Algorithm 3.2 RWPT algorithm for $N \geq 2$ interfaces

- Consider particle (k) with mass m_k and position X_k.
- **while** particle (k) crosses interfaces **do**
  - **If** $R_{1,2} \geq 0$ **then**
    1. **If** $[\![R_{1,2}]\!] = 0$; **then** the particle (k) is $refracted$ to the position X_k^{Rr} as in Eq.3.3.11 **endif**
    2. **If** $[\![R_{1,2}]\!] = 1$; **then** the particle (k) is $reflected$ to the position X_k^{Rl} as in Eq.3.3.11 **endif**
  - **Else** (case $R_{1,2} < 0$)
    1. The particle (k) is $refracted$ to the position X_k^{Rr}.
    * **If** $[\![R_{1,2}]\!] = 1$; **then** Create two particles "1" and "2":
      1. with mass m_k and at the $refracted$ position X_k^{Rr}.
      2. with mass $-m_k$ and at the $reflected$ position X_k^{Rl}.
    * **endif**
  - **end**
- **end**

for $R < 0$). After this (step 2), if the new particle position does not belong to its initial subdomain, nor to the adjacent subdomains, then go back to "step 1". Thereafter, the particle continues undergoing this algorithm within a conditional loop, until the particle does not cross an interface (it then reaches its final position within the loop). See Algorithm 3.2 (Negative particles algorithm).

This algorithm will be tested in section 3.4, with the analytical solution defined in subsection 3.2.3. Then, it will be compared with a generalized analytical solution for a pure diffusion problem with two interfaces and three different diffusion coefficients and water contents: the detailed analytical solution for this 3-layer case is presented in Eq.3.3.21. And finally, it will be validated with an even more generalized semi-analytical solution which algorithm has been detailed in the previous subsection 3.3.6.1.

3.3.7 Post processing: from particles to concentrations

Post-processing in Random Walk method is very essential since the primary objective of the simulation is to get the concentration (temperature or pressure) field. A special attention should be given to Negative unit mass and Adaptive mass particle methods in particular, since they are very different from the classical Random Walk simulation. Here the mass conservation is still maintained, since each time we create negative mass, we create also positive one.

The concentration is determined from distribution of particle positions X_t weighted by their respective masses. $dm_t = C(X_t, t)\, dX_t$. This can be expressed formally as[4] :

$$C(x,t) = \int_{\mathbb{R}} C(X_t, t)\, \delta(X_t - x)\, dX_t \tag{3.3.23}$$

$$C(x,t) = \int_{\mathbb{R}} \delta(X_t - x)\, dm_t \tag{3.3.24}$$

There are mainly three types of methods to obtain a spatial distribution of concentration $C(\mathbf{x}, t)$ from particle positions :

1. The most basic one is Fixed windows method. The domain is meshed, and the concentration is simply calculated by summing the masses of the particles in each cell and dividing it by the size of the cell. It is basically a histogram method. Note here that if the cells are very small, then some cells may not contain any particle or worse they could contain negative mass particles, thus the concentration would be negative in those cells. That is why, the size of the concentration cells should be less refined if adaptive or negative mass particles exist. Even without negative masses, the size of the concentration cells should be selected in consideration of the number of particles and the domain size (or the difference between

[4]More precisely, in a given domain Ω, the local concentration $C(\mathbf{x}, t)$ is related to the PDF of particle positions$f_{X_t}(\mathbf{x}; t)$ by $C(\mathbf{x}, t) = M_\Omega(t)\, f_{X_t}(\mathbf{x}; t)$ where $M_\Omega(t)$ is the total mass of the particles inside the domain Ω at time t

the maximum and minimum particles positions). This has been studied mathematically for instance by Raviart [Raviart, 1983].

2. The second method is the Mobile window method. It consists in : (i) Moving a window across the domain; (ii) Putting the center of the cell at the position where we want to calculate the concentration; (iii) Summing the masses of the particles in this cell and divide it by the size of the cell. This method, gives more freedom to the user to calculate the concentration at whatever position he chooses, compared to simple meshed methods.

3. The third method is called Convoluted filter method. Particle contributions to the local concentration are described by Gaussian-type windows centered on particles positions. The concentration at (x,y,z) is then obtained by summing the contribution of each particle on that point.

In this study we have used the first post-processing method the Fixed windows method.

3.4 Results and discussion

In this section, we present test results for the three main particle schemes presented earlier for diffusion problems with discontinuous diffusion coefficient and porosity. The results are presented in terms of concentration profiles (histograms) computed from particle positions using the fixed window method (see subsection 3.3.7). Then, they will be compared with the generalized analytical solution, for a diffusion problem with two interfaces and three different discontinuous diffusion coefficients and porosities, as described in subsection 3.3.6.1.

x	$]-\infty;0]$	$[0;100]$	$[100;+\infty[$
D	1	10^2	10^1
θ	10^{-2}	1	10^{-1}

Table 3.1: Diffusion and porosity contrasts of Figure 3.4.3

3.4.1 Concentration profiles

Figure 3.4.1 shows the results of diffusion of an initial source in a discontinuous domain. Unlike the following methods, the method used here (Reflection/Refraction) have restrictions on the time step. Therefore, although the method converges towards the analytical solution, this proposed method was abandoned, because of its restrictions, in favor of the following methods with no restrictions on the time step.

In Figure 3.4.2, we simulate a diffusion problem for an initial source located in the sub-domain with the lowest diffusion coefficient (left sub-domain). This corresponds to the complex configuration with negative R_{1-2}), as seen in subsection 3.3.5. The algorithm here uses Homing Particles. The particle positions were obtained here by setting the time step equal to the final simulation time, for more efficiency (minimizing calculation time).

The figure shows the final concentration profile as a histogram, computed from particle positions using the fixed window method (cf. section3.3.7): concentrations are obtained in each histogram box, by dividing the mass of all particles contained in that box, by the total pore volume of that box.

We note that histogram fluctuations in sub-domain 1 (left, with lowest porosity) are due to the fact that particles in regions with low porosity represent higher concentrations than in regions with higher porosity. Thus, the concentration in low porosity regions has more fluctuations because of fewer particles for same level of concentration.

Note in all tables, the coefficient D is dimensionless, as well as space and

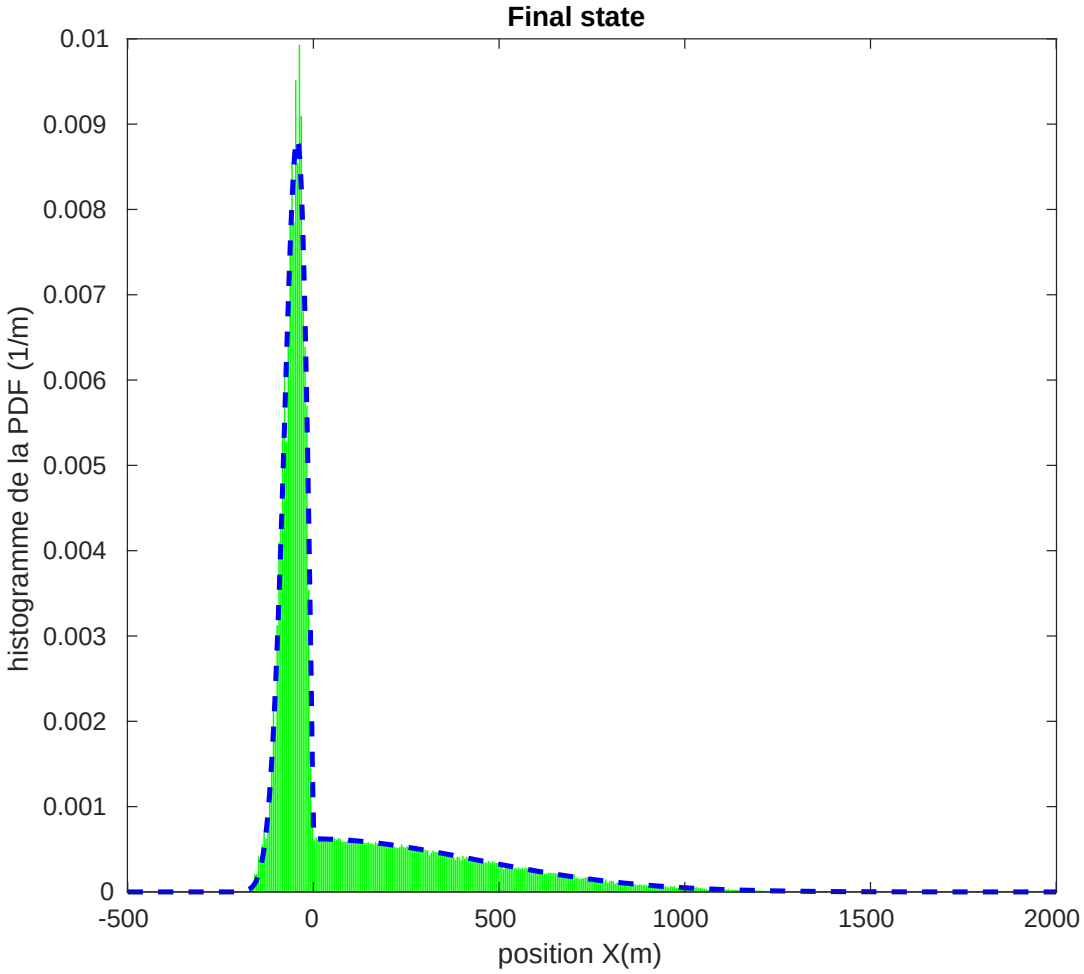

Figure 3.4.1: Comparison between analytical (PDE) and numerical (RWPT) concentration histogram using Reflection/Refraction particles, for a 1D infinite domain with an initial Dirac mass at $x_0 = -1$ ("source"). The diffusion coefficient $D(x)$ and porosity $\theta(x)$ are discontinuous. The dashed blue bold curve is the analytical solution of the diffusion PDE, Eq.3.2.19. The slightly fluctuating histogram is the result obtained by the RWPT with 100,000 particles. The diffusion contrast is $D_2/D_1 = 100$ and the porosity contrast $\theta_2/\theta_1 = 100$.

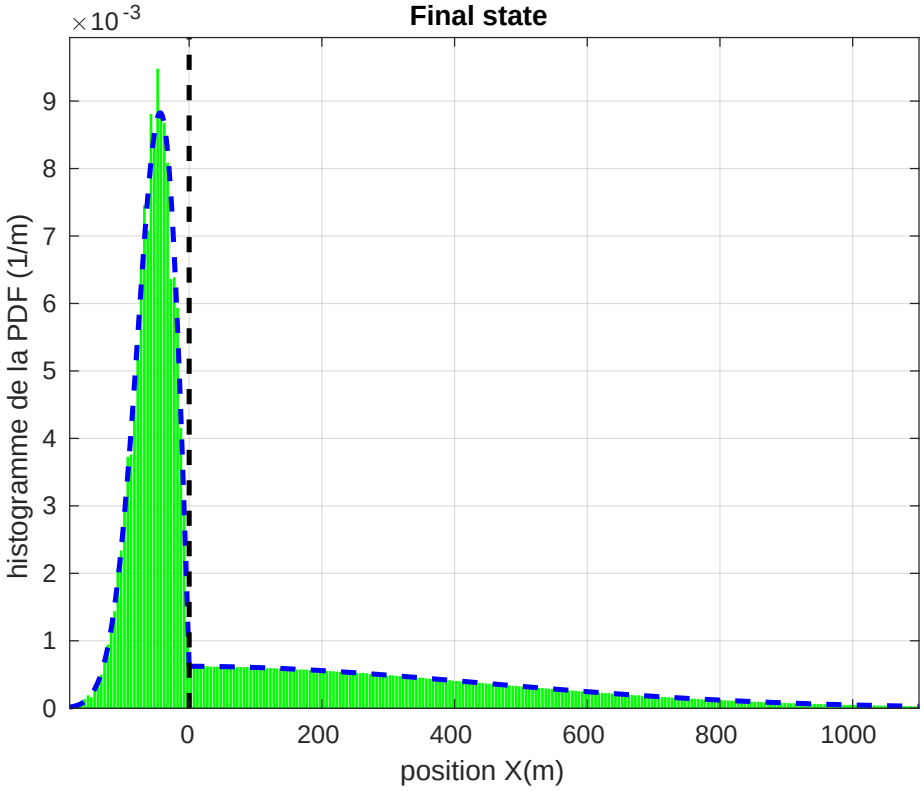

Figure 3.4.2: Comparison between analytical (PDE) and numerical (RWPT) concentration histogram using Homing particles, for a 1D infinite domain with an initial Dirac mass at $x_0 = -1$ ("source"). The diffusion coefficient $D(x)$ is discontinuous at $x = 0$ (black dashed line). The dashed bold curve is the analytical solution of the diffusion PDE, Eq.3.2.19. The slightly fluctuating histogram is the result obtained by the RWPT with one million initial particles. The diffusion contrast is $D_2/D_1 = 100$ and the porosity contrast $\theta_2/\theta_1 = 100$.

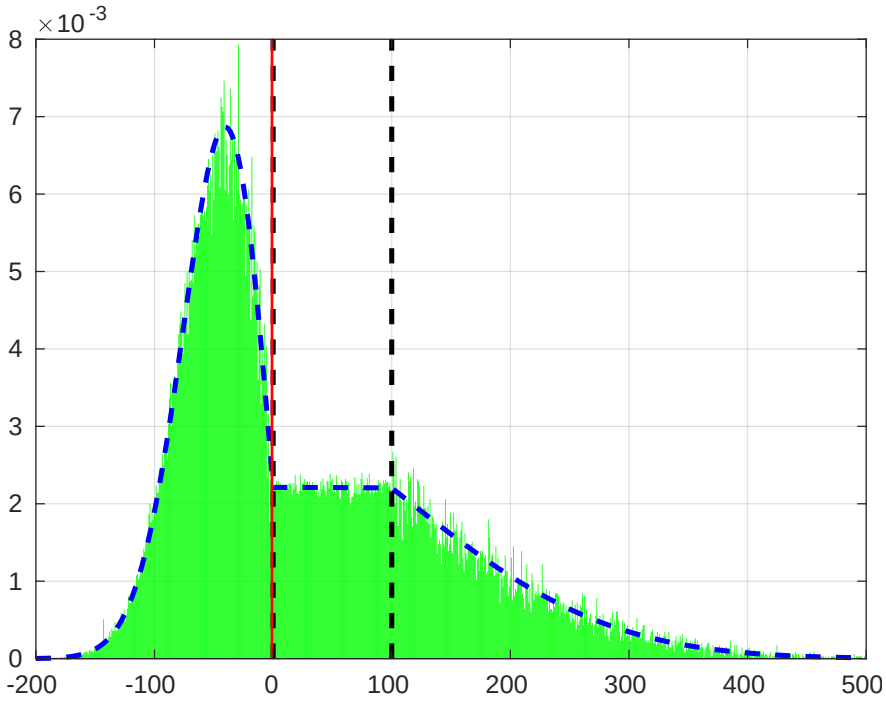

Figure 3.4.3: Comparison between analytical (PDE) (See Appendix) and numerical (RWPT) concentration histogram using Adaptive mass particles, for a 1D infinite domain problem with an initial Dirac mass at $x_0 = -1$ ("source" red line). The diffusion coefficient $D(x)$ is discontinuous at $x_{1-2} = 0$ and $x_{2-3} = 100$ (black dashed line). The dashed bold curve is the analytical solution of the diffusion (PDE) in the appendixB.1. The slightly fluctuating histogram is the result obtained by the RWPT with one hundred million initial particles. The diffusion and porosity contrasts are given in Table 3.1. This result was obtained by setting the time step equal to the final simulation time, for more efficiency and minimum calculation time.

x	$]-\infty;-300]$	$[-300;-100]$	$[-100;100]$	$[100;300]$	$[300;+\infty[$
D	1	10^5	1	10^5	1
θ	10^{-1}	1	10^{-1}	1	10^{-1}

Table 3.2: Diffusion and porosity contrasts of Figure 3.4.4

time units.

In Adaptive mass particles algorithm, some particles may have more mass than others, and some could have also a negative mass. This dispersion of particles masses in addition to the difference in porosities, explain the fluctuations seen in the histogram in Figure 3.4.3. On the other hand, these fluctuations could be smoothed when using a different post-processing method instead of the fixed window. Overall, the histogram obtained still follows the shape of the analytical solution, while using one single macro time step.

In Figure 3.4.4, the histogram is the result obtained by the RWPT with ten million particles initially. The diffusion and porosity contrasts are given in Table 3.2. This result was obtained by setting the time step equal to the final simulation time, for more efficiency. Such fluctuations are inherent to the RWPT method for a finite number of particles, but they appear quite moderate here given the large contrast ratio of the discontinuous coefficients (10/1 for porosity, and 100,000/1 for diffusion).

3.4.2 Time evolution of concentration profiles

Figure 3.4.5 and Figure 3.4.6 display the analytical vs. simulation results, at three times, of diffusion with one interface and two interfaces (where $D(x)$ and $\theta(x)$ are discontinuous). Figure 3.4.5 has diffusion contrast $D_2/D_1 = 100$ and porosity contrast $\theta_2/\theta_1 = 4$. The values of diffusion and porosity for Figure 3.4.6 are shown in Table 3.3. The initial source is at $x = -1$; it is located in the left subdomain with the lowest diffusion and porosity coefficients. Thus, in

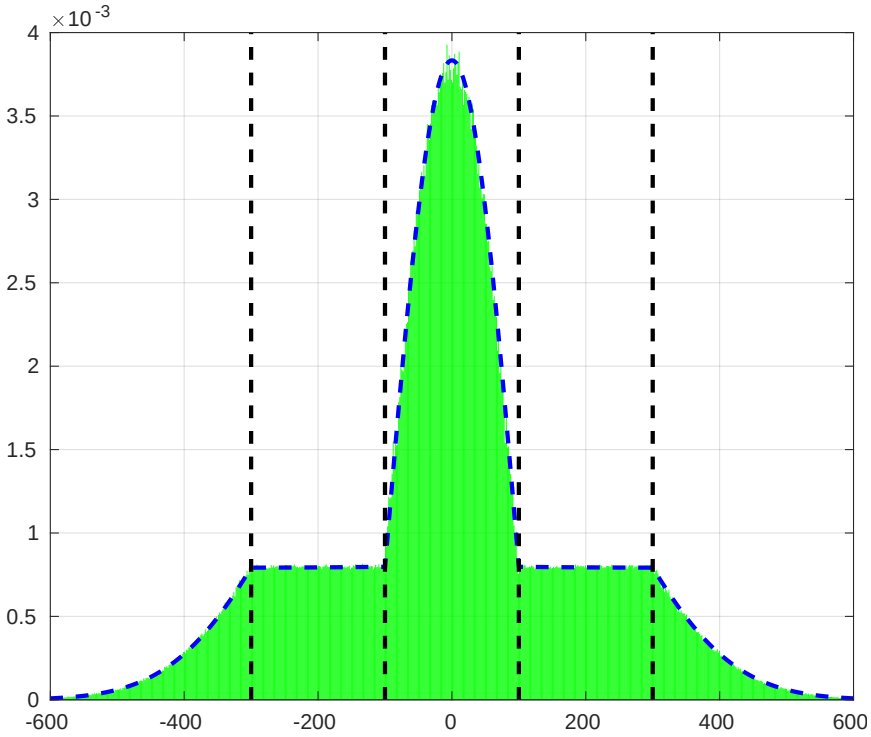

Figure 3.4.4: Comparison between analytical (PDE) and numerical (RWPT) concentration histogram using negative particles, for a 1D infinite domain with an initial Dirac mass at $x_0 = 0$ ("source"). The diffusion and the porosity coefficients $D(x)$ and $\theta(x)$ are discontinuous at the black dashed lines (see Table 3.2). The dashed blue curve is the semi-analytical solution of the diffusion (See subsection 3.3.6.1). The histogram is the result obtained by the RWPT with ten million initial particles. The diffusion and porosity contrasts are given in Table 3.2. This result was obtained by setting the time step equal to the final simulation time, for more efficiency and minimum calculation time.

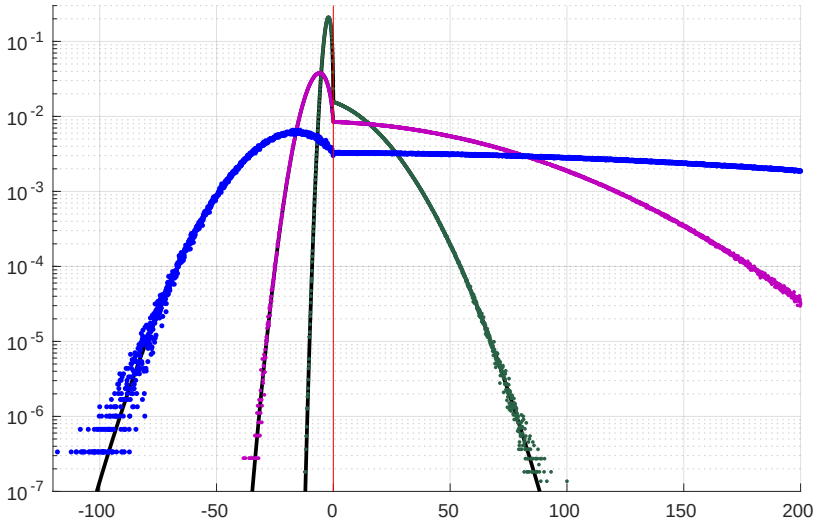

Figure 3.4.5: Time evolution of concentration profiles using the negative mass algorithm. The vertical red line corresponds to the position of the interface $x = 0$. The green, magenta and blue bold dots correspond to the simulation results at times t_1, t_2 and t_3 respectively. The bold black curves correspond to the analytical solution of Eq.3.2.20.

x	$]-\infty;0]$	$[0;100]$	$[100;+\infty[$
D	1	10^2	10^1
θ	0.25	1.00	0.50

Table 3.3: Diffusion and porosity values of Figure 3.4.6

both figures, particles initially encounter an interface with negative reflection coefficient R. Particles are either reflected at the interfaces and stay in the subdomain, or they cross the interface and enter the next subdomain. The simulation results were obtained by using 100 million particles and setting the time step equal to final simulation time ($\Delta t = T_f$). The fit is excellent in all cases, including near discontinuities.

Figure 3.4.7 is the result of a pure diffusion problem with two interfaces (where $D(x)$ and $\theta(x)$ are discontinuous see Table 3.4) at three different times $t_3 = 2t_2 = 10t_1$. The initial source is at $x = 0$, in the subdomain in the

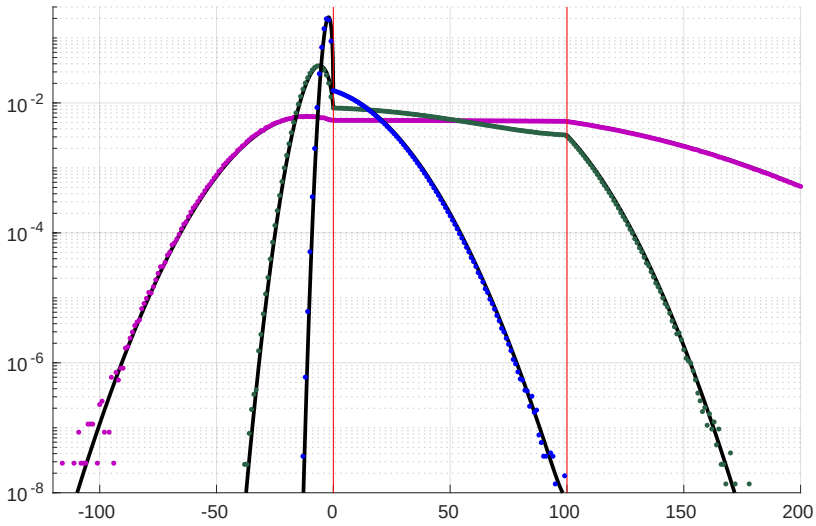

Figure 3.4.6: Time evolution of concentration profiles using the Stop&Go algorithm with negative mass particles for 100 million particles. The red vertical lines correspond to the interfaces $x = 0$ and $x = 100$. The green, magenta and blue bold dots correspond to the simulation results at times t_1, t_2, t_3. The bold black curves correspond to the semi-analytical solution of subsection 3.3.6.1.

x	$]-\infty;-100]$	$[-100;100]$	$[100;+\infty[$
D	10	1	10^2
θ	5.10^{-1}	$2,5.1$	1.00

Table 3.4: Diffusion and porosity contrasts of Figure 3.4.7

center and with the lowest diffusion and porosity coefficients. Thus, in this configuration, where we set the time step equal to the final simulation time, particles only encounters interfaces with a negative reflection coefficient R. Particles are either reflected at the interfaces and stay in the subdomain, or they cross the interface and enter the next subdomain which is semi-infinite here. This result was obtained by using 100 million particles.

Figure 3.4.8 is the result of a pure diffusion problem with two interfaces (where $D(x)$ and $\theta(x)$ are discontinuous see Table 3.5) at three different times $t_3 = 10^2 t_2 = 10^4 t_1$. The initial source is at $x = 0$ in the subdomain in the

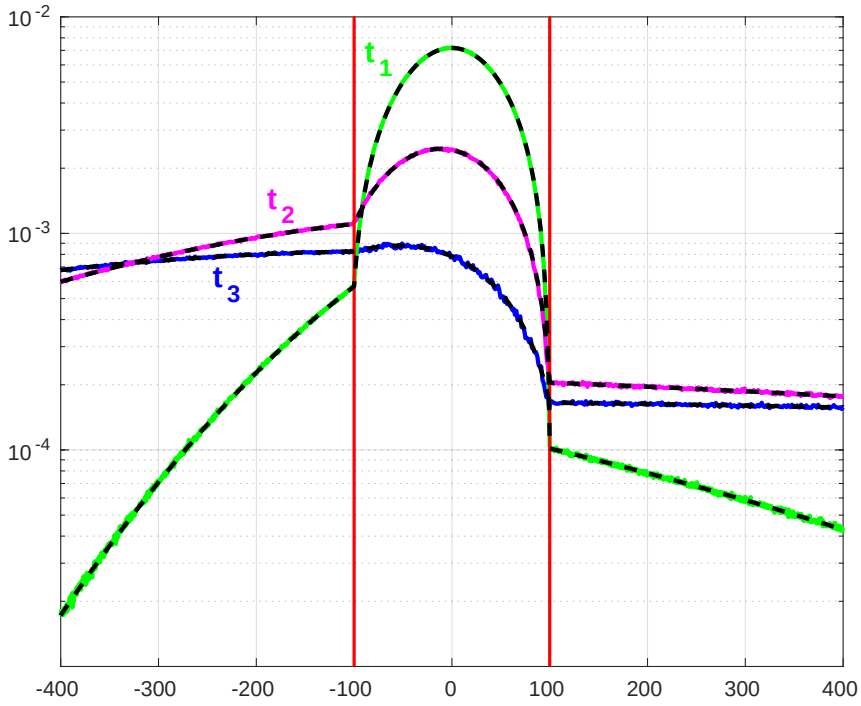

Figure 3.4.7: Time evolution of concentration profiles using Negative unit mass algorithm. The red bold lines correspond to the position of the interfaces $x = -100$ and $x = 100$. The green, magenta and blue bold curves correspond to the result of the simulation of the negative unit mass method at three different times t_1, t_2, t_3 respectively. The dashed black curves correspond to the corresponding semi-analytical solutions described in subsection 3.3.6.1.

x	$]-\infty;-100]$	$[-100;100]$	$[100;+\infty[$
D	1	10^4	10^2
θ	0.25	1.00	0.50

Table 3.5: Diffusion and porosity contrasts of Figure 3.4.8

center and with the highest diffusion and porosity coefficients. Similarly to what have been explained in the paragraph above, particles only encounters interfaces with a positive reflection coefficient R. This result was obtained by using 100 million particles.

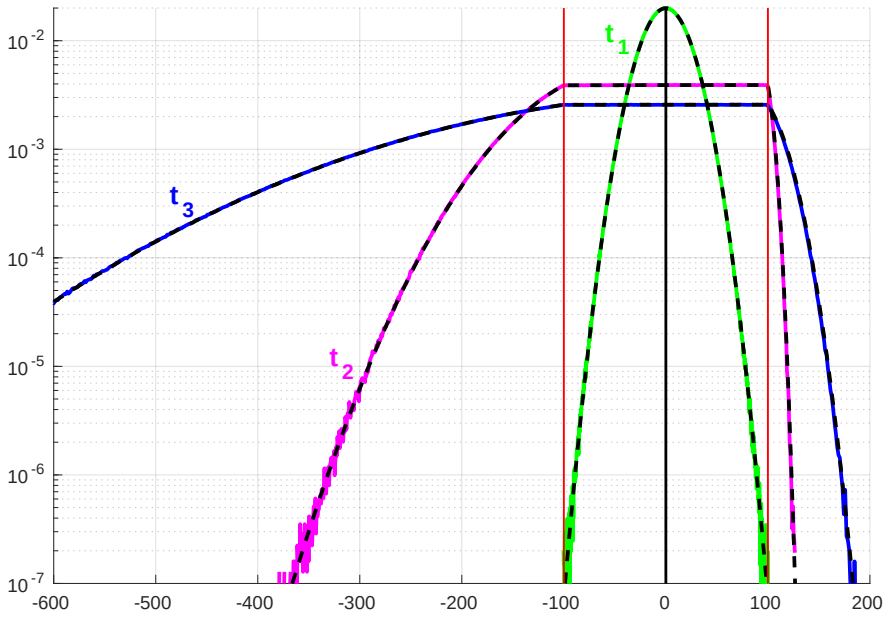

Figure 3.4.8: Time evolution of concentration profiles using the Stop & Go algorithm. The red bold lines correspond to the position of the interfaces $x = -100$ and $x = 100$. The green, magenta and blue bold curves correspond to the result of the simulation of the negative unit mass method at three different times t_1, t_2, t_3 respectively. The dashed black curves correspond to the corresponding semi-analytical solutions described in subsection 3.3.6.1.

3.4.3 Discussion on CPU Time

Explicit time-stepping methods usually have a linear evolution of CPU Time vs. simulation time. We observe from Figure 3.4.9 that the CPU Time of the Stop&Go algorithm behaves as a power law, then reaches a constant plateau in a second stage. In Figure 3.4.9, the magenta curve with squares corresponds to the two-layer problem of Figure 3.4.7, while the blue curve with circles corresponds to the three-layer problem of Figure 3.4.8. For very small simulation time, particles have not yet reached the interface. Therefore, the algorithm does not need to deal with discontinuity, and the CPU Time remains constant. For intermediate simulation time, CPU Time evolves as the power 0.39 of sim-

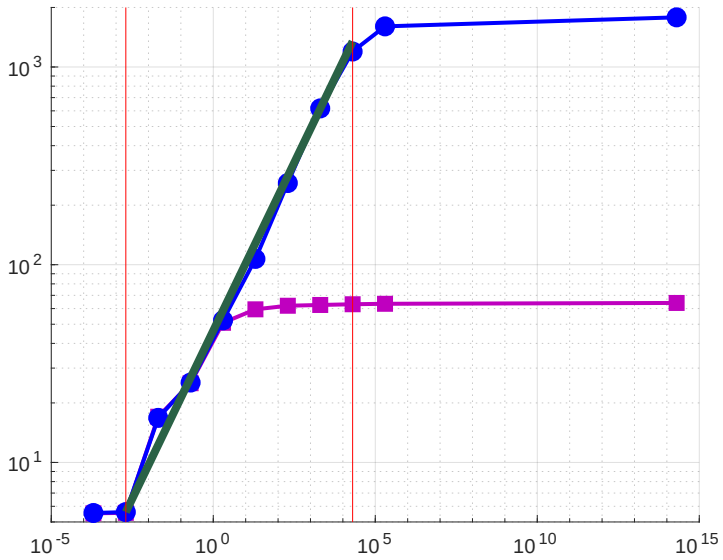

Figure 3.4.9: CPU Time versus Final Simulation Time. The bold blue curve corresponds to the study of Figure 3.4.8, the dashed green line corresponds to the final simulation time power 0.3867.

ulation time T_f (Figure 3.4.9). This exponent depends probably on diffusion and porosity contrasts, number of interfaces, etc. Finally, as can be seen in Figure 3.4.9, CPU Time reaches a plateau for $T_f > 2$ for the two-layer problem, and for $T_f > 2.10^4$ for the three-layer problem.

For larger simulation times, more and more particles succeed in crossing the outer interfaces (after many trials). This is because the transmission probability $(1 - R_{1-2})$, although small, is strictly non null. Once this crossing has occured, particles only need to do a single step to reach their final position at time T_f in the left or right semi-infinite layers. In summary, the computational performance of the negative mass Stop&Go RWPT scheme is encouraging; the CPU time evolves sub-linearly with simulation time, while it evolved linearly in previous RWPT methods.

3.5 Conclusion and perspective

To test the new stop-and-go RWPT schemes, we develop analytical and semi-analytical solutions for diffusion in the presence of multiple interfaces (discontinuous multi-layered medium). The results show that the proposed stop-and-go RWPT schemes (with adaptive, negative, or homing particles) fits extremely well the semi-analytical solutions, even for very high contrasts and in the neighborhood of interfaces. The three schemes provide a correct diffusive solution in only a few macro-time steps, with a precision that depends only on the number of particles, and not on the macro-time step.

The new methods presented in this chapter could be considered as a modified type of "Partial reflection scheme". The idea behind these new algorithms come from the semi-analytical solution of the diffusion of an initial source in an infinite domain, in the presence of many material interfaces where the diffusion coefficient and porosity are discontinuous $D(x)$ and $\theta(x)$ (see Subsection3.3.6.1). With the concept of these exotic particles (Homing, negative unit mass and adaptive mass particles), the scheme converges to the correct solution while keeping computational efficiency and robustness. In that configuration, it leads to the exact diffusion equation instead of approaching it. The method is combined with an asynchronous algorithm that solves the overshoot problem. Several test cases were investigated. For example, we have shown in Subsection 3.4 the solution of the discontinuous diffusion problem at a given time solved in one single time step, taking the time step equal to the final simulation time. This method has been verified analytically, and it is validated in 1D by comparing the concentration profile obtained by the RWPT algorithm with the analytical solution.

The three schemes provide a correct diffusive solution in only a few macro-time steps, with a precision that depends only on the number of particles, and

not on the macro-time step. These schemes seem promising with a view to extensions towards more complex 3D geometries (ongoing work).

The three variant schemes could also be considered in implementing boundary conditions, or in modeling other phenomena like chemical reactions or well production. This gives a new degree of freedom, that could be discussed in another paper in a future study.

Chapter 4

Dirichlet Conditions for Random Walk particle methods for diffusion in discontinuous media

4.1 Introduction

4.1.1 Preamble

This chapter is formatted as a paper to be submitted soon (whence the partial redundancy between this Introduction with the general introduction of the thesis).

4.1.2 Overview

This study develops new Lagrangian particle methods for modeling flow and transport phenomena in finite complex porous media. Particle methods are well known for modeling transport problems [Noetinger et al., 2016]. They reduce or avoid some of the problems of Eulerian methods (e.g. instabilities, excessive diffusion, or oscillations that could lead to negative concentrations). Random Walk algorithms are used to model diffusion processes in the Lagrangian particle approach.

However, discontinuities and heterogeneities are difficult to treat, particularly discontinuous diffusion $D(x)$. The difficulties are different for the Eulerian PDE approach and for the Lagrangian Random Walk approach. In the literature on particle Random Walks, previous methods used to handle this problem could be characterized into two main types: the first one is called "Interpolation technique" [Labolle et al., 1996] which smooths the discontinuity of the parameters, and therefore creates many cells near the interface that smooths it, so that it could be considered as a continuously variable rather than discontinuous coefficient. The second one is called "Partial reflection method", introduced by Uffink [Uffink, 1985]. The discontinuous interface is taken into account by assigning probabilities for particle reflection and transmission across the interface [Ackerer, 1985, Cordes et al., 1991, Hoteit et al., 2002]. One of the main

drawbacks is the decrease in time step size required in order to converge to the expected solution. All these restrictions on the time step, lead to inefficient algorithms.

In this study, we propose a novel approach without any restrictions in the treatment of the particles jump and time step size. Moreover, the algorithm proposed here does not approach the solution but gives a semi-analytical solution with a maximum precision that depends solely on the number of particles. The new method could be considered as a modified type of "Partial reflection method". The idea behind this new algorithm is inspired, from the analytical solution of the diffusion of an initial source in an infinite domain with an interface where the diffusion parameter is discontinuous. With the concept of negative mass particles, it allows to converge to the expected solution while keeping efficiency and robustness. In that configuration, it leads to the exact equation instead of approaching it. The method is combined with an asynchronous algorithm [Lim, 2006] that solves the overshoot problem [Bechtold et al., 2011].

4.1.3 Dirichlet boundary conditions

Dirichlet conditions[1] are difficult to implement in particle methods. Chandrasekhar [Chandrasekhar, 1943] was among the first to study Random Walk inside finite and semi-infinite domains. He introduced absorbing and reflecting barriers in Random Walk methods. Then Feller [Feller, 1957] studied Stochastic Differential Equations using the Method of Images. Uffink [Uffink, 1985] used Feller [Feller, 1957] Method of Images for SDE's to propose a partial reflection method algorithm for RWPT to model discontinuous diffusion.

This chapter discusses four different methods on how to implement Dirichlet BC's with a random walk algorithm. Each has its drawbacks and advantages.

[1] In this chapter, the term Dirichlet conditions is used in relation to both: the PDE problem based on concentration $C(x,t)$, and the corresponding RWPT implementation of such BC's.

The different methods could be used for different problems. The first method is the one used in literature [Delay et al., 2005, Spiller, 2004], it is based on a volume filled with particles that are distributed at a given time. The volume is taken as large as the maximum step that a particle could do during a time step and is refilled every time step. In the second method, method proposed in this Chapter, the volume is taken as large as the maximum displacement that a particle could do during the time of the simulation. The third method is a flux one, where the particles are injected with a predetermined step: particles are injected with a certain distribution.

The methods used to implement Dirichlet conditions in this chapter are mainly for diffusion transport problems. These methods could be applied for a mass transport by diffusion in fluid either in a whole volume or in porous media. Or it could be a heat conduction problem. In this case the particles would represent heat energy and their density would be the temperature. In addition, for some cases, the diffusion transport equation could also be rearranged to model the pressure of a fluid in porous media, and in that case the particles would represent pressure energy and their density would be the pressure of the fluid.

This chapter is organized as follows. Section 4.2, discusses the theory and properties of Gaussian functions, their role as PDF's and CDF's in the characterization of Gaussian Random Variables, and their role as PDE's solutions. Section 4.3 proposes several new RWPT algorithms to model diffusion problems in domains with Dirichlet BC's. Then, results of simulations compared to semi-analytical solutions are presented in section 4.4. Finally, section 4.5 concludes this chapter and gives perspectives.

4.2 Theory

4.2.1 Gaussian PDF's & CDF's

This subsection defines properties and notations of Gaussian PDF's and CDF's that will later be used in this Chapter.

4.2.1.1 Gaussian PDF's

Let us define $x \to G\left(\mu, \sigma^2; x\right)$ which represents a Gaussian function with a mean μ and a variance σ^2. The Probability Density Function PDF of a Gaussian Markovian process is :

$$G\left(\mu, \sigma^2; x\right) = \frac{1}{\sigma\sqrt{2\pi}} exp\left(-\frac{1}{2}\left(\frac{x-\mu}{\sigma}\right)^2\right) \tag{4.2.1}$$

A Gaussian random variable (RV) with a mean μ and a variance σ^2, which means it has the probability density function (PDF) $x \to G\left(\mu, \sigma^2; x\right)$, is : $N\left(\mu, \sigma^2\right)$. The normal centered PDF is defined as the PDF of a Gaussian Markovian process with a mean $\mu = 0$ and a variance $\sigma^2 = 1$, so the normal centered PDF is $x \to G\left(0, 1; x\right)$.

$\delta\left(x\right)$ represents the Dirac pseudo-function (δ distribution) defined by Schwartz [Schwartz, 1951]; it can be defined via test functions; and it can also be defined in a certain sense as the limit of a Gaussian PDF as the standard deviation σ goes to zero:

$$\forall x \epsilon \mathbb{R}^n; \delta\left(x\right) = \lim_{\sigma \to 0^+} G\left(0, \sigma^2; x\right) \tag{4.2.2}$$

4.2.1.2 Gaussian CDFs

Let us also define the Cumulative Distribution Function (CDF) of the normal centered PDF $G\left(0, 1; x\right)$.

$$\Phi(x) = \int_{-\infty}^{x} \frac{1}{\sqrt{2\pi}} e^{-\frac{x'^2}{2}} dx' \tag{4.2.3}$$

$\Phi(x)$ can also be written as a function of the error function $erf(x)$ or $erfc(x)$:

$$\Phi(x) = \frac{1}{2}\left[1 + erf\left(\frac{x}{\sqrt{2}}\right)\right] = \frac{1}{2} erfc\left(-\frac{x}{\sqrt{2}}\right) \tag{4.2.4}$$

with the error function defined as:

$$erf(x) = \frac{2}{\sqrt{\pi}} \int_{0}^{x} e^{-t^2} dt \tag{4.2.5}$$

and the complementary error function:

$$erfc(x) = \frac{2}{\sqrt{\pi}} \int_{x}^{+\infty} e^{-t^2} dt \tag{4.2.6}$$

For the more general case of a Gaussian RV $N\left(\mu, \sigma^2\right)$, its CDF is of the form:

$$F(x) = \Phi\left(\frac{x-\mu}{\sigma}\right) = \frac{1}{2}\left[1 + erf\left(\frac{x-\mu}{\sigma\sqrt{2}}\right)\right] \tag{4.2.7}$$

Reminder: the CDF $F(x)$ of a RV represents the probability that the RV X has a value smaller than x:

$$F_X(x) = \mathbb{P}(X \leq x) = \mathbb{P}(]-\infty; x]) \tag{4.2.8}$$

4.2.2 Dirichlet BC's

4.2.2.1 Problem statement and analytical solutions of PDE's

RWPT method used in this study and in general are based on initial value problems (Cauchy's problem Eq.4.2.9). Cauchy's problems solve PDE's in infinite domains with a Dirac initial condition. In RWPT, each particle is represented by the initial Dirac condition. And the algorithm of the particles must reproduce the concentration based PDE. The aim would be to have the PDF equivalent to the solution of the concentration based PDE. This study,

uses some theorems that generalizes the solutions Cauchy's problems to propose new algorithms for RWPT.

$$\forall t \geq 0, \forall x \epsilon \mathbb{R}^n; \frac{\partial C}{\partial t}(x;t) = D\Delta C(x;t) \tag{4.2.9a}$$

$$\forall t \geq 0; \lim_{|x| \to \infty} C(x;t) = 0 \tag{4.2.9b}$$

$$\forall x \epsilon \mathbb{R}^n; C(x;0) = \frac{M_0}{\theta}\delta(|x - x_0|) \tag{4.2.9c}$$

$$\forall t \geq 0; \int_{\mathbb{R}^n} C(x;t)\, dx = \frac{M_0}{\theta} \tag{4.2.9d}$$

with n is the dimension number.

Eq.4.2.9d represents the conservation of mass throughout the simulation, and it allows to have a unique solution. The solution of Eq.4.2.9 is:

$$\forall t > 0; \forall x \epsilon \mathbb{R}^n;\ C(x,t) = \frac{M_0}{\theta} \frac{1}{(4\pi D t)^{\frac{n}{2}}} exp\left(-\frac{|x - x_0|^2}{4Dt}\right) \tag{4.2.10}$$

Theorem [Evans, 2010] Let us consider the problem described by Eq.4.2.11:

$$\forall t, x \epsilon \mathbb{R}^n; \frac{\partial C}{\partial t}(x;t) = D\frac{\partial^2 C}{\partial x^2}(x;t) \tag{4.2.11a}$$

$$\forall t \geq 0; \lim_{|x| \to \infty} C(x;t) = 0 \tag{4.2.11b}$$

$$\forall x \epsilon \mathbb{R}^n; C(x;0) = g(x) \tag{4.2.11c}$$

The solution of problem Eq.4.2.11 is the following Eq.4.2.12

$$\forall t > 0; \forall x \epsilon \mathbb{R};\ C(x;t) = \frac{1}{(4\pi D t)^{\frac{n}{2}}} \int_{\mathbb{R}^n} exp\left(-\frac{\left|x - x'\right|^2}{4Dt}\right) g(x')\, dx' \tag{4.2.12}$$

The result of this Theorem is expected if $g(x)$ is seen as a function of the Dirac function:

$$g(x) = \int_{\mathbb{R}^n} \delta(x - x')\, g(x')\, dx' \tag{4.2.13}$$

Then, the solution Eq.4.2.12 is found by replacing $\delta(x - x')$ in Eq.4.2.13 by the solution of the δ initial problem Eq.4.2.12. This, transition from the solution

of an initial Dirac to the solution of any function $g(x)$ is possible because of the linearity of the problem.

For a one dimensional problem $n = 1$ and in an infinite domain with a Heaviside initial condition the problem becomes:

$$\forall t \geq 0, x \epsilon \mathbb{R}; \frac{\partial C}{\partial t}(x;t) = D \frac{\partial^2 C}{\partial x^2}(x;t) \tag{4.2.14a}$$

$$\forall t \geq 0; \lim_{|x| \to \infty} C(x;t) = 0 \tag{4.2.14b}$$

$$\forall x \leq 0; C(x;0) = 2C_0 \tag{4.2.14c}$$

$$\forall x > 0; C(x;0) = 0 \tag{4.2.14d}$$

Using the above Theorem 4.2.2.1 with $\forall x \leq 0; g(x) = 2C_0$, the solution of Eq.4.2.14 is:

$$\forall t > 0; \forall x \epsilon \mathbb{R};\ C(x;t) = \frac{1}{(4\pi D t)^{\frac{1}{2}}} \int_{-\infty}^{0} exp\left(-\frac{\left(x - x'\right)^2}{4Dt} \right) 2C_0 dx' \tag{4.2.15}$$

On the other hand, the equation governing a pure diffusion transport (C) problem in a semi-infinite domain ($x \geq 0$), with a Dirichlet condition (constant value $C = C_0$) at a boundary($x = 0$), and with a constant diffusion coefficient D.

$$\forall t, x > 0; \frac{\partial C}{\partial t}(x;t) = D \frac{\partial^2 C}{\partial x^2}(x;t) \tag{4.2.16a}$$

$$\forall t \geq 0; \lim_{x \to +\infty} C(x;t) = 0 \tag{4.2.16b}$$

$$\forall t \geq 0; C(0;t) = C_0 \tag{4.2.16c}$$

The analytical solution of this problem is [Carslaw & Jaeger, 1959]:

$$\forall t; x \geq 0; C(x;t) = \frac{2C_0}{\sqrt{\pi}} \int_{\frac{x}{2\sqrt{Dt}}}^{+\infty} e^{-t'^2} dt' \tag{4.2.17}$$

Eq.4.2.17 could also be written using the complementary error function of Eq.4.2.6:

$$\forall t; x \geq 0; C(x;t) = C_0 erfc\left(\frac{x}{2\sqrt{Dt}}\right) \tag{4.2.18}$$

4.2.2.2 Equivalence of Dirichlet with an infinite domain problem

The diffusion of an initial Heaviside function in an infinite domain $x\epsilon\mathbb{R}$ Eq.4.2.14, has the solution Eq.4.2.15. This analytical solution Eq.4.2.15 can also be written in the form of Eq.4.2.17. The equivalence between the two solutions (the solution of the initial infinite domain and the Dirichlet BC) induce that this same equivalence could be used in RWPT methods. Since the study of RWPT is well known in infinite domains, this study proposes to use this parallel between the solutions of the two problems to model the Dirichlet BC. Hence, this study proposes to replace a Dirichlet BC in RWPT by a an initial semi-infinite reservoir filled with particles with two times the concentration of the fixed Dirichlet BC.

4.3 Methods and algorithms

4.3.1 Dirichlet BC in RWPT methods

The RWPT algorithms proposed in this study are inspired from the analytical solutions of initial value problems studied in subsection 4.2.2. These initial value problems (Cauchy's problems) take the Dirac distribution as an initial condition. And the Dirac pseudo-function $\delta(x - x_0)$ represents particles at position x_0 in RWPT. Gaussian functions in the analytical solutions are replaced by Gaussian RVs in RWPT. Thus, the solution of the diffusion of an initial Dirac in an infinite domain Eq.4.3.1:

$$\forall t > 0; \forall x\epsilon\mathbb{R};\ C(x,t) = \frac{M_0}{\theta} G(x_0, 2Dt; x) \tag{4.3.1}$$

In RWPT Eq.4.3.1 becomes Eq.4.3.2:

$$X_t = N\left(x_0, 2Dt\right) \tag{4.3.2}$$

with each particle has a mass $m_{particle} = \frac{M_0}{N_{particles}}$, particles positions with their mass will be used to induce the concentration based solution. Using basic Gaussian RVs properties, Eq.4.3.2 could also be written as:

$$X_t = x_0 + \sqrt{2Dt}\, N\left(0, 1\right) \tag{4.3.3}$$

For problems like the one described by Eq.4.2.11, the initial condition is a function $g\left(x\right)$ instead of the Dirac $\delta\left(x - x_0\right)$. This $g\left(x\right)$ initialization is translated in RWPT, into initializing the PDF of the positions of the particles as $g\left(x\right)$ instead of initializing all particles at the position x_0.

4.3.1.1 External Mesh method

In previous work in literature of RWPT, the implementation of the Dirichlet BC used an External Mesh method. This method, creates a mesh adjacent to the domain of study. This mesh is, then, maintained at a constant concentration at each time step. Either by adding the number of particles that left the mesh in the previous time step. Or by completely updating the distribution of particles in this mesh every time step.

This External Mesh method presents many problems. First, the time step has to be very small for more precision. Theoretically, it has to tend towards zero for maximum precision. Second, the process of updating or replacing the particles in the mesh at every time step increases the CPU Time significantly.

Therefore, the next subsection (subsection 4.3.1.3) proposes a new method to implement the Dirichlet BC. This new Dirichlet BC method is called External Reservoir Method. It has no restriction on the time step.

4.3.1.2 Finite Dirichlet Flux method

In this subsection we propose a new method to implement Dirichlet BC's, using a Flux method based on Finite Difference scheme. This method uses the finite difference scheme in the mesh adjacent (number $i = 1$) to the BC:

$$C_i^{n+1} = C_i^n + \frac{D\Delta t}{2\Delta X^2} C_0 + \frac{D\Delta t}{2\Delta X^2} C_{i+1}^n - \frac{D\Delta t}{2\Delta X^2} 2C_i^n \tag{4.3.4}$$

with n corresponds to time $t_n = n\Delta t$ and i the number of the mesh frontier to the Dirichlet BC.

- The red $-\frac{D\Delta t}{2\Delta X^2} 2C_i^n$ term in Eq.4.3.4 corresponds to the particles that will leave the mesh i to meshes $i+1$ and $i-1$, here the mesh $i-1$ is outside the domain.
- The blue $+\frac{D\Delta t}{2\Delta X^2} C_{i+1}^n$ term in Eq.4.3.4 corresponds to the particles that will enter the mesh i coming from mesh $i+1$.
- The green $+\frac{D\Delta t}{2\Delta X^2} C_0$ term in Eq.4.3.4 corresponds to the particles that will enter the mesh i from the Dirichlet BC. We notice here, that the green term is constant.

Using the above analysis of the Finite Difference scheme Eq.4.3.4, we propose to model the Dirichlet BC in RWPT methods by injecting at each time step a constant number of particles corresponding to the green $+\frac{D\Delta t}{2\Delta X^2} C_0$ term in Eq.4.3.4:

$$N_{Particles}^{Injected} = \frac{D\Delta t}{2\Delta X} C_0 \tag{4.3.5}$$

The advantage of this method, compared to the previous one External Mesh method, is: it does not need to model the entire external mesh and update it at each time step. Here, we inject only the particles that will enter the domain (the number of particles injected is constant).

However, this method, as the previous one, still has restrictions on the time step and mesh sizes. Thus, we propose, in the following subsections, methods with no restrictions on the time step.

4.3.1.3 External Reservoir method

RWPT methods are based on Initial value problems (Cauchy's Problems). These problems are in infinite domains. Hence the idea of transforming the semi-infinite problem, with Dirichlet BC, into an infinite domain problem with an initial condition.

Using this similarity, to model the Dirichlet problem, this study proposes to model the Dirichlet BC in RWPT by an External Reservoir adjacent to the domain of study. This adjacent External Reservoir is initiated at $t = 0$, but it does not need to be updated during the simulation time.

In theory, this External Reservoir should be semi-infinite. But, particles, that are initially in the External Reservoir and will not reach the domain of study during the simulation time, do not need to be simulated. Hence, the width of the External Reservoir will be set equal to the maximum displacement that a particle might have:

$$L_{Res} = \Delta X_{max} = max\left(X_{T_{Simu}} - x_0\right) = \sqrt{2DT_{Simu}}\, M_{GAUSS} \tag{4.3.6}$$

with $M_{GAUSS} = max\left(N\left(0,1\right)\right)$ is the numerically maximum value that a normal centered Gaussian RV might have. In theory, $N\left(0,1\right)$ is unbounded. But numerically, the probability for $N\left(0,1\right)$ to exceed a value x is:

$$\mathbb{P}\left(X_{T_{Simu}} \geq x\right) = 1 - \Phi\left(x\right) = \frac{1}{2}\left[1 - erf\left(\frac{x}{\sqrt{2}}\right)\right] = \frac{1}{2} erfc\left(\frac{x}{\sqrt{2}}\right) \tag{4.3.7}$$

By choosing $x = 6$, $\mathbb{P}\left(N\left(0,1\right) \geq 7\right) = 9.87.10^{-10}$, which is a very small probability. It means that if the RV $N\left(0,1\right)$ is generated 10^9 times, one of the 10^9 values will likely be higher than 6. In all simulations used in this study the RV

$N(0,1)$ will be generated no more than 10^9 times. Therefore, $max(N(0,1))$ in Eq.4.3.6 is replaced by 6 and becomes:

$$L_{Res} = 6\sqrt{2DT_{Simu}} \tag{4.3.8}$$

Eq.4.3.8 shows that the width of the External Reservoir L_{Res} is correlated with the square root of the simulation time T_{Simu}. With the finite External Reservoir with a width L_{Res} instead of the semi-infinite reservoir the analytical solution Eq.4.2.15 becomes: $\forall t > 0; \forall x \epsilon \mathbb{R}$;

$$C(x;t) = \frac{1}{(4\pi Dt)^{\frac{1}{2}}} \int_{-L_{Res}}^{0} exp\left(-\frac{\left(x - x^{'}\right)^2}{4Dt}\right) 2C_0 dx' \tag{4.3.9}$$

The External Reservoir is initially filled uniformly with a concentration $2C_0$ of particles Eq.4.3.10:

$$X_0 = -L_{Res} U_{[0;1]} \tag{4.3.10}$$

with $U_{[0;1]}$ is the RV with the continuous uniform distribution.

Eq.4.3.11 describe the relation between the total initial number of particles $N_{particles}$ (inside the External Reservoir and the domain of study), the mass of one particle $m_{particle}$, the Dirichlet physical concentration C_0, the numerical parameter L_{Res}. The mass of one particle $m_{particle}$ is correlated to the precision of the simulation, the smaller $m_{particle}$ is, the greater the precision. While the number of particles $N_{particles}$ evolves linearly with the CPU Time.

$$2C_0 = \frac{m_{Particle} N_{Particles}}{L_{Res}} \tag{4.3.11}$$

After initializing the positions, particles undergo the same algorithm Eq.4.3.2 they would if they were in an infinite domain. Then, in post-processing, only particles that are inside the domain of study are considered. The next subsection, proposes a method that reduces the number of particles that will not have an effect on the domain of study.

4.3.1.4 Semi-Reservoir method

This method is based on the External Reservoir method described in subsection 4.3.1.3. As mentioned in the previous subsection, the number of particles that will not be used in the post-processing must be reduced to reduce the CPU Time and Memory. Even though these particles are not used in the post-processing, they are still CPU Time consuming since all particles undergo the algorithm Eq.4.3.2. Hence, this subsection proposes to reduce the total number of particles $N_{particles}$ by reducing (halving) the size of the External Reservoir L_{Res} in Eq.4.3.11.

In subsection 4.3.1.3, for a domain of study $[0;+\infty[$ with a Dirichlet BC at $x = 0$, the External Reservoir is located in $[-L_{Res};0]$. This subsection proposes to halve the width of the Reservoir $\left[-\frac{L_{Res}}{2};0\right]$ with a full reflecting barrier (method of images) at $x = -\frac{L_{Res}}{2}$ (inside the reservoir).

The reflecting barrier adds a symmetric solution to the one without this barrier. The solution Eq.4.3.1, of the initial value problem in an infinite domain, becomes in a semi-infinite domain with a reflecting barrier: $\forall t > 0; \forall x \epsilon \mathbb{R}$;

$$C(x,t) = \frac{M_0}{\theta} G(x_0, 2Dt; x) + \frac{M_0}{\theta} G(2x_{BC} - x_0, 2Dt; x) \tag{4.3.12}$$

Eq.4.3.12 adds the symmetric of Eq.4.3.1 relative to the position $x = x_{BC}$ of the reflecting barrier. Hence, by applying the same principle to the Semi-Reservoir with $x_{BC} = -\frac{L_{Res}}{2}$: $\forall t > 0; \forall x \epsilon \mathbb{R}$;

$$C(x;t) = \int_{-\frac{L_{Res}}{2}}^{0} 2C_0 \left(G(x', 2Dt; x) + G((-L_{Res}) - x', 2Dt; x)\right) dx' \tag{4.3.13}$$

Using integral properties, it can be shown that Eq.4.3.13 and Eq.4.3.9 are equivalent.

The Semi-Reservoir method improves the performances of the previous External Reservoir method by halving the Reservoir, i.e. halving the number of particles, while keeping the same level of precision $m_{particle}$.

4.3.1.5 Erfc Flux method (for Dirichlet BC)

This subsection proposes a new method for implementing Dirichlet BC via a type of "flux" condition, rather than a concentration condition. As the methods proposed in subsection 4.3.1.3 and 4.3.1.4, the method here has no restriction on the time step. In addition, it does not use an External Reservoir, thus, less particles outside the domain.

This Erfc Flux method proposes to inject particles, inside the domain, with a distribution that follows the analytical solution Eq.4.3.9 of the Dirichlet problem with $C = C_0$ at left. Thus, by combining Eq.4.3.10 (used to fill the External Reservoir) with the algorithm Eq.4.3.2 (particles displacements), equation 4.3.14 is obtained:

$$X_t = \sqrt{2Dt}\left(N\left(0,1\right) - M_{GAUSS}U_{[0;1]}\right) \tag{4.3.14}$$

Then, only particles that verifies $X_t > 0$ will be kept. The other particles are discarded, they correspond to the one that stays inside the External Reservoir in the method of External Reservoir. $X_t > 0$ means that all the negative values of the RV $N\left(0,1\right)$ will be discarded. And since, $N\left(0,1\right)$ is an even RV then it could be replaced, in Eq.4.3.14, with its absolute value $\left|N\left(0,1\right)\right|$ for more efficiency.

The operation Eq.4.3.14 is similar to injecting particles with a distribution $\frac{1}{2}erfc\left(\frac{x}{\sqrt{2}}\right)$. In addition, the sum of two independent RV's is an RV with a PDF that is the convolution of the PDF's of the two independent RVs. Thus, the PDF of X_t is:

$$P\left(x;t\right) = \int_{-M_{GAUSS}\sqrt{2Dt}}^{0} G\left(x', 2Dt; x\right) dx' \tag{4.3.15}$$

On the other hand $P = \frac{C}{2C_0}$, thus the solution obtained is once again equivalent to the one with the External Reservoir method Eq.4.3.9.

4.3.2 Dirichlet BC combined with multiple layers with discontinuous diffusion and porosity

4.3.2.1 Zero concentration Dirichlet BC

The Zero concentration Dirichlet BC is a particular case of Dirichlet BC's. Carslaw & Jaeger propose to solve the PDE associated to this BC using the Method of Images [Carslaw & Jaeger, 1959] with a negative coefficient. Whence, in this chapter we propose to implement the Zero concentration Dirichlet BC by a negative full reflecting boundary. Which means that: each particle, crossing the boundary, will be fully reflected and its mass will be multiplied by -1. This allows to deal with the zero concentration Dirichlet BC with no restriction on the time step.

4.3.2.2 From Semi-infinite to finite Dirichlet BC's

To implement Dirichlet BC in both ends of a finite domain, the methods proposed in this section can be implemented in both ends of the domain. For example, the External Reservoir method needs two External Reservoirs at both ends of the domain. Similarly, the Semi-Reservoir and the Erfc Flux methods need to be applied in both ends of the domain.

4.3.2.3 Algorithm of the semi-analytical solution

This subsection uses the same principle used in section 4.2. Note here, that the analytical solution in a finite two-layered domain with two Dirichlet BC's has been described by Carslaw & Jaeger [Carslaw & Jaeger, 1959] as rather complicated, instead they gave the solution in a very specific case (square root of the contrast of diffusivities rational). This subsection, proposes a novel method that gives a semi-analytical solution for an N-layered domain and with no conditions on the contrasts. The principle transforms an initial value problem

Algorithm 4.1 Semi-analytical solution for discontinuous diffusion with $N \geq 2$ interfaces and Dirichlet BCs

1. C_k concentration in sub-domain k
2. Initialize $Ci_k = C_S$ with C_S the solution of a diffusion problem with no discontinuity.
3. $u_k = \pm 1$ the direction towards the interfaces limiting sub-domain (k).
4. **while** (C_k) not converged **do**
   a) $C_k = C_k + L_{k,k+u_k}(Ci_k)$ and $C_{k+u_k} = C_{k+u_k} + L^*_{k,k+u_k}(Ci_k)$
   b) $u_{k+u_k} = u_k$ and $u_k = -u_k$
   c) $Ci_k = L_{k,k+u_k}(Ci_k)$ and $Ci_{k+u_k} = Ci_{k+u_k} + L^*_{k,k+u_k}(Ci_k)$
5. **end**

in an infinite domain (Cauchy's Problem), into a semi-infinite problem with Dirichlet BC. This transformation is a superposition of initial Dirac functions located in a semi-infinite domain (adjacent) outside of the domain of study. Hence, the solution of the Dirichlet BC problem is a superposition of solutions of initial value problems. In this study, the superposition is seen as an integral. Therefore, to solve the Dirichlet BC problem with multiple layers, this study proposes to integrate the semi-analytical solution of the initial value multi-layer problem presented in Chapter 3. This integration starts from $-\infty$ to the Dirichlet BC location. Consequently, the algorithm of the semi-analytical solution presented in Chapter 3 for an infinite domain stays the same here for a Dirichlet BC, however, The Gaussian function used as a "seed" is replaced by the complementary error function as in Eq.4.2.18.

4.3.2.4 RWPT in a heterogeneous discontinuous media with Dirichlet BCs

The RWPT algorithm used in this subsection is similar to the Negative Particles Algorithm described in Chapter 3. The implementation of the Dirichlet

Algorithm 4.2 RWPT algorithm for $N \geq 2$ interfaces

1. Initialize the particles positions and their first step:

$$X_t = \sqrt{2Dt}\left(N(0,1) - M_{GAUSS}U_{[0;1]}\right) \tag{4.3.16}$$

2. Consider particle (k) with mass m_k and position X_k.

3. **while** particle (k) crosses interfaces **do**

   - **If** $R_{1,2} \geq 0$ **then**
     - **If** $[\![R_{1,2}]\!] = 0$; **then** the particle (k) is $refracted$ to the position X_k^{Rr}**endif**
     - **If** $[\![R_{1,2}]\!] = 1$; **then** the particle (k) is $reflected$ to the position X_k^{Rl} **endif**
   - **Else** (case $R_{1,2} < 0$)
     - The particle (k) is $refracted$ to the position X_k^{Rr}.
     - **If** $[\![R_{1,2}]\!] = 1$; **then** $m_k = 2m_k$ and create one particle (k^*) with:
       - The mass of $k^*$is $m_{k^*} = -m_k$
       - The position of (k^*) is the position of (k) if (k) was $reflected$ $X_{k^*} = X_k^{Rl}$
     - **endif**
   - **endif**

4. **end**

BC consists on the initialization of the particles positions and their first displacement. This algorithm allows the implementation of a Dirichlet BC with no restriction on the time step and with maximum precision.

x	$[-300; -100]$	$[-100; 100]$	$[100; 300]$
D	100	10	1
θ	100%	40%	10%

Table 4.1: Diffusion and porosity contrasts of Figure 4.4.1

4.4 Results and discussions

4.4.1 PDE's solutions: Time evolution of concentration profiles

4.4.1.1 PDE's solutions: Dirichlet BC's equal to 1 in the left and to 0 in the right

Figure 4.4.1 shows the results of the semi-analytical solution of the pure diffusion in a three-layered medium with discontinuous diffusion and porosity at four different times. The medium is bounded by two Dirichlet boundary conditions equal to 1 in the left and to 0 in the right. The diffusion coefficient and porosity are discontinuous, Table 4.1 shows the values that they have.

4.4.1.2 PDE's solutions: Dirichlet BC's equal to 1 in the left and in the right

The second analytical solution, of Figure 4.4.2, is the result of the semi-analytical solution Algorithm 4.1 in a three-layered domain. The diffusion coefficient and porosity of the domain are discontinuous their values are shown in Table4.2. The position of the interfaces and the values of the porosity and diffusion coefficient are chosen so that the domain would be symmetrical. In this case, both BC's of the domain are kept at constant concentrations $C = 1$. It can be seen that the solutions are symmetrical. This was expected since the domain and the BC's are symmetrical about the center of the domain ($x = 0$).

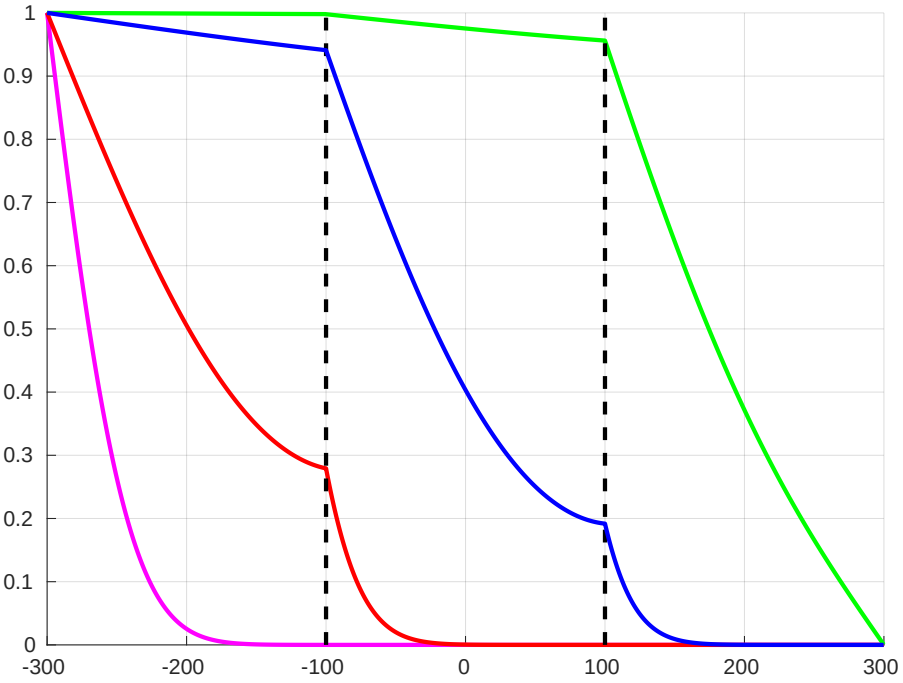

Figure 4.4.1: The magenta, red, blue and green curves are the results of different times of the analytical solution. The vertical dashed black lines represent the interfaces between sub-domains that have different porosities and diffusivities. The Dirichlet boundary conditions are in the left $C = 1$ and in the right $C = 0$.

x	$[-300; -100]$	$[-100; 100]$	$[100; 300]$
D	1	100	1
θ	10%	100%	10%

Table 4.2: Diffusion and porosity contrasts of Figure 4.4.2

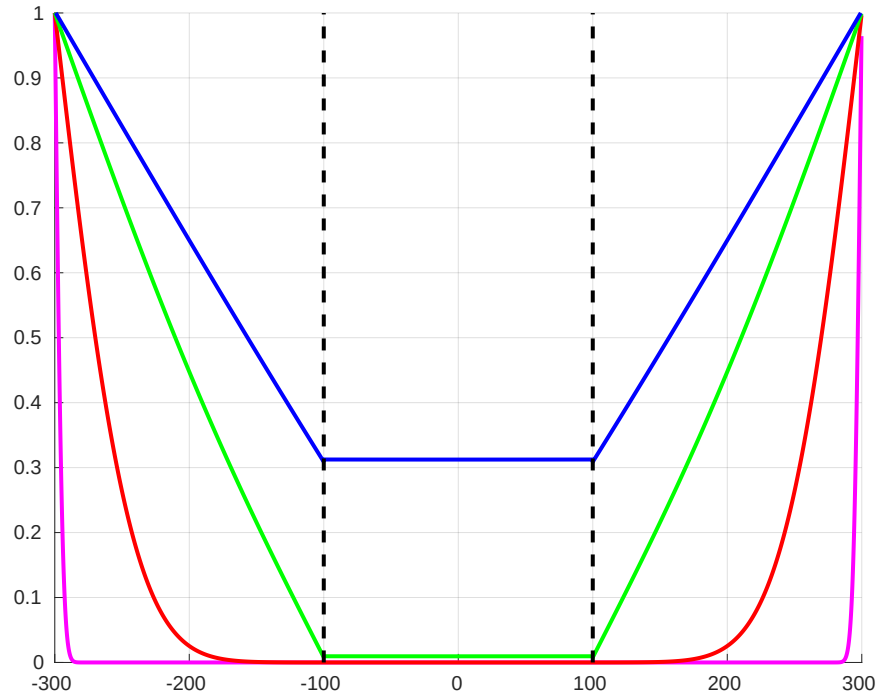

Figure 4.4.2: The blue, green, red and magenta curves are the results of different times of the analytical solution. The vertical dashed black lines represent the interfaces between sub-domains that have different porosities and diffusivities. The Dirichlet boundary conditions in the left and in the right are $C = 1$.

4.4.2 RWPT method with Dirichlet BC's

4.4.2.1 Homogeneous semi-infinite domain

Figure 4.4.4 shows the results of different simulations using the External Reservoir method. Different sizes of reservoirs were used. The figure shows all reservoirs with a size than $L_{Res} = 2\sqrt{2Dt}$, fit the analytical solution (Black curve). Using Eq.4.3.7, the error for a reservoir with a size $L_{Res} = 2\sqrt{2Dt}$ is less than 2%.

Figure 4.4.5 shows the results of a Dirichlet BC simulation using different sizes of Semi-Reservoirs. This Figure shows that we can obtain results with

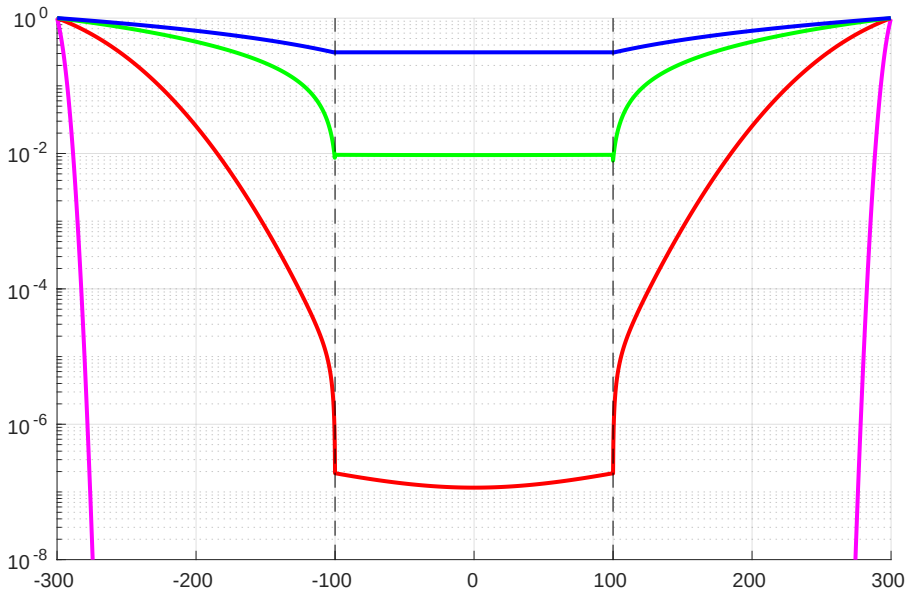

Figure 4.4.3: The blue, green, red and magenta curves are the results of different times of the analytical solution. The vertical dashed black lines represent the interfaces between sub-domains that have different porosities and diffusivities. The Dirichlet boundary conditions in the left and in the right are $C = 1$.

the same precision as the one of the External Reservoir method, while using 2 times less particles, i.e. 2 times more efficient in CPU Time.

4.4.2.2 Heterogeneous semi-infinite domain

Figure 4.4.6 shows the results of simulations using Algorithm 4.2 compared to the results of the semi-analytical solution Algorithm 4.1 at different times t_1, t_2 and t_3. The domain is semi-infinite with a Dirichlet BC, two interfaces and three sub-domains that have different porosities and diffusivities (see Table 4.3).

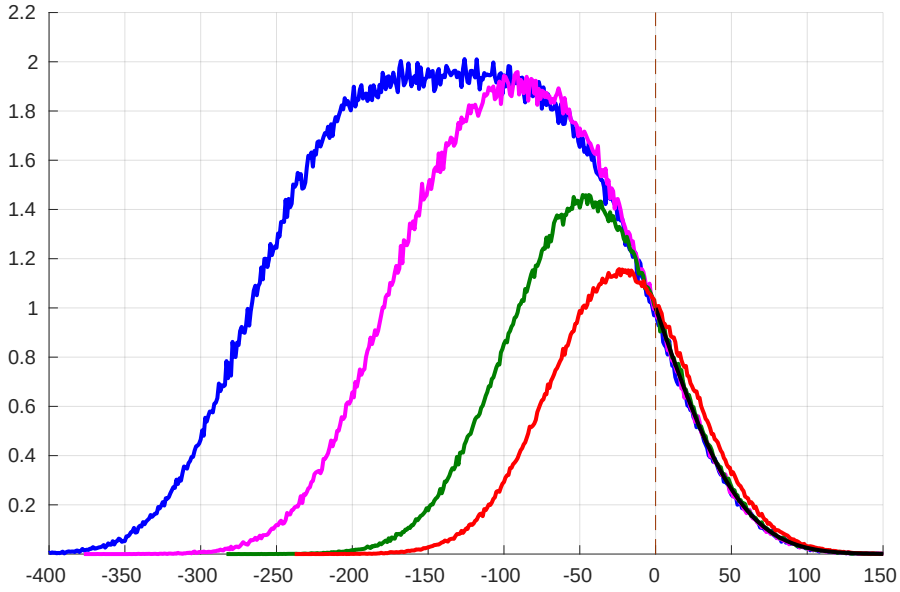

Figure 4.4.4: Concentration profiles using the External Reservoir method: The blue, magenta, green and red bold curves represent the concentrations with a Reservoir with a size of $6\sqrt{2Dt}$, $4\sqrt{2Dt}$, $2\sqrt{2Dt}$ and $\sqrt{2Dt}$ respectively. The black bold curve represent the analytical solution for a semi-infinite domain with a Dirichlet BC.

x	$[-300; -100]$	$[-100; 100]$	$[100; +\infty]$
D	100	10	50
θ	50%	5%	30%

Table 4.3: Diffusion and porosity contrasts of Figure 4.4.6

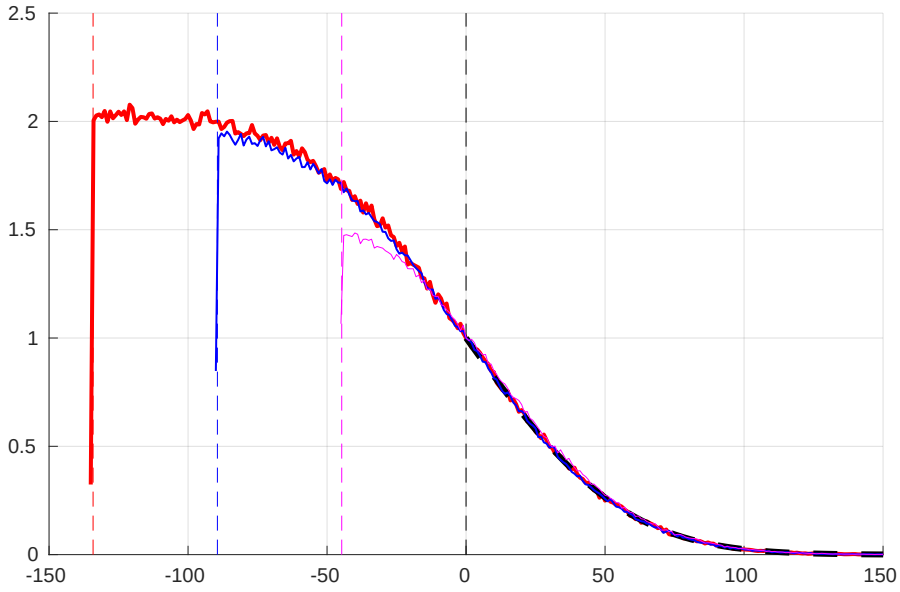

Figure 4.4.5: Concentration profiles using the External Semi-Reservoir method: The red, blue and magenta curves represent the concentrations with a Semi-Reservoir with a size of $3\sqrt{2Dt}$, $2\sqrt{2Dt}$, $\sqrt{2Dt}$ respectively. The black dashed curve represents the analytical solution for a semi-infinite domain with a Dirichlet BC.

4.4.2.3 Heterogeneous finite domain

In Figure 4.4.7, we compare the analytical solution found in [Carslaw & Jaeger, 1959] book, to the RWPT algorithm with Dirichlet BC's implemented using the Finite Dirichlet Flux method described in subsection 4.3.1.2. The Figure shows a deficit of concentration near the left Dirichlet BC (non nul). This deficit is related to the time step and mesh size used.

Figure 4.4.8 shows a comparison between the results of the semi-analytical solution described in subsection 4.3.2.3 and the RWPT simulation using algorithm 4.2. The case studied here, is a diffusion problem in a three layer domain with discontinuous diffusion coefficient and porosity (see Table 4.4). The domain is bounded with two Dirichlet BC's. The left one is kept at $C = 1$, while

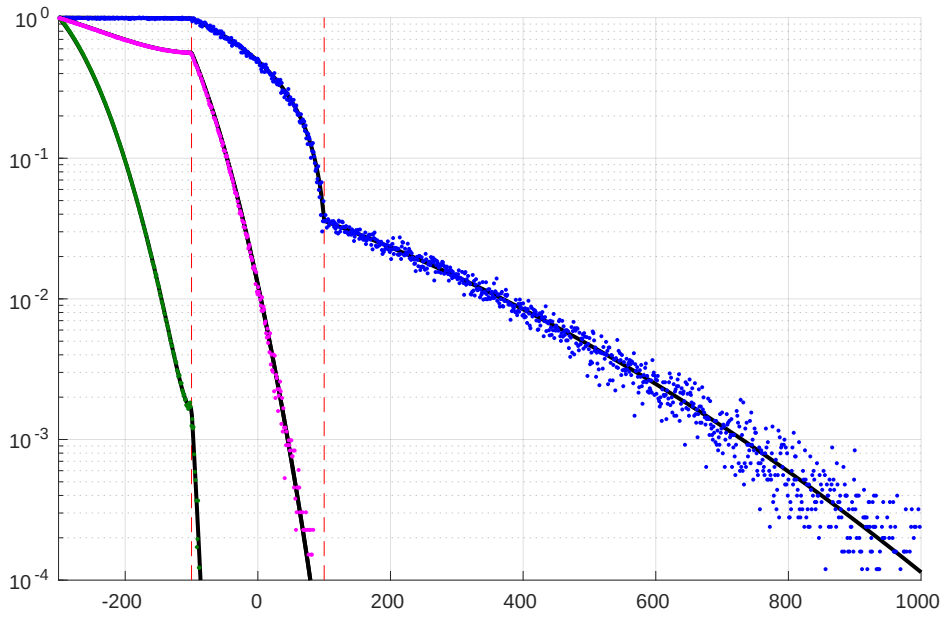

Figure 4.4.6: Time evolution of log-concentration profiles using Algorithm 4.2 with the Erfc method and negative mass particles. The red dashed vertical lines correspond to the interfaces $x = -100$ and $x = 100$. The green, magenta and blue bold dots correspond to the simulation results. The bold black curves correspond to the semi-analytical solution of algorithm 4.1. The Dirichlet boundary conditions in the left is $C = 1$ at $x = -300$.

x	$[-300; -100]$	$[-100; 100]$	$[100; 300]$
D	10^2	10^4	1
θ	50%	100%	25%

Table 4.4: Diffusion and porosity contrasts of Figure 4.4.8

the right BC is at $C = 0$.

4.5 Conclusion and perspectives

- This Chapter studies diffusion in discontinuous finite and semi-infinite domains with Dirichlet Boundary Conditions (BC's) via particle-based

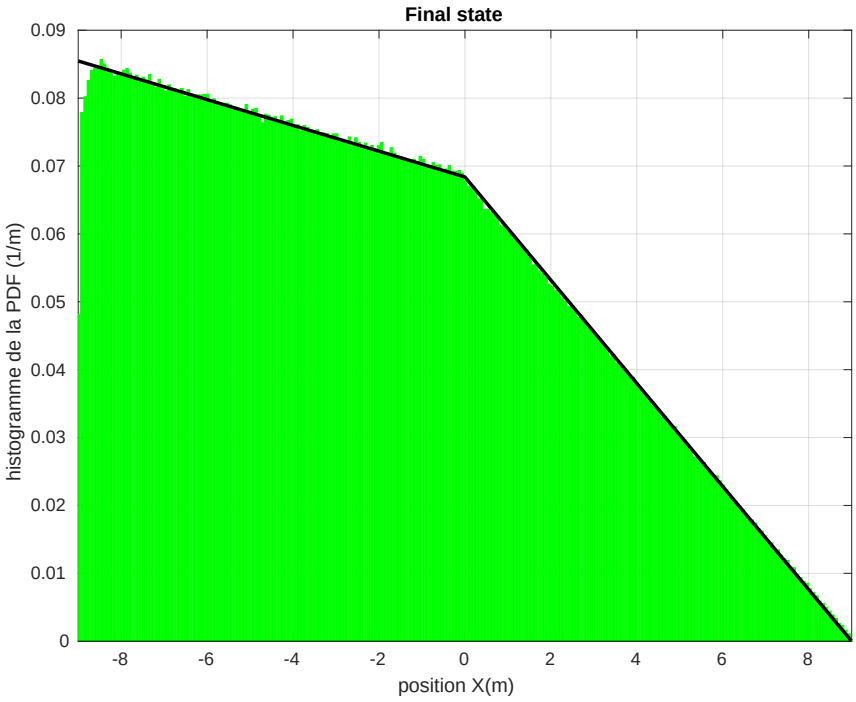

Figure 4.4.7: Comparison between the RWPT algorithm and analytical solution. The black bold curve corresponds to the analytical solution. The green histograms correspond to the PDF of particles positions.

methods (RWPT).

- The heterogeneity consists in the discontinuity of the properties of the domain. The domain can be divided into sub-domains with different porosities and diffusivities.

- This study extends the algorithm of Chapter 3 that solves semi-analytically diffusion PDE's in heterogeneous infinite domains, into solving the same problem but also in semi-infinite and finite domains with Dirichlet BC's.

- It proposes also an extension of the RWPT Algorithm of Chapter 3 that solves discontinuous diffusion and porosity using particle methods in infi-

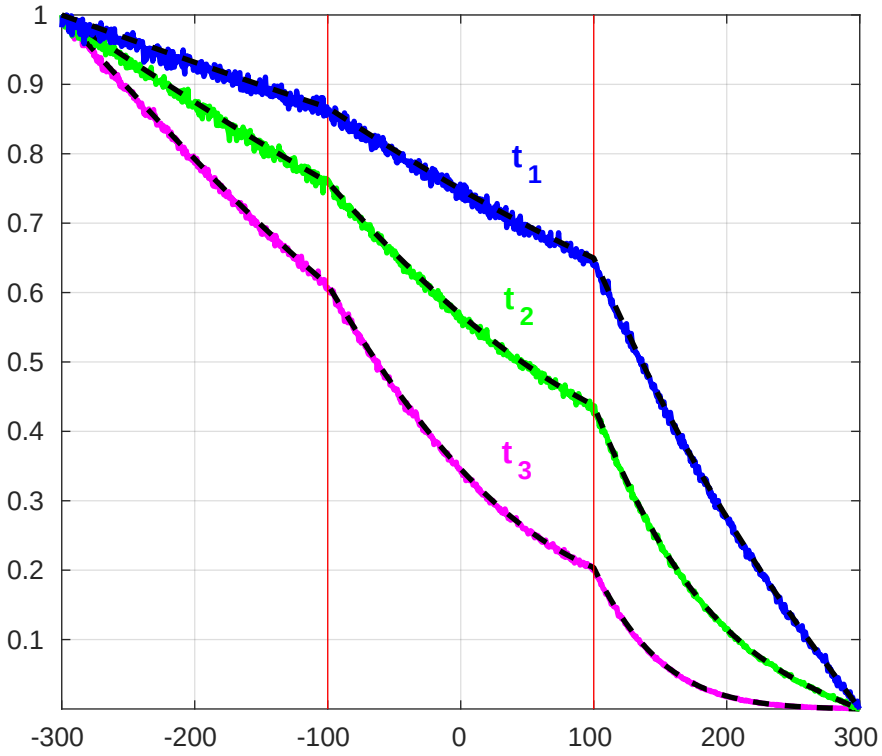

Figure 4.4.8: The blue, green and magenta curves are the results of different times $t_1 > t_2 > t_3$ of the Algorithm. The dashed black curves are the analytical solutions of the same different times t_1, t_2 and t_3. The two vertical red lines represent interfaces between three sub-domains with different properties (different porosities, and different diffusion coefficients).

nite domains, so that it handles also semi-infinite and finite heterogeneous domains with Dirichlet BC's. This extension of the algorithm is based on the analytical solutions proposed in this Chapter.

- The methods have been checked analytically and verified for various configurations.

Chapter 5

Chapter 5: Multi-scale study of diffusion in composite Grain-Pore systems using Random Walk

5.1 Introduction

Transport processes concern a broad class of porous reservoir flow and transport problems, including: solute mass transport, heat transport, and Darcy flow (pressure diffusion). Diffusion processes, in particular, are important in transport phenomena, either directly (solute diffusion, heat diffusion, pressure diffusion) or indirectly (when the hydrodynamic dispersion of transported quantities is modeled as a diffusion-type process).

This chapter studies diffusion processes at different scales in composite media (whether natural or man-made (industrial)). Considering a binary grain/pore medium, at the "microscopic" level (micro-scale), diffusion occurs inside the pore elements, while the grain elements are assumed inaccessible to diffusion (extensions to aggregates instead of grains are discussed in the conclusion Section 5.5). A zero-flux condition is assumed locally at the grain/pore interfaces. At the macro-scale level, diffusion occurs in a homogeneous medium with macroscopic parameters (porosity and effective diffusion coefficients) induced from moments upscaling methods.

Particle methods have been extensively used for modeling transport problems in porous soils, aquifers, and reservoirs. They reduce or avoid some of the problems of Eulerian methods, e.g. instabilities, excessive artificial diffusion, mass balance, and/or oscillations that could lead to negative concentrations. In the Lagrangian particle approach diffusion processes are modeled by Random Walk algorithms. The numerical (modeling) issues are different for the Eulerian PDE approach and for the Lagrangian Random Walk approach (for more details, see Introduction Chapter 3, and see Oukili et al. 2019 [J.Compt.Phys., Submitted]).

In this study, the Random Walk Particle Tracking (RWPT) method is based on 2D/3D analytical solutions in finite and semi-infinite domains with zero flux

boundary conditions. The RWPT algorithm induced from the analytical solutions is then applied to more complex geometries of grains and pores (that are difficult to solve analytically). Different configurations or structures at the micro-scale level (e.g. grains and pores in a porous media) will be chosen in order to obtain composite isotropic media at the macro-scale level with different porosities. Then, by choosing elongated micro-structures, anisotropic media emerge at the macroscopic level. These configurations will be of the form of motifs of grains and pores with different porosities, repeated periodically and indefinitely (infinite domain with grains and pores). Effective macro-scale properties (porosities, effective diffusion tensors, tortuosities) are then calculated using moments of particles positions.

This chapter is organized as follows. The next section, section 5.2, presents the theory behind Random Walk Particle Tracking methods (RWPT), and the corresponding concentration based PDE, particularly for diffusion problems with zero flux BC's (Boundary Conditions). Section 5.3 presents a generalization of particle-based methods and algorithms for solving diffusion transport problems using RWPT in media with multiple zero flux interfaces. In section 5.4, the results obtained for different geometries of grains and pores are presented and discussed. An upscaling method using spatial moments (such as $\sigma_{xx}^2(t)$) is applied to the micro-scale simulation results to deduce macroscopic properties. The conclusive section 5.5 recapitulates results and discusses extensions.

5.2 Theory

5.2.1 PDE's for initial-value problems in infinite domains and with one zero-flux BC

5.2.1.1 The Gaussian function (PDF)

Let us define the initial-value problem (Cauchy's problem) in an infinite porous domain:

$$\begin{cases} \forall t>0; \forall x \epsilon \mathbb{R}; & \frac{\partial C}{\partial t}(x,t) = -V \frac{\partial C}{\partial x}(x,t) + D \frac{\partial^2 C}{\partial x^2}(x,t) \\ \forall t>0; & \lim\limits_{x \to \pm\infty} C(x,t) = 0 \\ \forall x \epsilon \mathbb{R}; & C(x,0) = \frac{M_0}{\theta} \delta(x - x_0) \end{cases} \tag{5.2.1}$$

where θ is the porosity, M_0 the initial mass of solute at $x = x_0$, and C is the mass concentration of solute per volume of solvent [kg/m in 1D].

The solution of Eq.5.2.1, is:

$$\forall t>0; \forall x \epsilon \mathbb{R};\ C(x,t) = \frac{M_0}{\theta} \frac{1}{\sqrt{4\pi D t}} exp\left(-\frac{(x-(x_0+Vt))^2}{4Dt} \right) \tag{5.2.2}$$

Eq.5.2.2 can be written as follows:

$$\forall t>0; \forall x \epsilon \mathbb{R};\ C(x,t) = \frac{M_0}{\theta} G(x_0 + Vt, 2Dt; x) \tag{5.2.3}$$

where $G(x_0 + Vt, 2Dt; x)$ is the Gaussian function (PDF) with mean $x_0 + Vt$ and variance $2Dt$. For instance, $G(0, 2t; x)$ is the fundamental solution of the heat equation [Evans, 2010].

$N\left(\mu, \sigma^2\right)$ denotes a Gaussian Random Variable (RV) with mean μ and variance σ^2, which means it has the probability density function (PDF) $x \to G\left(\mu, \sigma^2; x\right)$.

The initial value PDE problem for pure diffusion ($V = 0$) in 2D space is:

$$\begin{cases} \forall t > 0; \forall (x,y)\, \epsilon \mathbb{R}^2; & \frac{\partial C}{\partial t}(x,y,t) = D\left(\frac{\partial^2 C}{\partial x^2}(x,y,t) + \frac{\partial^2 C}{\partial y^2}(x,y,t)\right) \\ \forall t > 0; & \lim\limits_{x,y \to \pm\infty} C(x,y,t) = 0 \\ \forall (x,y)\, \epsilon \mathbb{R}^2; & C(x,y,0) = \frac{M_0}{\theta}\delta(x - x_0, y - y_0) \end{cases} \tag{5.2.4}$$

The solution of Eq.5.2.4 is:

$$\forall t > 0; \forall x \epsilon \mathbb{R};\ C(x,y,t) = \frac{M_0}{\theta} G\left((x_0,y_0), 2Dt; (x,y)\right) \tag{5.2.5}$$

where $G\left((x_0,y_0), 2Dt; (x,y)\right)$ is the bi-variate Gaussian PDF with mean (x_0, y_0) and isotropic variance $\sigma_x^2(t) = \sigma_y^2(t) = 2Dt$. The bi-variate Gaussian of Eq.5.2.4 will be used in subsequent subsections.

5.2.1.2 Semi-infinite domain with zero flux BC

In a semi-infinite 1D domain with a zero flux boundary condition at $x = x_{BC}$ the diffusion of an Initial-value located at $x = x_0$ is governed by the following system of equations:

$$\begin{cases} \forall t > 0; \forall x \epsilon\,]-\infty; x_{BC}]\,; & \frac{\partial C}{\partial t}(x,t) = D\frac{\partial^2 C}{\partial x^2}(x,t) \\ \forall t > 0; & \lim\limits_{x \to -\infty} C(x,t) = 0 \\ \forall t > 0; & -\theta D \frac{\partial C}{\partial x}(x_{BC},t) = 0 \\ \forall x \epsilon\,]-\infty; x_{BC}]\,; & C(x,0) = \frac{M_0}{\theta}\delta(x - x_0) \end{cases} \tag{5.2.6}$$

The solution of Eq.5.2.11 is Eq.5.2.8 (similar to the one found in [Carslaw & Jaeger, 1959]):$\forall t > 0; \forall x \epsilon\,]-\infty; x_{BC}]\,;$

$$C(x,t) = \frac{M_0}{\theta}\left(G(x_0, 2Dt; x) + G(2x_{BC} - x_0, 2Dt; x)\right) \tag{5.2.7}$$

Eq.5.2.8 could be written as:

$$C(x,t) = \frac{M_0}{\theta}\left(G(x_0, 2Dt; x) + L_{BC}\left(G(x_{BC}, 2Dt; x)\right)\right) \tag{5.2.8}$$

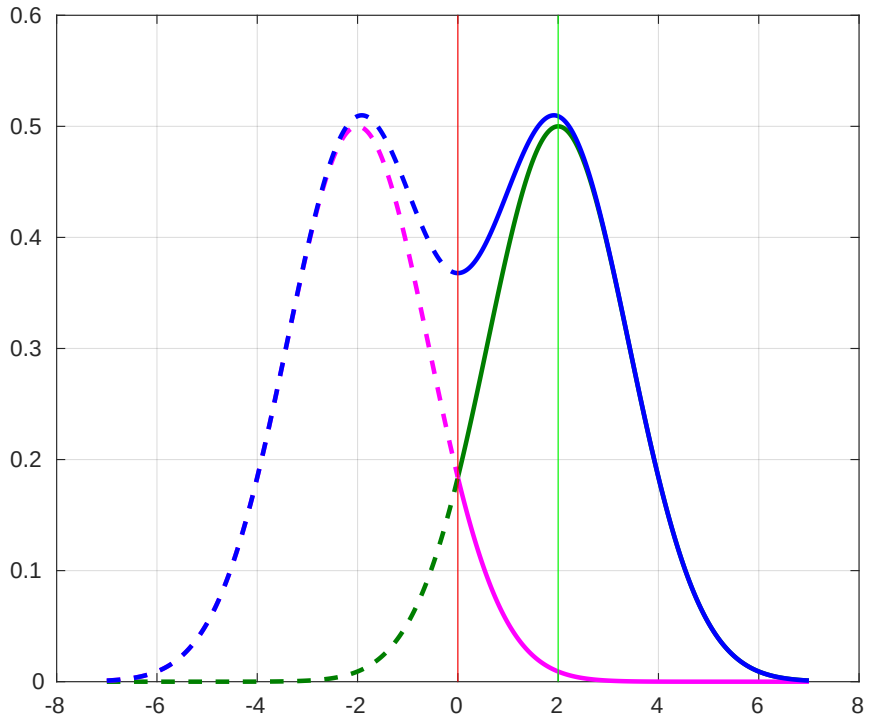

Figure 5.2.1: Plot of different terms of Eq.5.2.8 and Eq.5.2.8. The red vertical line represents the interface: BC with zero-flux. The green vertical line is the initial source position located at $x = 2$. The bold curves are the solutions inside the domain of interest, while the dashed curves are the same solutions extended outside the domain. The green bold curve is a Gaussian: the source solution in an infinite domain. The magenta curve is the symmetric Gaussian of the green one relative to the interface. The bold blue curve is the left hand side of Eq.5.2.8 and Eq.5.2.8, it is the sum of the green and magenta curves.

where L_{BC} is a linear application that transforms $G(x_0, 2Dt; x)$ into $G(2x_{BC} - x_0, 2Dt; x)$. Notice here, that $L_{BC}(G(x_0, 2Dt; x))$ is the symmetric of $G(x_0, 2Dt; x)$ relative to $x = x_{BC}$ (see Figure 5.2.1).

In the 2D case Eq.5.2.11 becomes:

$$\begin{cases} \forall t>0; \forall x \epsilon \left]-\infty; x_{BC}\right]; \forall y \epsilon \mathbb{R}; & \frac{\partial C}{\partial t}(x,y,t) = D\left(\frac{\partial^2 C}{\partial x^2} + \frac{\partial^2 C}{\partial y^2}\right)(x,y,t) \\ \forall t>0; & \lim\limits_{x,y\to-\infty} C(x,y,t) = 0 \\ \forall t>0; \forall x \epsilon \left]-\infty; x_{BC}\right]; & \lim\limits_{y\to+\infty} C(x,y,t) = 0 \\ \forall t>0; \forall y \epsilon \mathbb{R}; & -\theta D \frac{\partial C}{\partial x}(x_{BC},y,t) = 0 \\ \forall x \epsilon \left]-\infty; x_{BC}\right]; \forall y \epsilon \mathbb{R}; & C(x,y,0) = \frac{M_0}{\theta}\delta(x-x_0, y-y_0) \end{cases} \tag{5.2.9}$$

The solution of this equation (Eq.5.2.9) is the following combination of Gaussians:

$\forall t>0; \forall x \epsilon \left]-\infty; x_{BC}\right]; \forall y \epsilon \mathbb{R};$

$$C(x,y,t) = \frac{M_0}{\theta}\left(G\left((x_0,y_0), 2Dt; (x,y)\right) + G\left((2x_{BC}-x_0, y_0), 2Dt; (x,y)\right)\right) \tag{5.2.10}$$

The half-domain solution Eq.5.2.9 (with zero-flux BC) will be used in subsequent subsections.

5.2.2 PDE solutions under various geometries with zero-flux BC's

The concentration based analytical solutions shown in this section have been checked by direct substitution in their respective system of equations and their initial and boundary conditions. They take the form of infinite series. Their convergence is studied in C. Using the same concept shown in this section for 2D analytical solutions, these solutions could be extended to solve 3D problems. An analogous method, to the one used (in this subsection 5.2.2) to find these analytical solutions, will be applied to RWPT (in the next subsection 5.3.2) to develop an algorithm that treats multiple interfaces.

5.2.2.1 1D Zero Flux, finite domain

As explained in subsection 5.2.1.2 and 5.3.1.2, the solution of a semi-infinite domain with a zero flux boundary condition can be expressed as: the sum of the solution in an infinite domain G and of its symmetric relative to the position of the boundary $L_{BC1}(G)$[1]. Thus, $L_{BC1}(G)$ added to G could be considered as a correction so that it fits the zero flux BC number 1.

$$\begin{cases} \forall t > 0; \forall x \epsilon [x_{BC1}; x_{BC2}]; & \frac{\partial C}{\partial t}(x,t) = D\frac{\partial^2 C}{\partial x^2}(x,t) \\ \forall t > 0; & -\theta D\frac{\partial C}{\partial x}(x_{BC1},t) = 0 \\ \forall t > 0; & -\theta D\frac{\partial C}{\partial x}(x_{BC2},t) = 0 \\ \forall x \epsilon [x_{BC1}; x_{BC2}]; & C(x,0) = \frac{M_0}{\theta}\delta(x - x_0) \end{cases} \tag{5.2.11}$$

Therefore, in this chapter, to solve the problem of Eq.5.2.11 with two zero flux BC's, we propose to apply the same concept for both BC's, i.e. add also $L_{BC2}(G)$ to the solution G so that it fits zero flux BC number 2 too. However, although G has now been corrected to fit both BC's, $L_{BC1}(G)$ and $L_{BC2}(G)$ do not fit zero flux $BC2$ and $BC1$ respectively. Hence, once again, using the same algorithm $L_{BC1}(G)$ is corrected by adding $L_{BC2}(L_{BC1}(G))$, so that $L_{BC1}(G) + L_{BC2}(L_{BC1}(G))$ does fit zero flux $BC2$. Similarly, $L_{BC2}(G)$ is corrected by adding $L_{BC1}(L_{BC2}(G))$, so that $L_{BC2}(G) + L_{BC1}(L_{BC2}(G))$ does fit zero flux $BC1$. Eq.5.2.12 shows how G (the solution of the infinite domain) is corrected by adding the red and blue terms to fit $BC1$ and $BC2$ respectively. Then, the red and blue terms are corrected by adding. The difference in color is to show that for each correction we add a new layer of corrections and so on and so forth.

$$C = G + L_{BC1}(G) + L_{BC2}(G) + L_{BC2}(L_{BC1}(G)) + L_{BC1}(L_{BC2}(G)) + ... \tag{5.2.12}$$

[1] Analogy with the method of images

Eq.5.2.12 becomes an infinite series (Eq.5.2.13) after applying the concept of correction (or superposition) indefinitely.

$$C = \sum_{i=0}^{+\infty} (id + L_{BC1}) (L_{BC2} L_{BC1})^i (id + L_{BC2}) (G) \tag{5.2.13}$$

Eq.5.2.13 can also be written as the following infinite series:

$$\forall t > 0; \forall x_{BC1} \leq x \leq x_{BC2}; \frac{\theta}{M_0} C^x_{BC12}(x,t) = G(x_0, 2Dt, x) +$$

$$+ \sum_{i=1}^{+\infty} (G(-2il_{x1-2} + x_0, 2Dt, x) + G(2il_{x1-2} + x_0, 2Dt, x) +$$

$$+ G(-2il_{x1-2} + x_{BC1} - x_0, 2Dt, x) + G(2il_{x1-2} + x_{BC2} - x_0, 2Dt, x)) \tag{5.2.14}$$

where $l_{x1-2} = x_{BC1} - x_{BC2}$.

5.2.2.2 2D Zero Flux, finite in X and infinite in Y

In 2D, the solution is the product obtained by multiplying the 1D solution in X direction and in Y direction. Thus, the solution in the X and Y directions are independent. In Figure 5.2.2, the 2D Zero Flux finite domain in X direction and infinite in Y direction, there is no BC in the Y direction. Therefore, the solution is a Gaussian in the Y direction multiplied by the solution in the X direction Eq.5.2.14 obtained in subsection 5.2.2.1. This yields:

$\forall t \geq 0; \forall x_{1:2} \leq x \leq x_{2:3}; \forall y \epsilon \mathbb{R};$

$$\frac{\theta}{M_0} C(x,y,t) = G(y_0, 2Dt, y) \times \frac{\theta^x}{M_0} C^x_{BC12}(x,t) \tag{5.2.15}$$

5.2.2.3 2D Zero Flux, semi-infinite domain in X and Y directions

In this problem, there is one zero flux BC for the X and Y directions. Hence, the principle of correction (explained in subsection 5.2.2.1) must be applied so that the solution fits the zero flux BC in X and Y directions (instead of

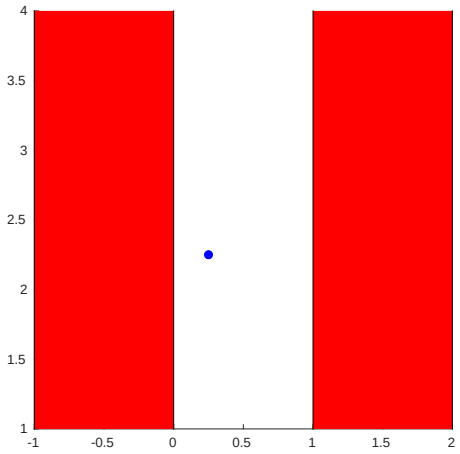

Figure 5.2.2: 2D parallel zero flux interfaces

$BC1$ and $BC2$ of the same direction as in subsection 5.2.2.1). Since X and Y are independent, then the solution of this problem (see Figure 5.2.3) is the solution of the 1D semi-infinite problem in X multiplied by the solution of the 1D semi-infinite problem in Y. Hence, in this case the solution is not an infinite series but only the sum of four Gaussian functions.

$$C = (id + L^x_{BC})\,(id + L^y_{BC})\,(G) \tag{5.2.16}$$

$$\frac{\theta}{M_0} C\,(x, y, t) = G\,((x_0, y_0)\,, 2Dt, (x, y)) + G\,((2x_{12} - x_0, y_0)\,, 2Dt, (x, y)) + \\ + G\,((x_0, 2y_{23} - y_0)\,, 2Dt, (x, y)) + G\,((2x_{12} - x_0, 2y_{23} - y_0)\,, 2Dt, (x, y)) \tag{5.2.17}$$

5.2.2.4 2D Zero Flux, finite domain in X, finite or semi-infinite in Y

The solution of the initial value problem finite in X and semi-infinite in Y (see Figure 5.2.4) is the solution of the 1D finite in X problem multiplied by the solution of the 1D semi-infinite in Y problem.

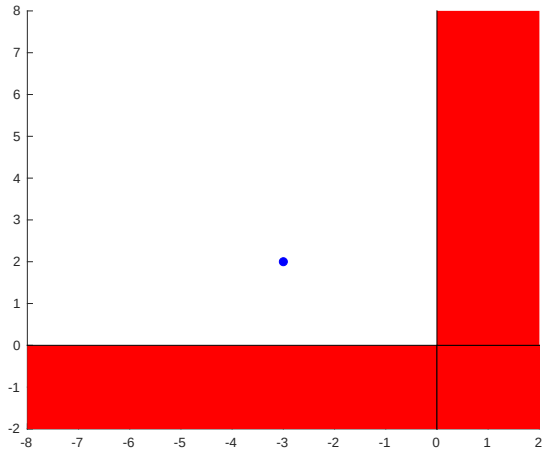

Figure 5.2.3: 2D semi-infinite domain in X and Y directions

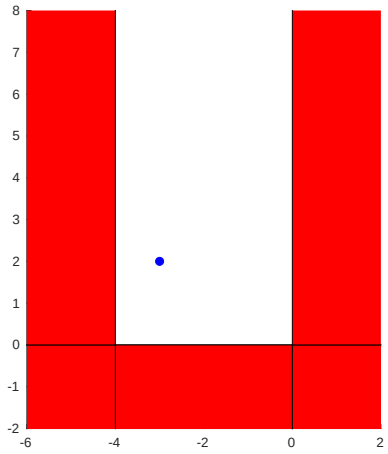

Figure 5.2.4: 2D finite domain in X and semi-infinite in Y

$\forall t \geq 0; \forall x_{1:2} \leq x \leq x_{2:3};$

$$\frac{\theta}{M_0} C(x,y,t) = \left[G(y_0, 2Dt, y) + G(2y_{BC} - y_0, 2Dt, y)\right] \frac{\theta^x}{M_0} C^x_{BC12}(x,t) \tag{5.2.18}$$

The solution of the initial value problem finite in X and Y (see Figure 5.2.5)

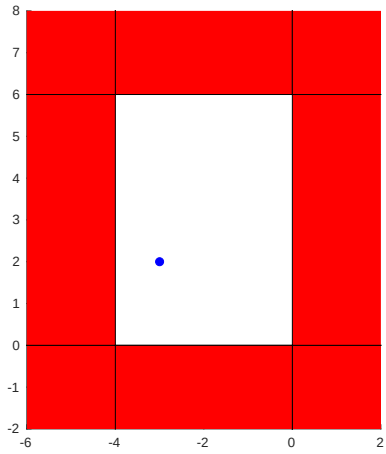

Figure 5.2.5: 2D finite domain in X and Y

is the solution of the 1D finite in X multiplied by the solution of the 1D finite in Y problem.

$\forall t \geq 0; \forall x_{1:2} \leq x \leq x_{2:3};$

$$\frac{\theta}{M_0} C(x,y,t) = \frac{\theta^y}{M_0} C^y_{BC12}(y,t) \frac{\theta^x}{M_0} C^x_{BC12}(x,t) \tag{5.2.19}$$

5.2.2.5 Recapitulation

The method, used here to find concentration based solutions $C(x,y,t)$, was applied to different initial-Boundary-value problems with cartesian parallel interfaces serving as zero-flux planes. In these problems, each and every interface is infinite. Even when the domain is finite in one direction, the interface of this same direction is supposed to be infinite. This last condition restricts the application of this method to geometries with the above configurations (Figure 5.2.2, 5.2.3, 5.2.4, 5.2.5). These configurations, allow the solution to be the product of the 1D solution in one direction multiplied by the 1D solution of the other direction. In the following subsection 5.3.2, it is suggested that the

independence between the two directions in these concentration based solutions implies an independence between the $X(t)$ and $Y(t)$ positions of particles in RWPT.

5.2.3 From particle positions to concentration

Let us consider now a particle based method to solve Initial-value problems. The concentration will be determined from the particles positions distribution PDF.

$$C(x,t) = \int_{\mathbb{R}} C(X_t,t)\,\delta(X_t - x)\,dX_t \tag{5.2.20}$$

$$C(x,t) = \int_{\mathbb{R}} \delta(X_t - x)\,dm_t \tag{5.2.21}$$

where X_t and dm_t represent, respectively, the position and mass of an infinitesimal concentration packet (to be discretized as a "particle").

5.3 Methods and Algorithms

This section uses the same principle to solve concentration based PDE's (see subsection 5.2.2) to induce a RWPT algorithm that solves diffusion problems in more complex geometries (compared to the geometries of subsection 5.2.2).

5.3.1 RWPT methods with one zero flux BC

RWPT methods are primarily inspired from initial-value problems (see Subsection 5.2.1). These methods consider particles to be independent. Therefore, if a particle does not encounter any interface, then it will be considered as if it were in an infinite domain, and follows the corresponding algorithm. While particles that do encounter interfaces (e.g. interface with zero flux BC), their algorithm will be altered.

5.3.1.1 RWPT in an infinite domain

To solve Eq.5.2.1 using particle methods. For a time t. We need to generate particles with a PDF equivalent to Eq.5.2.2. Thus, these particles must follow the RV $N\left(x_0 + Vt, 2Dt\right)$, hence:

$$X_t = N\left(x_0 + Vt, 2Dt\right) \tag{5.3.1}$$

Using simple Gaussian RV operations, we obtain:

$$X_t = x_0 + V\,t + \sqrt{2\,D\,t}\;N\left(0,1\right) \tag{5.3.2}$$

where $N\left(0,1\right)$ is a Gaussian RV, with 0 mean and unit variance.

In conclusion, the PDF of RV X_t is identical to the concentration solution in Eq.5.2.2 divided by $\frac{M_0}{\theta}$.

In 2D, to solve a pure isotropic diffusion problem Eq.5.2.4 using a particle method $\mathbf{X}_t$ must be:

$$\mathbf{X}_t = \begin{pmatrix} x_0 \\ y_0 \end{pmatrix} + \sqrt{2\,D\,t}\;\begin{pmatrix} N_x\left(0,1\right) \\ N_y\left(0,1\right) \end{pmatrix} \tag{5.3.3}$$

where $N_x\left(0,1\right)$ and $N_y\left(0,1\right)$ are Gaussian RV, with 0 mean and unit variance.

5.3.1.2 RWPT in semi-infinite domain with zero flux BC

Let us define Ω_{BC} and Ω^*_{BC} as: $\Omega_{BC} =]-\infty; x_{BC}]$ and $\Omega^*_{BC} = [x_{BC}; +\infty[$, so $\Omega_{BC} \bigcup \Omega^*_{BC} = \mathbb{R}$. In subsection 5.2.1.2, we have shown that, the solution of the semi-infinite domain with zero flux BC could be written as the sum of: the solution of the infinite domain G and its symmetric $L_{BC}\left(G\right)$ relative to the position of the interface $x = x_{BC}$. Both are truncated on the semi-infinite domain Ω_{BC}. On the other hand, $L_{BC}\left(G\right)$ truncated on Ω_{BC} is the symmetric of G truncated on Ω^*_{BC}. Therefore, in RWPT methods, G truncated on Ω_{BC} represent the particles that did not reach the interface. These particles algorithm (i.e. infinite domain algorithm) is not altered because G is the solution

of the infinite domain[2]. Whereas, $L_{BC}(G)$ truncated on Ω_{BC} symmetry is considered as if the particles that crossed the interface were totally reflected (i.e. their final position is the symmetric relative to the interface). Hence, the particles Random Walk algorithm becomes, in the presence of a zero-flux plane at $x = x_{BC}$:

$$\begin{cases} \forall p & X_t^p = N^p(x_0, 2Dt) \\ If\,(X_t^p > x_{BC}) & X_t^p = 2x_{BC} - x_0 - \sqrt{2\,D\,t}\;N^p(0,1) \end{cases} \tag{5.3.4}$$

Note here that N^p is a Gaussian random variate, i.e. a given realization of the Gaussian Random Variable, for particle number p. Since its outcome is known, it can be compared to the interface position x_{BC}.

5.3.2 Multiple zero flux interfaces for RWPT

In RWPT methods, after crossing one interface, particles may eventually cross multiple interfaces. First, because the spatial step depends on a Gaussian RV, which has unbounded values. Secondly, in multidimensional problems, particles located near a corner, e.g. around two perpendicular interfaces, might cross the interfaces forming this corner [Uffink, 1985, Labolle et al., 1996, Salamon et al., 2006, Bechtold et al., 2011]. Thus, the algorithm governing particles displacements must take into account such possibility. Therefore, this subsection proposes a generalization, analogous to the concept of subsection 5.2.2, of the algorithm used to a single interface with zero flux boundary Eq.5.3.4 to treat multiple interfaces.

[2]These considerations (properties) are due to the linearity of the corresponding PDE problem. A superposition principle is being applied; and there are analogies with Green's functions approach and with the method of images as well.

Algorithm 5.1 RWPT algorithm in a bounded domain with zero flux BC's

$$\begin{cases} \forall p & X^p\left(t^{n+1}\right) = X^p\left(t^n\right) + \sqrt{2D\left(t^{n+1}-t^n\right)}\, N^{n;p}\left(0,1\right) \\ \textbf{While } \left(X^p\left(t^{n+1}\right) \notin \left[x_{BC1}; x_{BC2}\right]\right) & \\ \textbf{If } \left(X^p\left(t^{n+1}\right) < x_{BC1}\right) & X^p\left(t^{n+1}\right) = 2x_{BC1} - X^p\left(t^{n+1}\right) \\ \textbf{ElseIf } \left(X^p\left(t^{n+1}\right) > x_{BC2}\right) & X^p\left(t^{n+1}\right) = 2x_{BC2} - X^p\left(t^{n+1}\right) \\ \textbf{End} & \\ \textbf{End} & \end{cases}$$

5.3.2.1 RWPT zero flux BC in 1D

Using an analogous method to the one used to solve concentration based problem with two zero flux BC's (see subsection 5.2.2.1), and combining it with the RWPT algorithm for one zero flux BC described in subsection 5.3.1.2, the 1D RWPT for two zero flux BC's becomes:

The method, used in subsection 5.2.2.1 to solve the concentration based problem with two zero flux BC's, is similar to the use of the method of images through infinite superpositions. Each time it was used, it corrected the new term to fit the boundary condition.

In RWPT, the method of images becomes a total particle reflection. If the new particle position is outside the domain $[x_{BC1}; x_{BC2}]$, it represents, in term of PDE's, the tail of the solution that it is outside of the domain and needs to be corrected again. That is why reflections are repeated until the particle's final position becomes inside the domain $[x_{BC1}; x_{BC2}]$. Note here that the number of reflections is finite, because spatial particles steps are finite. This algorithm does not have restrictions on the time step. Therefore, the time step can be set equal to the final simulation time.

5.3.2.2 RWPT zero flux, interfaces in 2D

Subsection 5.2.2 presented 2D analytical solutions for various zero flux configurations. In all these configurations interfaces are infinite. This condition allows the concentration based solutions to be the product of the 1D solution in one direction multiplied by the 1D solution in the other direction. In RWPT, if the PDE of the stochastic process could be written as the product of the PDE's of its components, then the position of X and Y are independent. In this case, there are no restrictions on the time step and the 2D RWPT algorithm can be expressed as Algorithm 5.1 applied to X and Y.

On the other hand, if interfaces are not infinite, then it can be demonstrated that the concentration based solution cannot be written as a product of two functions with separate and independent variables. Therefore, the proposed following algorithm is a generalization of the infinite interface case taking into account the case of finite interfaces and complex geometries in a cartesian mesh.

5.3.2.3 Discussion on time step size

The algorithm 5.1 requires particles to encounter interfaces that are only parallel to each other. Hence, the generalization to Algorithm 5.2. However, this algorithm (Algorithm 5.2) requires a time step small enough that most particles do not encounter multiple horizontal and vertical interfaces during a single time step. Therefore, the maximum spatial step of a particle should not be greater than the characteristic length of the micro-geometry. This limitation could be interpreted in terms of constraints as follows:

$$max\left(\Delta X_{step}\right) \leq \lambda_{PORE} \tag{5.3.5}$$

$$max\left(\sqrt{2D\Delta t}\ Z\right) \leq \lambda_{PORE} \tag{5.3.6}$$

Algorithm 5.2 2D RWPT for infinite or not infinite interfaces with zero flux condition

1. Consider particle (p) with mass m_p and position $X_1^{(p)}$ and $X_2^{(p)}$.
2. For $i\epsilon\{1;2\}$;$X_i^{(p)}\left(t^{n+1}\right) = X_i^{(p)}\left(t^n\right) + \sqrt{2D\left(t^{n+1}-t^n\right)}N_i^{n;p}\left(0,1\right)$
3. $\begin{cases} X_i^{(p)}\left(t^{n+1}\right) = X_i^{(p)}\left(1\right); & X_i^{(p)}\left(t^n\right) = X_i^{(p)}\left(0\right) \\ u = sign\left(N^{n;p}\left(0,1\right)\right) & t^0 = 0 \end{cases}$
4. **while** particle (k) crosses interfaces **do**
   a) Calculate the times t_1 and t_2 when (k) reach the nearest interface in the X and Y directions
   b) $[I;t_I] = min(t_1,t_2)$; i is the direction that reached its interface first (I could be either direction 1 or 2) and t_I is its corresponding time
   c) $\begin{cases} X_I^{(p)}\left(0\right) = X_{Interface} \\ X_{3-I}^{(p)}\left(0\right) = X_{3-I}^{(p)}\left(0\right) + u_{3-I}\sqrt{2D}\left(\sqrt{t_I}-\sqrt{t^0}\right)N_I^{n;p}\left(0,1\right) \end{cases}$
   d) $\begin{cases} u_I = -u_I \quad t^0 = t_I \end{cases}$
   e) $\begin{cases} i\epsilon\{1;2\}; \quad X_i^{(p)}\left(1\right) = X_i^{(p)}\left(0\right) + u_i\sqrt{2D}\left(\sqrt{\left(t^{n+1}-t^n\right)}-\sqrt{t_I}\right)N_i^{n;p}\left(0,1\right) \end{cases}$
5. **end**

where Z is a normalized Gaussian RV $N\left(0,1\right)$.

$$\Delta t \leq \frac{\lambda_{PORE}^2}{2D\left(max\left(Z\right)\right)^2} \tag{5.3.7}$$

For this problem of 2D Grain/Pore, the maximum absolute value of the Gaussian RV will not exceed 7 in practice (knowing that the probability of the absolute value of a normal Gaussian RV to exceed 7 is around 10^{-12}). Hence Eq.5.3.7 becomes:

$$\Delta t \leq 10^{-2}\frac{\lambda_{PORE}^2}{D_{PORE}} \tag{5.3.8}$$

In addition, we should keep in mind that for the same simulation time, a small time step costs more in term of computational time compared to a larger time step. Hence, we choose the largest time step that verifies condition Eq.5.3.8. In the following subsection we take $\lambda_{PORE} = 1$ and $D_{PORE} = 1$,

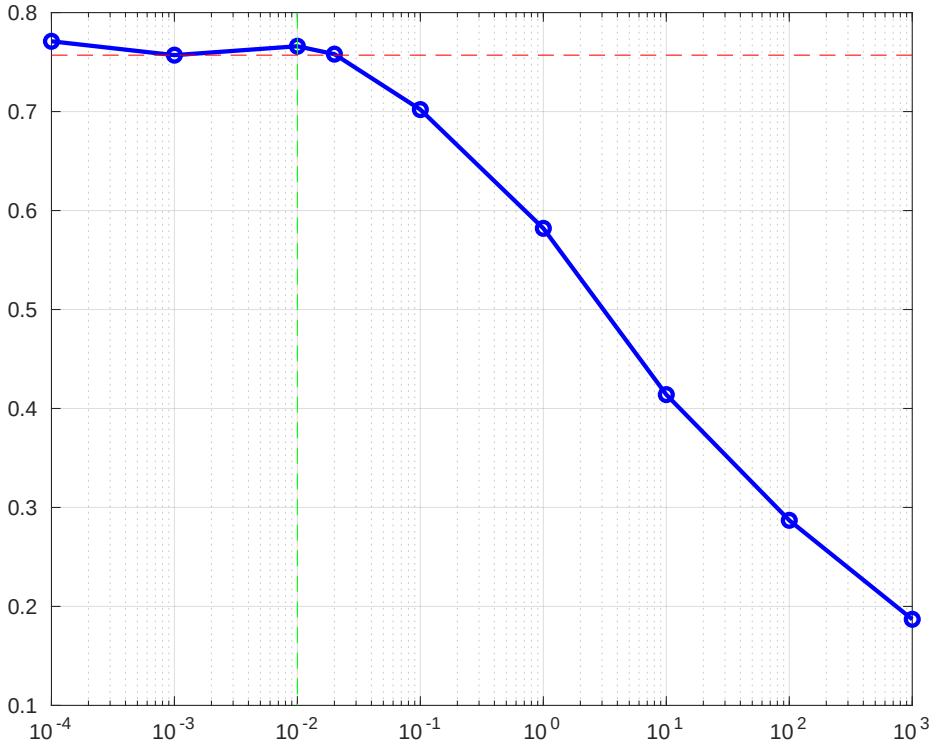

Figure 5.3.1: Effective diffusivity vs Time step. The bold blue curve represents the effective diffusivity plotted against the time step chosen for the simulation. The horizontal dashed red line correspond to the value of effective diffusivity using a time step $\Delta t = 10^{-3}$ (or roughly $\Delta t \leq 10^{-2}$). The vertical dashed green line corresponds to the time step $\Delta t = 10^{-2}$ used in all subsequent simulations.

therefore the time step is equal to $\Delta t = 10^{-2}$. Furthermore, to validate $\Delta t = 10^{-2}$, we repeated the same simulations with different time steps. The result in terms of the calculated effective Diffusion coefficient (explained later) is shown in Figure 5.3.1 versus time step size. It is clear that the $\Delta t \leq 10^{-2}$ is adequate and required.

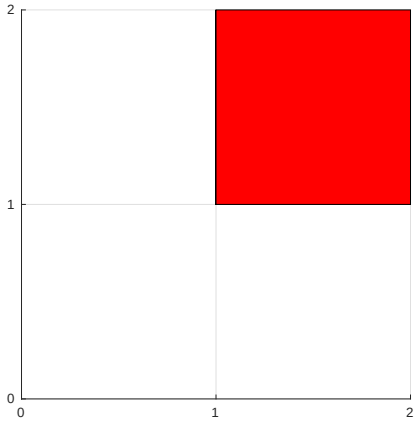

Figure 5.3.2: 2D Micro-model motif for a 75% porosity. The red square represents the Grain, the white region represents the pore.

5.3.3 Grain pore Micro-model

5.3.3.1 Grain/Pore motif and pattern

This subsection describes the first configuration of the geometry that will be studied. Figure 5.3.2 represents the Grain/Pore motif that will be repeated, periodically and indefinitely, to create the infinite domain geometry. The red square corresponds to the grain while the pore is in white. The area of the pore divided by the area of the whole motif (Grain/Pore), is the porosity of the motif (this case $\theta = 75\%$). Since the infinite domain geometry is a periodic repetition of the previous motif (see Figure 5.3.3), then the effective porosity of the infinite domain is the same: $\theta_{eff} = 75\%$.

5.3.3.2 Representative Elementary Volume (REV)

For this kind of periodic structure, we could naively imagine that the REV would be composed of one grain and three pores as shown in Figure 5.3.2. However, for this particular problem of the diffusion from an initial source in

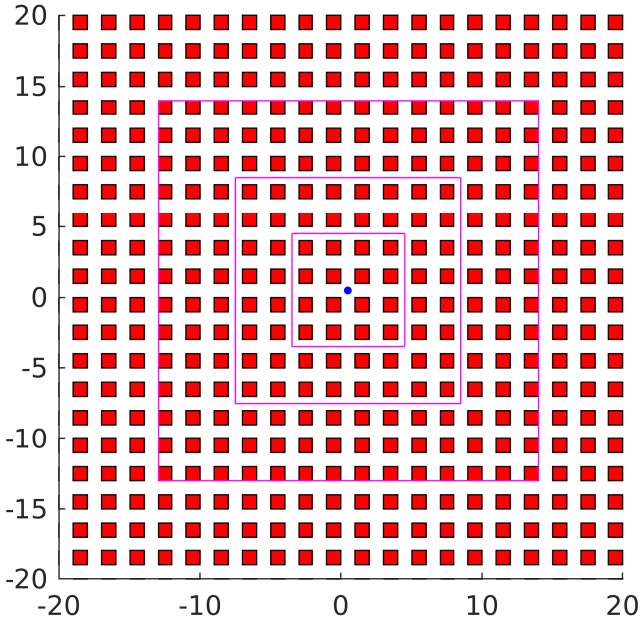

Figure 5.3.3: 2D Micro-model comprising 20×20 grains (red squares). The blue dot in the center is used as the initial source. The three examples of squares in magenta represent upscaling domains of various sizes .

an infinite domain, we will later define the REV using a convergence criterion for macroscopic properties (such as effective diffusivity).

The first macroscopic property to be studied here is the porosity (θ). To define the REV using the macroscopic porosity, we define first a square surface (in 3D we would have used a volume) in which the effective porosity is calculated. In most cases, the surface is taken as a disc (sphere in 3D), but here, in the interest of simplicity, we take a square. This area will be related to a "Radius" (distance from the center (the initial source position) to the area's edge). This "Radius" is equal to half the edge of the square, in the case of a disc this distance is the radius of the disc. Later we will use this "Radius" to define the limits of our REV.

Figure 5.3.4 plots the porosity inside a square against the "Radius" of this

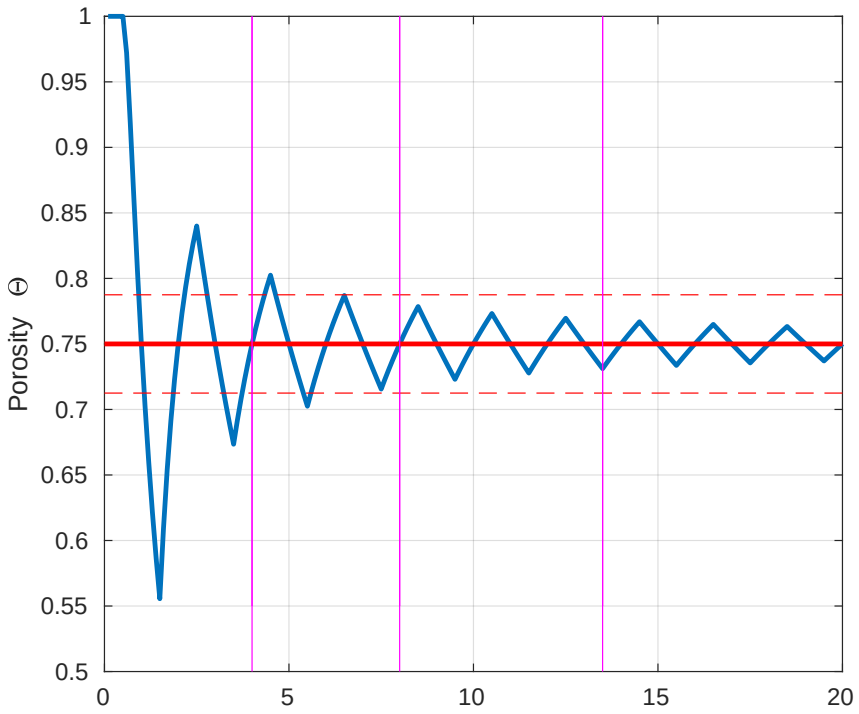

Figure 5.3.4: Porosity profile vs "Radius" of the upscaling domain expressed in pore size units in bold blue curve. The horizontal bold red line is the effective porosity of the infinite domain 75%. The horizontal dashed red lines are ±5% of the bold red line. The vertical magenta bold lines correspond to the three magenta squares in Figure 5.3.3.

square. In Figure 5.3.3 the blue dot represents the center of the square, and the three magenta squares are examples of areas over which the porosity is calculated. The three magenta vertical lines in Figure 5.3.4 correspond to the magenta squares in Figure 5.3.3.

Simulation time The simulation time should be large enough for the particles to explore the domain and the Representative Elementary Volume (REV). The simulation time can be estimated by equating the Domain Length (L_{REF})

to the standard deviation displacement (i.e. the so-called root-mean-square dispersion length). This yields the estimated simulation time for the particle cloud to reach the edges of the grain/pore domain:

$$T_{Simu} \sim \frac{L_{REF}^2}{2D_{eff}} \tag{5.3.9}$$

5.4 Results and Discussion

This section analyses the results of simulations of diffusion of an initial source inside pores of a composite media Pore/Grain. Different structures are studied, either isotropic or anisotropic and with different porosities. For each case, an upscaling method, using moments of particles positions, is applied to determine the macro-properties of the composite media (essentially, effective porosity tortuosity, and diffusion coefficient).

5.4.1 Isotropic grains ($\lambda_{Grain,X} = \lambda_{Grain,Y}$)

5.4.1.1 Porosity $\theta = 75\%$

The first Grain/Pore configuration, where the diffusion (Algorithm 5.2) will be tested, is the one described in Figure 5.3.3. An initial source diffuses inside the center of the pore at the position $(0.5; 0.5)$. The result of the simulation is shown in Figure 5.4.1. The blue dots represents the particles after time $t_F = 20$. This time is chosen so that enough particles have explored the periodic infinite domain.

Figure 5.4.2 is a zoom of Figure 5.4.1 centered on the position of the initial source $(0.5; 0.5)$. It shows clearly that particles are found anywhere but inside the squared grains. Algorithm 5.2 makes particles bounce off the grains.

After post-processing, as described in subsection 5.2.3, Figure 5.4.1 is obtained. In this Figure, concentrations $C(x, y)$ were computed as 2D histogram

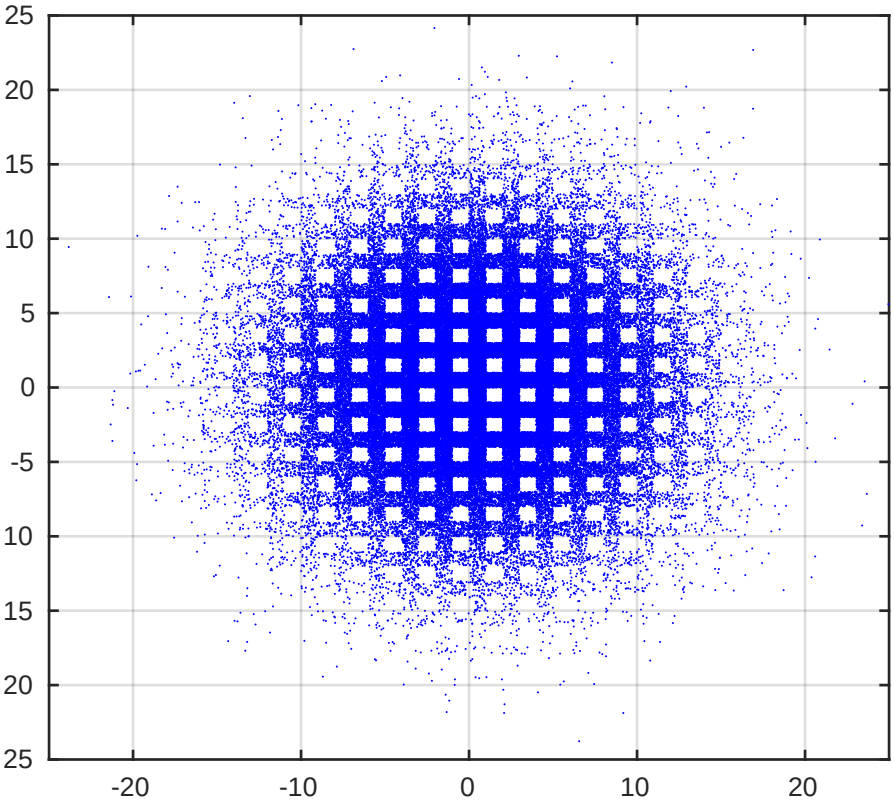

Figure 5.4.1: 2D plot of particles positions (blue dots): result of diffusion simulation at time $t_F > T_{Simu}$ in the geometry of Figure 5.3.3

based on the smallest histogram bins corresponding pore size λ_{PORE}. It represents the 2D concentration of particles. As one might predict, the highest concentrations are found near the center where the initial source was $(0.5; 0.5)$. Then, the concentration drops gradually while moving further away from the center, as expected.

Effective diffusivity There are different methods to calculate the effective diffusivity. The most common one in literature uses the concentration gradient in a Dirichlet bounded domain. This study uses the second order spatial

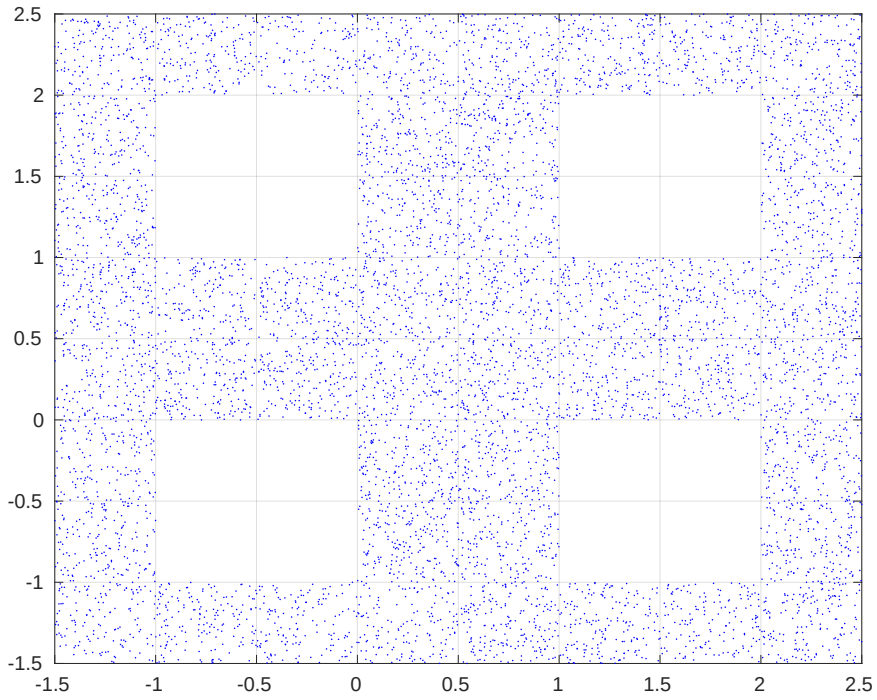

Figure 5.4.2: Zoom at the center of Figure 5.4.1: 2D plot of particles positions (blue dots) results of diffusion simulation at time $t_F > T_{Simu}$, in the geometry of Figure 5.3.3

moments of particles positions $M_2(t)$:

$$M_2(t) = \begin{pmatrix} \sigma_X^2 & \sigma_{XY} \\ \sigma_{YX} & \sigma_Y^2 \end{pmatrix} \tag{5.4.1}$$

If $M_2(t)$ is diagonal then $M_2(t) = \sigma^2(t) I$, with I is the identity matrix. Then, the effective diffusivity is determined by one of the two following equations:

$$D_{eff} = \frac{\sigma^2}{2t} \tag{5.4.2}$$

$$D_{eff} = \frac{1}{2} \frac{d\sigma^2}{dt} \tag{5.4.3}$$

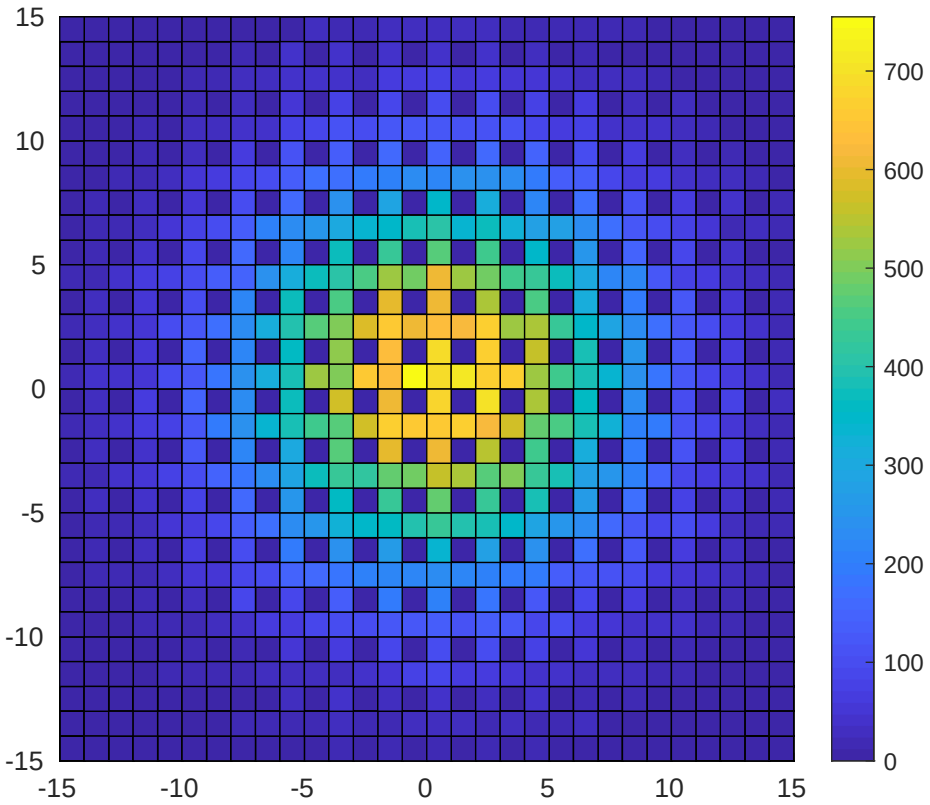

Figure 5.4.3: 2D plot of concentrations of the simulated particle cloud shown in Figure 5.4.1

Figure 5.4.4 and 5.4.5 plot the effective diffusivity as defined in Eq.5.4.2. The convergence of the effective diffusivity is defined as: it is convergent when its value stays between $\pm 1\%$ of its final mean value. This happens at around $t = 1$ close to the value predicted by Eq.5.3.9.

Initially, the effective diffusivity is equal to the diffusion coefficient inside the pore. D_{eff} stays equal to D_0 until particles start encountering grains interfaces. Then, as times goes by, particles bounce off the grains, which limits their diffusion, and D_{eff} starts slowly to decline, until it converges towards its

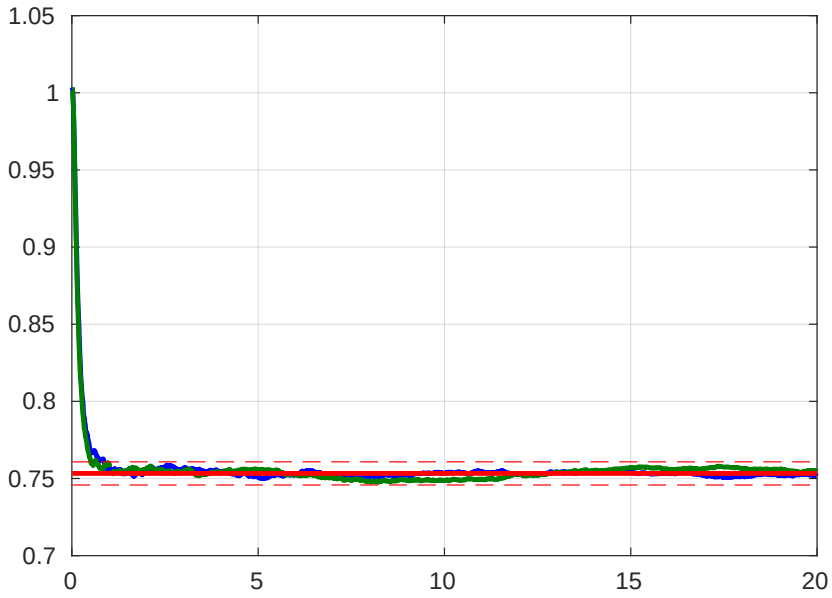

Figure 5.4.4: Effective diffusivity vs time. The blue and green bold curves are the variance of the position X and Y respectively divided by $(2 * t)$ with t is the time. The red bold line is the mean value of the variance 0.753. The red dashed lines are $\pm 1\%$ of the bold red line.

final value (because of the periodicity of the geometry).

5.4.1.2 Experiments with different porosities

Table 5.1 shows the results of different simulations with different Grain/Pore configurations. In all the configurations tested in this table, the grains are taken as squares, characterized by their size λ_{Grain}. Here the tortuosity is calculated as [Yong et al., 2014]:

$$\tau^2 = \frac{D_m}{D_{eff}} \tag{5.4.4}$$

with D_m the diffusion coefficient inside the pore.

Figure 5.4.6 shows the trajectories of 3 particles. The particles circumvent the grains (red squares), and that is what creates the tortuosity of the system.

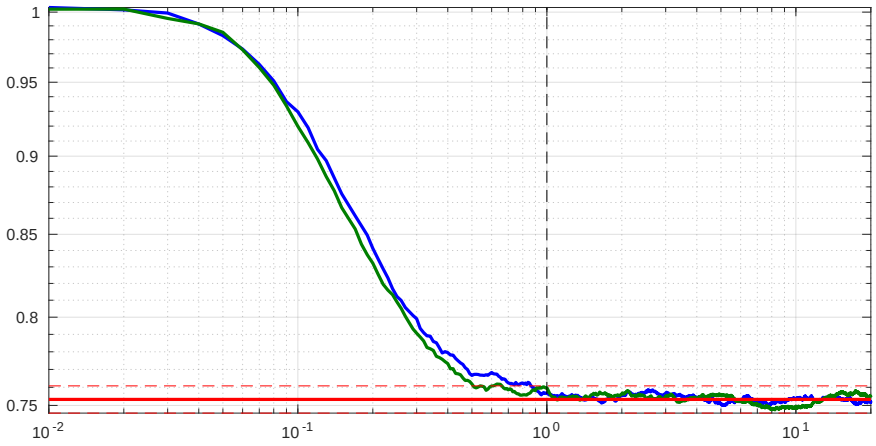

Figure 5.4.5: Log-log of Figure 5.3.1 effective diffusivity vs time. The blue and green bold curves are the variance of the position X and Y respectively divided by $(2 * t)$ with t is the time. The red bold line is the mean value of the variance 0.753. The red dashed lines are $\pm 1\%$ of the bold red line.

$\lambda_{Grain}/\lambda_{Pore}$	1	4	9	19	49	99
θ	75%	36%	19%	9,75%	3,96%	1,99%
D_{eff}	0.753	0.586	0.542	0.521	0.508	0.504
τ^2	1.33	1.71	1.84	1.92	1.97	1.98

Table 5.1: Porosity vs Effective diffusivity vs Tortuosity for different configurations

Figure 5.4.7 shows clearly that the effective tortuosity of the Grain/Pore geometry tends towards the geometric tortuosity:

$$\tau = \frac{\lambda_{Grain,X} + \lambda_{Grain,Y}}{\sqrt{\lambda^2_{Grain,X} + \lambda^2_{Grain,Y}}} \tag{5.4.5}$$

as found in the literature[Hunt & Sahimi, 2017]. When $\lambda_{Grain,X} = \lambda_{Grain,Y}$, then $\tau = \sqrt{2}$.

Figure 5.4.8 plots the tortuosity vs the porosity. This figure shows that for $\theta \in [0; 0.36]$ the tortuosity is linear with the porosity with a determination

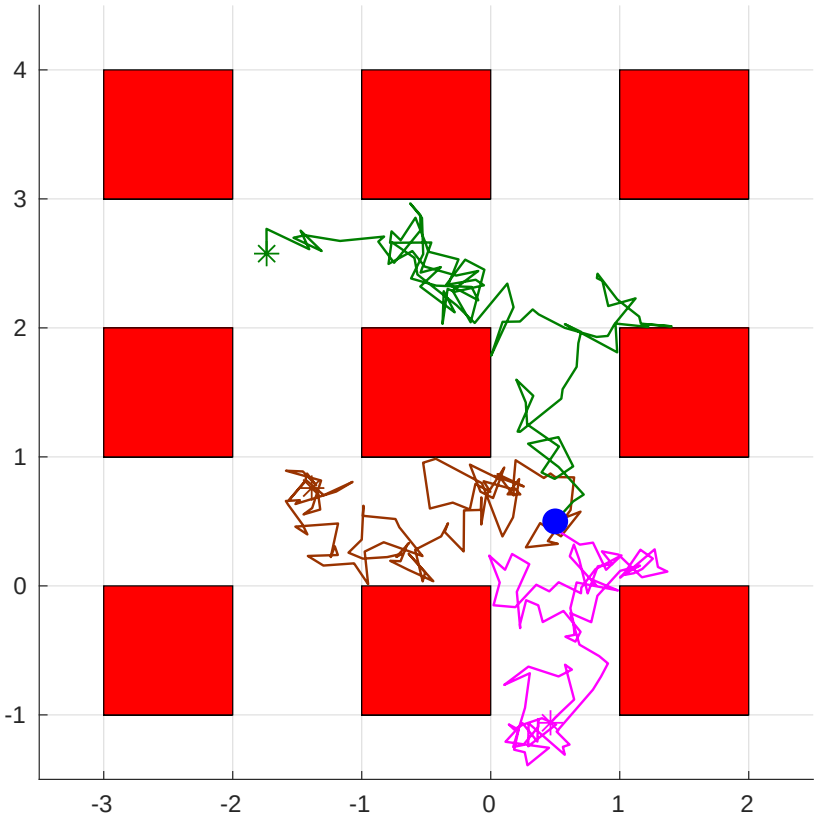

Figure 5.4.6: Plot of the trajectories (green, brown and magenta) of 3 particles inside the grain/pore system of Figure 5.3.3: the red squares are the grains and the white regions are the pores. The bold blue dot is the initial position $x = (0.5; 0.5)$ of the three particles. The green, brown and magenta stars are the final positions of the particles.

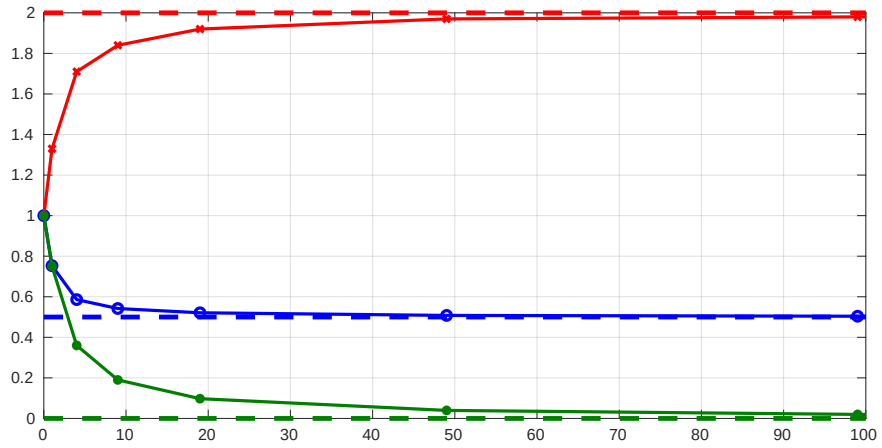

Figure 5.4.7: Plot of table5.1. Red, blue and green bold curves correspond, respectively, to the squared tortuosity, the effective diffusivity and the porosity. The dashed red, blue and green lines correspond to the squared geometric tortuosity ($\tau^2_{geo} = 2$), effective diffusivity ($D_{eff;geo} = 0,5$) and porosity ($\theta_{geo} = 0$).

coefficient $R^2 = 99.99\%$ and the corresponding empirical formula is:

$$\tau \approx \sqrt{2} - 0.3\theta = \tau_{geo} - 0.3\theta \tag{5.4.6}$$

5.4.2 Anisotropic grains ($\lambda_X > \lambda_Y$)

This subsection studies micro and macro-scopic diffusion in anisotropic geometries.

5.4.2.1 Anisotropic geometry with porosity $\theta = 75\%$

Figure 5.4.9 shows 2D concentration histogram of the result of an anisotropic test case with elongated grain $\lambda_X/\lambda_Y = 8$, and with the same porosity as previously used $\theta = 75\%$.

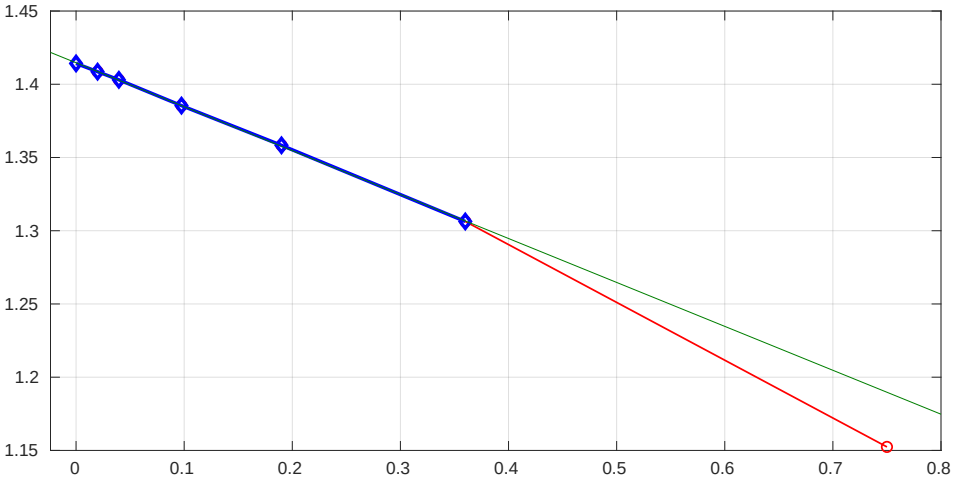

Figure 5.4.8: Tortuosity vs Porosity. The bold blue curve with diamonds is the tortuosity from $\theta \in [0; 0.36]$. The green line is a linear ($\tau = 1.41 - 0.3\theta$) fitting of the blue curve with an $R^2 = 99.99\%$. The red curve with circles is the torutosity from $\theta \in [0; 0.75]$.

5.4.2.2 Anisotropic geometry with porosity $\theta = 36\%$

Anisotropy ratio $\lambda_X/\lambda_Y = 2$. Figure 5.4.10,5.4.11 and 5.4.12 shows the results of the diffusion of an initial source inside the center of a pore. The domain is a periodic repetition of a motif Grain/Pore with rectangular grains. The grain's length is two times longer than its width, and six times longer than the width of the pore. The periodic repetition of this motif creates an anisotropic infinite domain with a porosity of $\theta = 36\%$.

Figure 5.4.13 and its zoom Figure 5.4.14 plots the mean normalized concentration on each direction and divided by the local porosity to obtain the concentration inside the pores. These 1D effective concentration profiles were obtained by directional averaging in X and Y:

$$\bar{C^Y}(x) = \frac{1}{L_Y} \int C(x, y)\, dy \tag{5.4.7}$$

It is clear, that the diffusion inside the pores at the micro-scopic level (inside

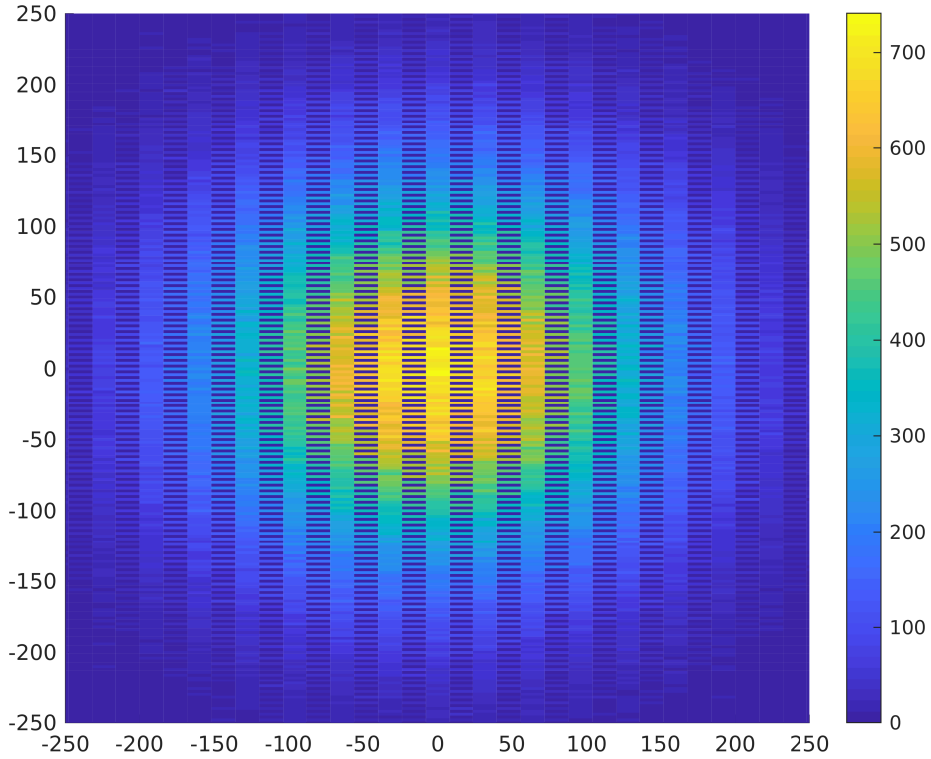

Figure 5.4.9: 2D concentrations of particles in anisotropic geometry with $\theta = 75\%$. The ratio between λ_X and λ_Y is 8

the pores) behaves as a pure diffusion in the macro-scopic level with the macro-properties calculated using moments particles positions.

Table 5.2 displays the results of different simulations in different configurations of Grains/Pores with the same porosity $\theta = 36\%$ and different anisotropy ratios.

5.4.2.3 Anisotropic geometry with porosity $\theta = 19\%$ and $\theta = 9.75\%$

The results shown in Table 5.2,5.3 and 5.4 suggest the following trends:

- The longer a grain is in one direction, the higher its effective diffusion is in this same direction.

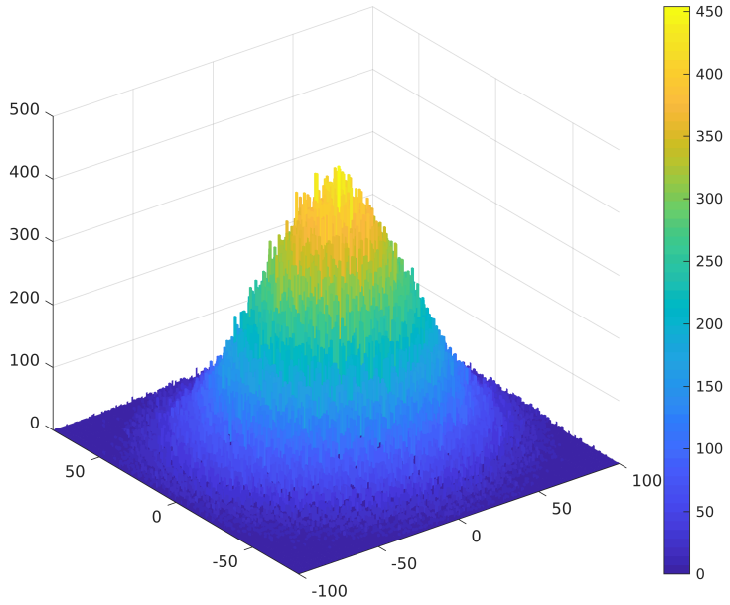

Figure 5.4.10: 3D Histogram of particles in anisotropic 2D geometry with $\theta = 36\%$. The ratio between λ_X and λ_Y is 2

λ_X/λ_Y	4/4	6/3	24/2
θ	36%	36%	36%
$D_{eff;X}$	0.586	0.726	0.930
$D_{eff;Y}$	0.586	0.429	0.126
τ_X^2	1.71	1.38	1.08
τ_Y^2	1.71	2.33	7.94

Table 5.2: Macroscopic properties (effective diffusion and tortuosity on the X and Y directions) for different configurations (different ratios of lengths of elongated grains) with a fixed porosity $\theta = 36\%$.

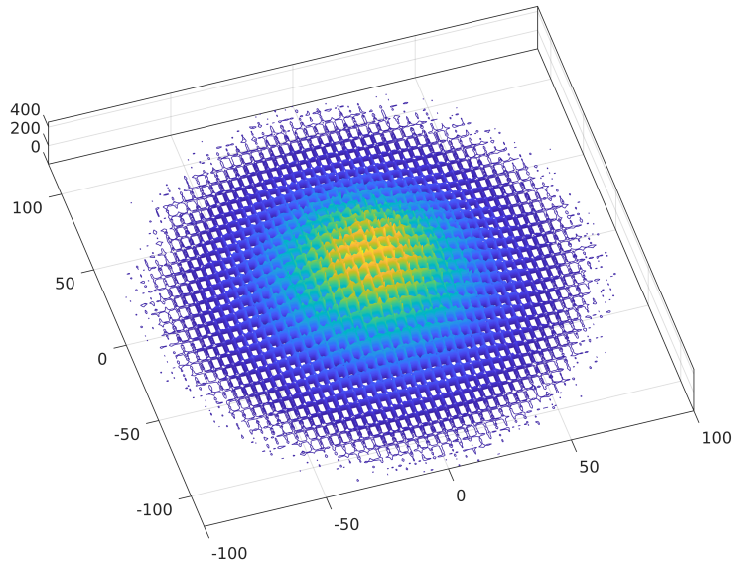

Figure 5.4.11: 3D Contour of particles positions in anisotropic 2D geometry with $\theta = 36\%$. The ratio between λ_X and λ_Y is 2

- When the anisotropic ratio $\frac{\lambda_X}{\lambda_Y}$ tends towards infinity, the effective diffusion tends towards 1 in the direction of the elongated grains (X), while in the opposite direction (Y) it tends towards 0.
- For a constant porosity, the sum of the effective diffusivity of both directions stays constant regardless of the anisotropic ratio (See Figure 5.4.16).

Figure 5.4.17 shows a fit of the tortuosity obtained numerically with the following analytical function:

$$\tau_{fit;Y} = (\tau_{iso} - \tau_\infty)\left(\frac{\lambda_X}{\lambda_Y}\right)^{(3/4)} + \tau_\infty \tag{5.4.8}$$

with τ_{iso} is the tortuosity in an isotropic configuration and $\tau_\infty = 1$ is the X tortuosity when $\frac{\lambda_X}{\lambda_Y} \to \infty$.

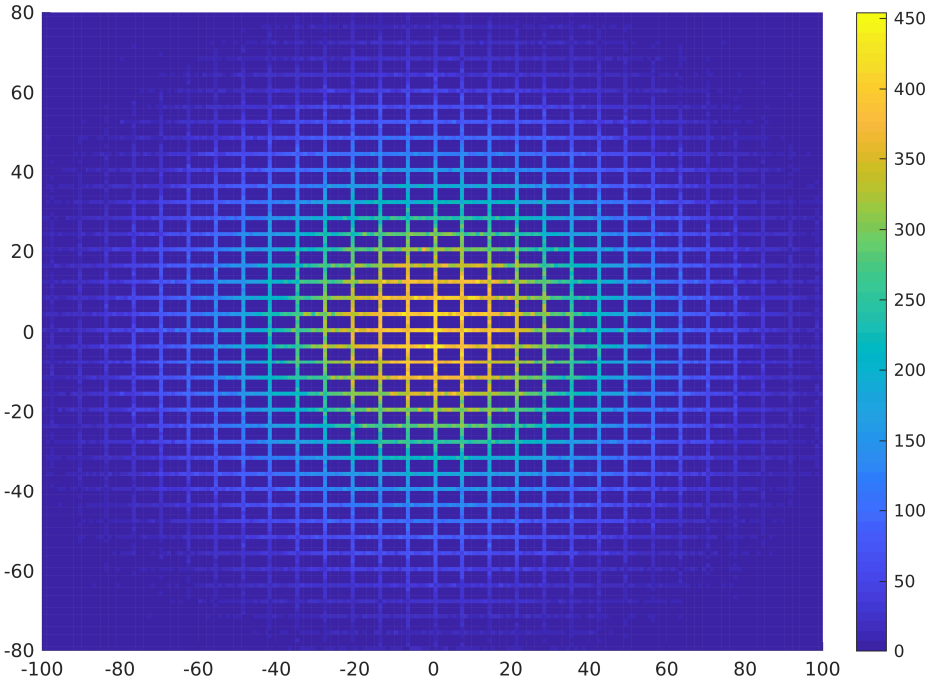

Figure 5.4.12: 2D concentrations of particles in anisotropic 2D geometry with $\theta = 36\%$. The ratio between λ_X and λ_Y is 2

λ_X/λ_Y	9/9	10/8	12/7	17/6	34/5
θ	19%	19%	19%	19%	19%
$D_{eff;X}$	0.542	0.593	0.654	0.763	0.881
$D_{eff;Y}$	0.542	0.500	0.412	0.309	0.159
τ_X^2	1.84	1.686	1.53	1.31	1.13
τ_Y^2	1.84	2.00	2.40	3.23	6.27

Table 5.3: Macroscopic properties (effective diffusion and tortuosity on the X and Y directions) for different configurations (different ratios of lengths of elongated grains) with a fixed porosity $\theta = 19\%$.

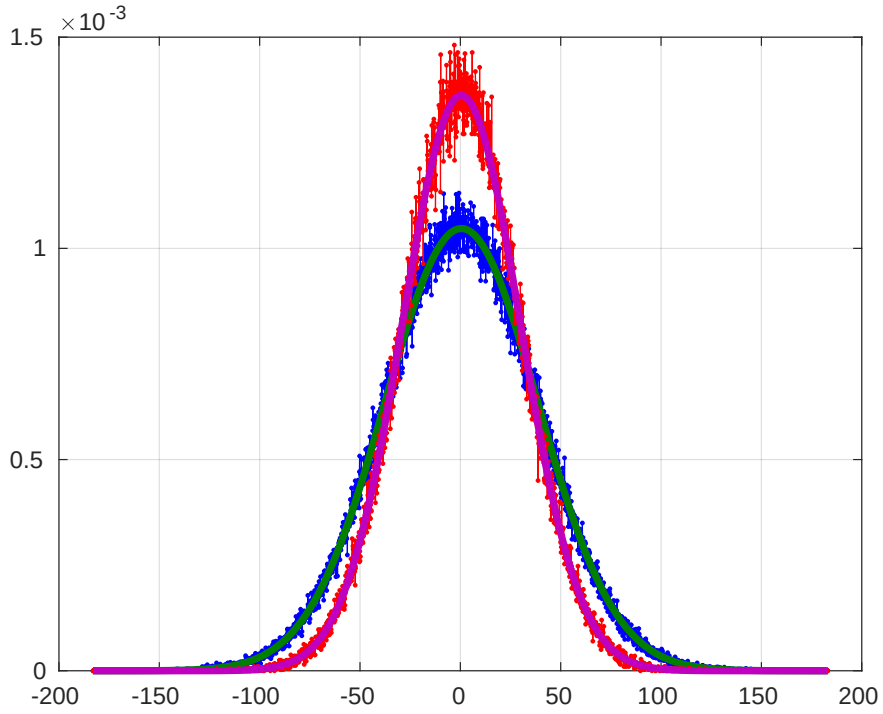

Figure 5.4.13: Effective concentration profiles $C(x)$ and $C(y)$ for anisotropic micro-geometry: The bold blue and red curves correspond, respectively, to the mean (on direction Y and X) concentration plotted against direction X and Y. The bold green and magenta curves correspond, respectively, to the analytical Gaussian functions with diffusive coefficient $D_{eff;X} = 0.726$ and $D_{eff;Y} = 0.429$.

λ_X/λ_Y	19/19	20/18	22/17	23/16	26/15	29/14	35/13	44/12	64/11	137/10
θ	9.75%	9.75%	9.75%	9.75%	9.75%	9.75%	9.75%	9.75%	9.75%	9.75%
$D_{eff;X}$	0.521	0.534	0.583	0.605	0.628	0.673	0.715	0.782	0.852	0.948
$D_{eff;Y}$	0.521	0.512	0.467	0.431	0.396	0.360	0.293	0.235	0.164	0.078

Table 5.4: Macroscopic properties (effective diffusion and tortuosity on the X and Y directions) for different configurations (different ratios of lengths of elongated grains) with a fixed porosity $\theta = 9.75\%$.

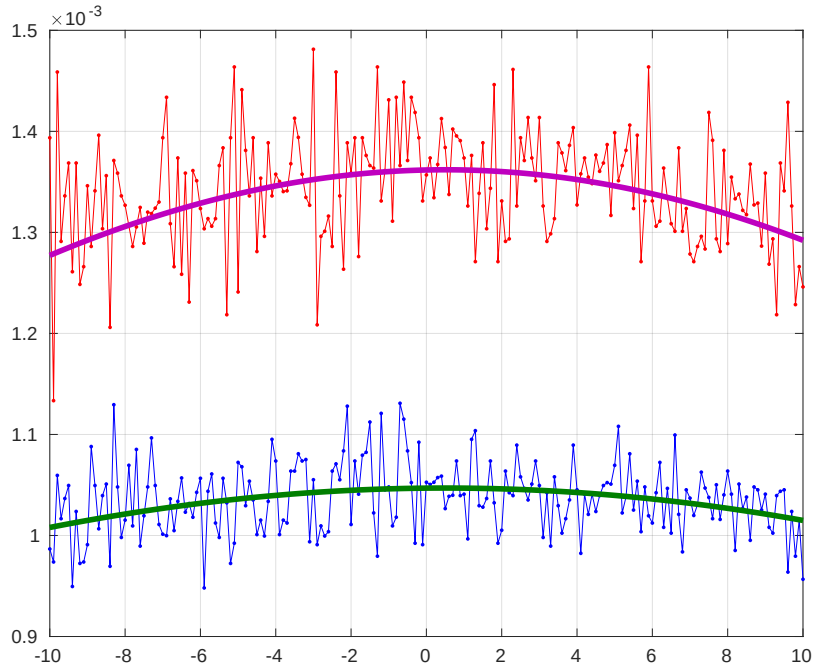

Figure 5.4.14: Effective concentration profiles $C(x)$ and $C(y)$: Zoom on the center of Figure 5.4.13

5.5 Conclusion and perspectives

5.5.1 Conclusion

- This study proposed a RWPT algorithm based on 2D/3D analytical solutions for zero flux conditions.
- The algorithm was applied for diffusion of an initial source in an infinite domain with different configurations of grains and pores (different porosities in isotropic systems, and constant porosity with different anisotropic configurations).
- A multi-scale study was developed from the micro-scale of grains and pores to the macro-scale level, leading to macro properties (porosity, effec-

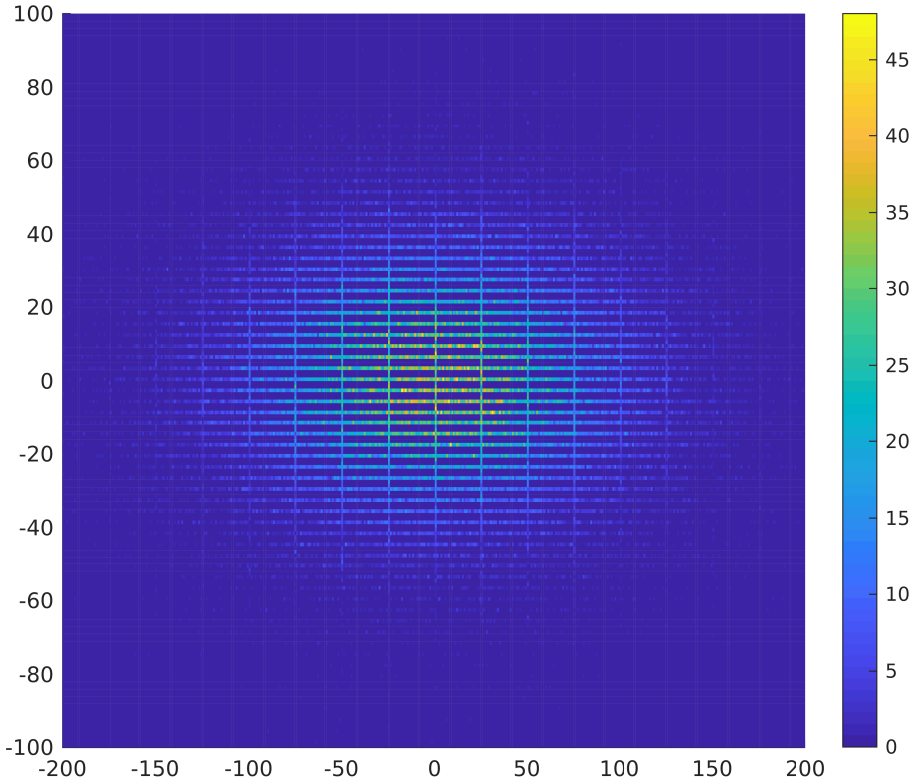

Figure 5.4.15: 2D concentrations of particles in anisotropic geometry with $\theta = 36\%$. The ratio between λ_X and λ_Y is 12

tive diffusivity, tortuosity in different directions). The upscaling method used moments of particles positions.

- Time step sensitivity study validated the time step choice for simulations. Convergence of macro properties in time simulation defines REV.

- Convergence of macro properties towards the geometric theoretical values when the Grain/Pore geometry's porosity tends towards zero.

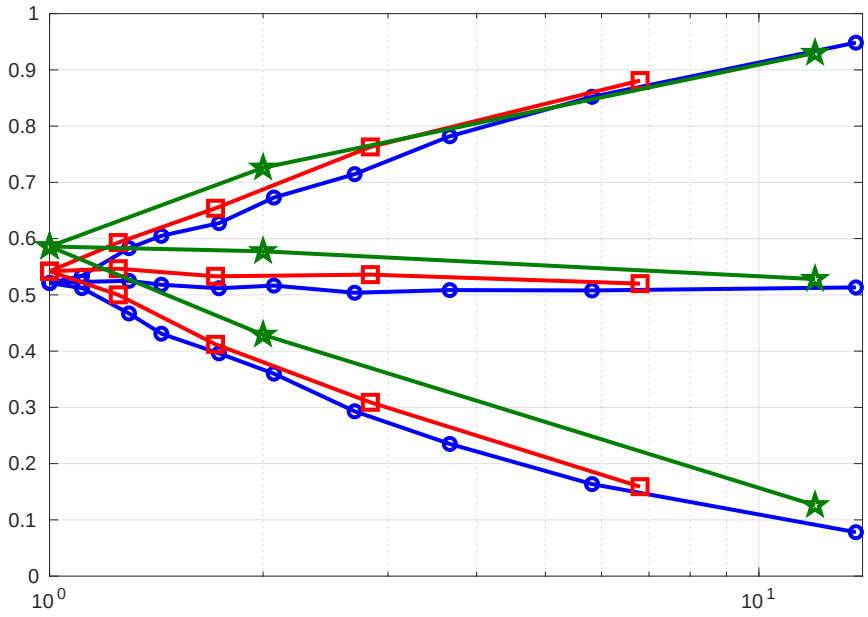

Figure 5.4.16: Effective diffusivity vs anisotropy ratio $\frac{\lambda_X}{\lambda_Y}$: The bold green curves with stars are for porosity $\theta = 36\%$. The bold red curves with squares are for porosity $\theta = 19\%$. The bold blue curves with circles are for porosity $\theta = 9.75\%$. For each color, the higher curve is $D_{eff,X}$.

5.5.2 Perspectives

- Grains replaced by porous aggregates with their own local porosity and diffusion coefficient (e.g., solute diffusion in a dual porous medium, or possibly, pressure diffusion in a dual porous medium).
- Random rather than deterministic micro-geometries and structures for pore-grain systems or pore-aggregate systems....
- Study in 3D instead of 2D.

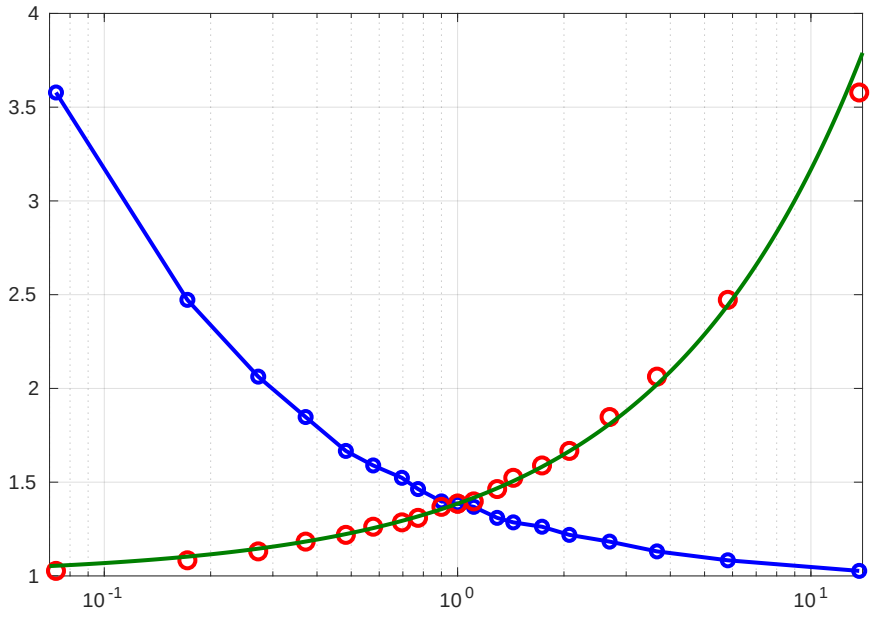

Figure 5.4.17: Tortuosity vs anisotropy ratio $\frac{\lambda_X}{\lambda_Y}$ for a porosity $\theta = 9.75\%$. The blue bold curve with circles is τ_X. The bold red circles are τ_Y. The bold green curve is the analytical function: $\tau_{fit;Y} = (\tau_{iso} - \tau_\infty)\left(\frac{\lambda_X}{\lambda_Y}\right)^{(3/4)} + \tau_\infty$.

Chapter 6

Conclusion and Perspectives

6.1 Conclusion and Perspectives (English)

6.1.1 Conclusion

This thesis, reviews, in Chapter 2, the theory behind stochastic processes, and gives the conditions for the Probability Density Function (PDF) of a stochastic process X(t) to follow the Fokker-Planck equation, and thus, the concentration based Partial Differential Equation (PDE) governing advective-diffusive transport. In short, the conditions are met if:

- Transport properties of the PDE are differentiable.
- The stochastic process is Markovian and continuous.

The second condition is satisfied for infinitesimal time steps. If transport properties are constant, then the PDF of particle positions is the Gaussian function, and the stochastic process $X(t)$ [also denoted X_t] verifies all the above conditions. In this case, at a fixed time t, X_t is a Gaussian Random Variable.

Chapter 3 presents new RWPT (Random Walk Particle Tracking) algorithms that can be considered as modified types of "Partial reflection schemes" (i.e., reflection/transmission schemes). Based on new concepts involving exotic particles (homing particles, negative unit mass particles, and adaptive mass particles), the new schemes converge to the correct solution while remaining computationally efficient and robust. These schemes lead to the exact diffusion equation instead of approaching it. The methods are combined with an asynchronous algorithm that solves the overshoot problem.

To test the new stop-and-go RWPT schemes, we develop analytical and semi-analytical solutions for diffusion in the presence of multiple interfaces (discontinuous multi-layered medium). The results show that the proposed stop-and-go RWPT schemes (with adaptive, negative, or homing particles) fit extremely well the semi-analytical solutions, even for very high contrasts and

in the neighborhood of interfaces. The three schemes provide a correct diffusive solution in only a few macro-time steps, with a precision that depends only on the number of particles, and not on the macro-time step.

Several test cases have been investigated. For example, we have shown that we can obtain the solution of the discontinuous diffusion problem, at a given time, in one single time step, by taking the time step equal to the final simulation time. These methods have been verified analytically, and they are validated in 1D by comparing the concentration profile obtained by the RWPT algorithm with the analytical solution for one or several interfaces of discontinuity of transport coefficients (diffusion and porosity).

Chapter 4 studies diffusion in discontinuous finite and semi-infinite domains with Dirichlet Boundary Conditions (BC's), where boundary concentration is imposed via particle-based methods (RWPT). The heterogeneity consists in the discontinuity of the properties of the domain. The domain can be divided into sub-domains with different porosities and diffusivities. This study extends the algorithm of Chapter 3 that solves semi-analytically diffusion PDE's in heterogeneous infinite domains, to semi-infinite and finite domains with Dirichlet BC's. It proposes also an extension of the RWPT Algorithm of Chapter 3 that solves discontinuous diffusion and porosity using particle methods in infinite domains, so that it handles also semi-infinite and finite heterogeneous domains with Dirichlet BC's. This extension of the infinite domain RWPT algorithm is based on the finite domain analytical solutions proposed in this Chapter (NB: here the term "finite" is understood as "bounded" or "partially bounded" domains). The methods have been checked analytically and verified for various configurations.

Chapter5 proposes an application of the RWPT algorithm multidimensional diffusion in grain-pore systems. The algorithm has been applied for diffusion

of an initial source in an infinite domain, with different configurations of grains and pores (different porosities in isotropic systems, and constant porosity with different anisotropic configurations). The diffusion algorithm used in this case is based on analytical solutions for zero flux conditions. The main results obtained by this diffusion algorithm in this chapter are as follows:

- A multi-scale study was developed from the micro-scale of grains and pores to the macro-scale level, leading to macro properties (porosity, effective diffusivity, tortuosity in different directions). The upscaling method used moments of particles positions.
- Time step sensitivity study validated the time step choice for simulations. Convergence of macro properties in time simulation defines REV.
- Convergence of macro properties towards the geometric theoretical values when the Grain/Pore geometry's porosity tends towards zero.

It will be useful, in the near future, to generalize several of the concepts and methods developed in this thesis: a list of possible extensions is proposed in the next section on "perspectives".

6.1.2 Perspectives

These perspectives are just written as a list of items. All of them could be considered as a short term study in order to enhance the complexity of the transport problems to be solved.

- The schemes presented in this thesis seem promising and are currently being extended to more complex multi-dimensional geometries (ongoing work).
- In addition to treating discontinuities, the three proposed types of "exotic" particle schemes (adaptive, negative, and homing particles) could

be considered in implementing boundary conditions. They could also be used for modeling other phenomena like chemical reactions or well production. This would give a new degree of freedom to algorithms, so that they would allow modeling different phenomena, this would be discussed in a future study.

- Extending and adapting the Dirichlet BC's schemes for multidimensional domains and spatially distributed concentration conditions on the boundaries.

- Implementation of "internal" concentration conditions based on the concepts already developed for particle-based implementations of Dirichlet Boundary Conditions (example problem for the Darcy-based pressure diffusion equation: imposed total pressure inside a subregion, corresponding to a lake or open water reservoir).

- Grains replaced by porous aggregates with their own local porosity and diffusion coefficient (e.g., solute diffusion in a dual porous medium, or possibly, pressure diffusion in a dual porous medium).

- Random rather than deterministic micro-geometries and structures for pore-grain systems or pore-aggregate systems....

- Considering advective as well as diffusive transport problems, i.e., adding a velocity component to the RWPT schemes, and implementing the resulting transport problem using one of the following methods:

  - Combining advective and diffusive transport in a single step.
  - One diffusive sub-step followed by one advective sub-step.
  - Transforming the Advective-diffusive equation into a pure diffusion problem by changing variables.

6.2 Conclusion et Perspectives (Français)

6.2.1 Conclusion

Cette thèse passe en revue, au chapitre 2, la théorie sous-jacente aux processus stochastiques et donne les conditions pour que la fonction de densité de probabilité (PDF) d'un processus stochastique X_t suive l'équation de Fokker-Planck et, partant, la concentration. Equation différentielle (PDE) régissant le transport advectif-diffusif. En bref, les conditions sont remplies si:

1. Les propriétés de transport de la PDE sont différentiables.

2. Le processus stochastique est markovien et continu.

La deuxième condition est remplie pour des pas de temps infinitésimaux. Si les propriétés de transport sont constantes, le PDF des positions des particules est la fonction gaussienne, et le processus stochastique $X(t)$ [également noté X_t] vérifie toutes les conditions ci-dessus. Dans ce cas, à une heure fixe t, X_t est une variable aléatoire gaussienne. Le chapitre 3 présente les nouveaux algorithmes RWPT (Random Walk Particle Tracking) qui peuvent être considérés comme des types modifiés de «schémas de réflexion partielle» (c'est-à-dire de schémas de réflexion / transmission). Basés sur de nouveaux concepts faisant appel à des particules exotiques (particules de référence, particules à masse unitaire négative et particules à masse adaptative), les nouveaux systèmes convergent vers la solution correcte tout en restant efficaces et robustes sur le plan informatique. Ces schémas conduisent à l'équation de diffusion exacte au lieu de s'en approcher. Les méthodes sont combinées à un algorithme asynchrone qui résout le problème de dépassement.

Pour tester les nouveaux schémas RWPT stop-and-go, nous développons des solutions analytiques et semi-analytiques pour la diffusion en présence de multiples interfaces (milieu multicouche discontinu). Les résultats montrent que les

schémas RWPT stop-and-go proposés (avec des particules adaptatives, négatives ou homing) conviennent extrêmement bien aux solutions semi-analytiques, même pour des contrastes très forts et au voisinage des interfaces. Les trois schémas fournissent une solution de diffusion correcte en quelques incréments de macro-temps, avec une précision qui ne dépend que du nombre de particules et non du pas de macro-temps. Plusieurs cas de test ont été examinés. Par exemple, nous avons montré que nous pouvons obtenir la solution du problème de diffusion discontinue, à un moment donné, en un seul pas de temps, en prenant le pas de temps égal au temps de simulation final. Ces méthodes ont été vérifiées analytiquement et elles sont validées en 1D en comparant le profil de concentration obtenu par l'algorithme RWPT à la solution analytique pour une ou plusieurs interfaces de discontinuité des coefficients de transport (diffusion et porosité). Le chapitre 4 étudie la diffusion dans des domaines finis et semi-infinis discontinus avec des conditions aux limites de Dirichlet (BC), où la concentration aux limites est imposée via des méthodes basées sur les particules (RWPT). L'hétérogénéité consiste en la discontinuité des propriétés du domaine. Le domaine peut être divisé en sous-domaines avec différentes porosités et diffusivités. Cette étude étend l'algorithme du chapitre 3 qui résout les PDE à diffusion semi-analytique dans des domaines infinis hétérogènes, à des domaines semi-infinis et finis avec des systèmes de type BC de Dirichlet. Il propose également une extension de l'algorithme RWPT du chapitre 3, qui résout la diffusion discontinue et la porosité à l'aide de méthodes de particules dans des domaines infinis, afin de traiter également les domaines hétérogènes semi-infinis et finis avec les systèmes de fichiers de Dirichlet. Cette extension de l'algorithme RWPT à domaine infini est basée sur les solutions analytiques à domaine fini proposées dans ce chapitre (NB: dans ce cas, le terme «fini» est compris comme des domaines «liés» ou «partiellement liés»).

Les méthodes ont été vérifiées analytiquement et vérifiées pour diverses configurations. Le chapitre 5 propose une application de la diffusion multidimensionnelle de l'algorithme RWPT dans les systèmes à pores de grains. L'algorithme a été appliqué à la diffusion d'une source initiale dans un domaine infini, avec différentes configurations de grains et de pores (différentes porosités dans les systèmes isotropes et une porosité constante avec différentes configurations anisotropes). L'algorithme de diffusion utilisé dans ce cas est basé sur des solutions analytiques pour des conditions de flux nul. Les principaux résultats obtenus par cet algorithme de diffusion dans ce chapitre sont les suivants:

- Une étude multi-échelle a été développée de la micro-échelle des grains et des pores au niveau macro, conduisant à des propriétés macro (porosité, diffusivité effective, tortuosité dans différentes directions). La méthode d'upscaling a utilisé des moments de positions de particules.
- Une étude de sensibilité par pas de temps a validé le choix du pas de temps pour les simulations. La convergence des propriétés des macros dans la simulation temporelle définit REV.
- Convergence des propriétés macro vers les valeurs géométriques théoriques lorsque la porosité de la géométrie des grains / pores tend vers zéro.

Il sera utile, dans un avenir proche, de généraliser plusieurs des concepts et méthodes développés dans cette thèse: une liste d'extensions possibles est proposée dans la section suivante sur les "perspectives".

6.2.2 Perspectives

Ces perspectives sont simplement écrites sous forme de liste d'éléments. Tous pourraient être considérés à court terme afin d'accroître la complexité des problèmes de transport à résoudre.

- Les schémas présentés dans cette thèse semblent prometteurs et sont actuellement étendus à des géométries multidimensionnelles plus complexes (travaux en cours).

- Outre le traitement des discontinuités, les trois types de schémas de particules "exotiques" proposés (particules adaptatives, négatives et dérivantes) pourraient être pris en compte lors de la mise en œuvre de conditions aux limites. Ils pourraient également être utilisés pour modéliser d'autres phénomènes tels que les réactions chimiques ou la production de puits. Cela donnerait un nouveau degré de liberté aux algorithmes, de sorte qu'ils permettraient de modéliser différents phénomènes, cela serait discuté dans une étude future.

- Extension et adaptation des schémas de Dirichlet BC pour les domaines multidimensionnels et les conditions de concentration distribuées dans l'espace sur les limites.

- Mise en œuvre de conditions de concentration "internes" basées sur les concepts déjà développés pour les implémentations de Dirichlet Boundary Conditions basées sur les particules (exemple de problème pour l'équation de diffusion de pression basée sur la méthode de Darcy: pression totale imposée à l'intérieur d'une sous-région, correspondant à un lac ou à un réservoir d'eau ouvert).

- Grains remplacés par des agrégats poreux avec leurs propres porosités et coefficients de diffusion locaux (par exemple, diffusion de soluté dans un milieu double poreux ou, éventuellement, diffusion sous pression dans un milieu double poreux).

- Micro-géométries et structures aléatoires plutôt que déterministes pour les systèmes à grains poreux ou les systèmes à agrégats pores ....

- Prendre en compte les problèmes de transport tant advectifs que diffusifs, c'est-à-dire ajouter une composante de vitesse aux schémas RWPT et mettre en œuvre le problème de transport résultant en utilisant l'une des méthodes suivantes:
  - Combiner transport advectif et diffusif en un seul pas de temps.
  - Une sous-étape diffusive suivie d'une sous-étape advective.
  - Transformer l'équation de transport advectif diffusif en une équation purement diffusive.

Appendix A

Pawula's theorem

Definition Let us define the scalar product $f * g(x) = \int_{\mathbb{R}} P(x+\zeta; t+dt|x;t) f(\zeta) g(\zeta) d\zeta$

Cauchy Schwartz's Inequality : Let's f and g be a positive function.

$$(f * g(x))^2 \leq (f * f(x))(g * g(x)) \tag{A.0.1}$$

For $n, m \geq 1$; we take $f(\zeta) = \zeta^n$ and $g(\zeta) = \zeta^m$ and

$$\forall n \epsilon \mathbb{N}; M_n = \int_{\mathbb{R}} P(x+\zeta; t+dt|x;t) \zeta^n d\zeta \tag{A.0.2}$$

By combining Eq.A.0.2 and Eq.A.0.1 we find

$$\forall n, m \epsilon \mathbb{N}^*; (M_{n+m})^2 \leq M_{2n} M_{2m} \tag{A.0.3}$$

We divide Eq.A.0.3 by dt^2, and tend dt towards 0 and we obtain :

$$(P_{n+m})^2 \leq P_{2n} P_{2m} \tag{A.0.4}$$

Pawula's theorem For $n \epsilon \mathbb{N}^*$, if $P_{2n} = 0$; So $\forall k \geq 3; P_k = 0$

Proof by mathematical induction For $n \geq 1$ we define the statement $Q_n : if\ P_{2n} = 0$; So $\forall k \geq 3; P_k = 0$

Let's prove that $\forall n \geq 1$; Q_n is true

If $P_2 = 0$ so according to Eq.A.0.4

$$\forall m \geq 1; P_{1+m}^2 \leq P_2 P_{2m} = 0 \Rightarrow P_{1+m} = 0 \tag{A.0.5}$$

So $\forall k \geq 3; P_k = 0$, therefore Q_1 is true

If $P_4 = 0$ so according to Eq.A.0.4

$$\forall m \geq 1; P_{2+m}^2 \leq P_4 P_{2m} = 0 \Rightarrow P_{2+m} = 0 \tag{A.0.6}$$

So $\forall k \geq 3; P_k = 0$, therefore Q_2 is true

For $n \geq 2$, let's suppose that Q_n is true and prove that Q_{n+1} is true

Let's assume that $P_{2(n+1)} = 0$; So according to Eq.A.0.4 $\forall m \geq 1; P_{n+1+m} = 0$

So for $m = n - 1 \geq 1$ we have $P_{2n} = 0$ and according to the statement Q_n we have $\forall k \geq 3; P_k = 0$

So by mathematical induction we have proven that$\forall n \geq 1$ if $P_{2n} = 0$; So $\forall k \geq 3; P_k = 0$

Conclusion : Either $\forall k \geq 3; P_k = 0$ or there is an infinite number of $k \geq 3; P_k \neq 0$.

It either stops at the second order or it goes infinite.

Appendix B

Analytical solutions in infinite discontinuous domains and study of their convergence

B.1 Analytical solution of diffusion in two interface media

This Appendix presents the detailed analytical solution for diffusion in an infinite medium with 2 "interfaces" (located at $x = x_{1-2}$ and $x = x_{2-3}$) of discontinuity of the diffusion coefficient $D(x)$ and porosity $\theta(x)$, defining 3 regions or layers with coefficients $(D_1;\theta_1)$, $(D_2;\theta_2)$, $(D_3;\theta_3)$. The solution is described for the case of "initial" point source $C(x,0) = M_0.\delta(x - x_0)$ located at $x_0 < x_{1-2} < x_{2-3}$ (Similarly we could find the solution for $x_{1-2} < x_{2-3} < x_0$ at the right of the domain). This solution is used in the text in relation to the generalization of our Random Walk algorithm, and for comparison/validation of results (Section 3.4, Figure 3.4.3) .

$$\begin{cases} \forall t > 0; \forall x \leq x_{1:2}; & \frac{\partial C_1}{\partial t}(x,t) = D_1 \frac{\partial^2 C_1}{\partial x^2}(x,t) \\ \forall t > 0; \forall x_{1:2} \leq x \leq x_{2:3}; & \frac{\partial C_2}{\partial t}(x,t) = D_2 \frac{\partial^2 C_2}{\partial x^2}(x,t) \\ \forall t > 0; \forall x \geq x_{2:3}; & \frac{\partial C_3}{\partial t}(x,t) = D_3 \frac{\partial^2 C_3}{\partial x^2}(x,t) \end{cases} \tag{B.1.1a}$$

$$\begin{cases} \forall t \geq 0; & \lim_{x \to -\infty} C_1(x,t) = 0 \\ \forall t \geq 0; & \lim_{x \to +\infty} C_3(x,t) = 0 \end{cases} \tag{B.1.1b}$$

$$\begin{cases} \forall t \geq 0; & C_1(x_{1:2},t) = C_2(x_{1:2},t) \\ \forall t \geq 0; & C_3(x_{2:3},t) = C_2(x_{2:3},t) \\ \forall t \geq 0; & -\theta_1 D_1 \frac{\partial C_1}{\partial x}(x_{1:2},t) = -\theta_2 D_2 \frac{\partial C_2}{\partial x}(x_{1:2},t) \\ \forall t \geq 0; & -\theta_3 D_3 \frac{\partial C_3}{\partial x}(x_{2:3},t) = -\theta_2 D_2 \frac{\partial C_2}{\partial x}(x_{2:3},t) \end{cases} \tag{B.1.1c}$$

The solution is described for two cases of "initial" point sources $C(x,0) = M_0.\delta(x - x_0)$ located at $x_0 < x_{1:2} < x_{2:3}$ and $C(x,0) = M_0.\delta(x - x_1)$ located at $x_{1:2} < x_1 < x_{2:3}$. In the first case, the source is in the left layer, but similar

solutions are obtained for any source position. These solutions are used in the text in relation to the generalization of our Random Walk algorithm, and for comparison/validation of results (Section 3.4, Figure 3.4.8) .

For a source located at left ($x_0 < x_{1:2}$) the initial conditions for the diffusion problem of Eq.B.1.1 is:

$$\begin{cases} \forall x \leq x_{1:2}; & C_1(x,0) = \frac{M_0}{\theta_1}\delta(x - x_0) \\ \forall x_{1:2} \leq x \leq x_{2:3}; & C_2(x,0) = 0 \\ \forall x \geq x_{2:3}; & C_3(x,0) = 0 \end{cases} \tag{B.1.2}$$

The solution of the discontinuous diffusion problem (Eq.B.1.1) with initial condition (B.1.2) is:

$$\forall t \geq 0; \forall x \leq x_{1:2}; \frac{\theta_1}{M_0} C_1(x,t) = G(x_0, 2D_1 t, x) + R_{1:2} G(-x_0 + 2x_{1:2}, 2D_1 t, x) + \\ + \sum_{i=0}^{+\infty} (1 - R_{1:2}) R_{2:3} (R_{2:3} R_{2:1})^i (1 - R_{2:1}) \times \\ \times G\left(-x_0 + 2x_{1:2} + 2(i+1)\frac{\sqrt{D_1}}{\sqrt{D_2}}(x_{2:3} - x_{1:2}), 2D_1 t, x\right) \tag{B.1.3a}$$

$$\forall t \geq 0; \forall x_{1:2} \leq x \leq x_{2:3}; \frac{\theta_2}{M_0} C_2(x,t) = \sum_{i=0}^{+\infty} (1 - R_{1:2}) (R_{2:3} R_{2:1})^i \times \\ \times \left(G\left(\frac{\sqrt{D_2}}{\sqrt{D_1}}(x_0 - x_{1:2}) - (2i+1)(x_{2:3} - x_{1:2}) + x_{2:3}, 2D_2 t, x\right) + R_{2:3} \times \right. \\ \left. \times G\left(-\frac{\sqrt{D_2}}{\sqrt{D_1}}(x_0 - x_{1:2}) + (2i+1)(x_{2:3} - x_{1:2}) + x_{2:3}, 2D_2 t, x\right)\right) \tag{B.1.3b}$$

$$\forall t \geq 0; \forall x \geq x_{2:3}; \frac{\theta_3}{M_0} C_3(x,t) = \sum_{i=0}^{+\infty} (1 - R_{1:2}) (R_{2:3} R_{2:1})^i (1 - R_{2:3}) \times \\ \times G\left(\frac{\sqrt{D_3}}{\sqrt{D_1}}(x_0 - x_{1:2}) + (2i+1)\frac{\sqrt{D_3}}{\sqrt{D_2}}(x_{1:2} - x_{2:3}) + x_{2:3}, 2D_3 t, x\right) \tag{B.1.3c}$$

And the solution of Eq.B.1.1 with the initial condition

$$\begin{cases} \forall x \leq x_{1:2}; & C_1(x,0) = 0 \\ \forall x_{1:2} \leq x \leq x_{2:3}; & C_2(x,0) = \frac{M_0}{\theta_1}\delta(x - x_1) \\ \forall x \geq x_{2:3}; & C_3(x,0) = 0 \end{cases} \tag{B.1.4}$$

is:

$$\forall t \geq 0; \forall x \leq x_{1:2}; \frac{\theta_1}{M_0} C_1(x,t) = (1 - R_{2:1}) \sum_{i=0}^{+\infty} (R_{2:3} R_{2:1})^i \times$$

$$\times \left(G\left(x_{1:2} + \sqrt{\frac{D_1}{D_2}} \left(2i\left(x_{2:3} - x_{2:1}\right) + x_0 - x_{1:2}\right), 2D_1 t, x \right) + \right.$$

$$\left. + R_{2:3} G\left(x_{1:2} + \sqrt{\frac{D_1}{D_2}} \left(2i\left(x_{2:3} - x_{2:1}\right) + 2x_{2:3} - x_0 - x_{1:2}\right), 2D_1 t, x \right) \right) \tag{B.1.5a}$$

$$\forall t \geq 0; \forall x_{1:2} \leq x \leq x_{2:3}; \frac{\theta_2}{M_0} C_2(x,t) = -G(x_0, 2D_2 t, x) + \sum_{i=0}^{+\infty} (R_{2:3} R_{2:1})^i \times$$

$$\times \left(G\left(2i\left(x_{2:3} - x_{1:2}\right) + x_0, 2D_2 t, x\right) + G\left(2i\left(x_{1:2} - x_{2:3}\right) + x_0, 2D_2 t, x\right) + \right.$$

$$+ R_{2:3} G\left(2i\left(x_{2:3} - x_{1:2}\right) + 2x_{2:3} - x_0 - x_{1:2}, 2D_2 t, x\right) +$$

$$\left. + R_{2:1} G\left(2i\left(x_{1:2} - x_{2:3}\right) + 2x_{1:2} - x_0 - x_{2:3}, 2D_2 t, x\right) \right) \tag{B.1.5b}$$

$$\forall t \geq 0; \forall x \geq x_{2:3}; \frac{\theta_3}{M_0} C_3(x,t) = (1 - R_{2:3}) \sum_{i=0}^{+\infty} (R_{2:1} R_{2:3})^i \times$$

$$\times \left(G\left(x_{2:3} + \sqrt{\frac{D_3}{D_2}} \left(2i\left(x_{1:2} - x_{2:3}\right) + x_0 - x_{2:3}\right), 2D_3 t, x \right) + \right.$$

$$\left. + R_{2:1} G\left(x_{2:3} + \sqrt{\frac{D_3}{D_2}} \left(2i\left(x_{1:2} - x_{2:3}\right) + 2x_{1:2} - x_0 - x_{2:3}\right), 2D_3 t, x \right) \right) \tag{B.1.5c}$$

The above solutions have been checked by direct substitution in Eq.B.1.1a and the initial and boundary conditions Eq.B.1.1b, Eq.B.1.1c and Eq.B.1.2.

The infinite series obtained in this section for concentration $C(x,t)$ have the form of a function $h(x,t)$ defined as:

$$h(x,t) = \sum_{n=0}^{+\infty} \frac{A}{\sqrt{t}} z^n exp\left(-\frac{(x + Cn + D)^2}{Bt} \right) \tag{B.1.6}$$

with $B, t > 0$; $x, A, C, D \epsilon \mathbb{R}$ and $z = R_{2:1} R_{2:3}$ (product of partial reflection coefficients). Their convergence is studied in the next appendix (B.2).

B.2 Study of the convergence and continuity of the series h

In this appendix, we study the convergence of the infinite series $h(x,t)$ (B.1.6) which has the form of the solution found in B.1. This solution (concentration $C(x,t)$) was used in Figure 3.4.8 to validate the Random Walk Particle Tracking model proposed in this chapter for discontinuous diffusion.

B.2.1 Pointwise convergence using d'Alembert criteria

Theorem 1. *d'Alembert Ratio test [Rudin, 1976]*

Let $(a_n, n\epsilon\mathbb{N})$ *be a sequence of complexe numbers such that* $L = \lim_{n\to+\infty} \frac{|a_{n+1}|}{|a_n|}$ *exists.*

If $L < 1$, *then the series* $\sum_{n=0}^{+\infty} a_n$ *converges absolutely. Thus,* $\sum_{n=0}^{+\infty} a_n$ *is pointwise convergent.*

If $L > 1$, *then the series* $\sum_{n=0}^{+\infty} a_n$ *is divergent.*

If $L = 1$, *then the case is undecided.*

Using Theorem 1, we now show that our series $h(x,t)$ is pointwise convergent. This series is of the form $h(x,t) = \sum_{n=0}^{+\infty} U_n(x,t)$, where:

$$U_n = \frac{A}{\sqrt{t}} z^n exp\left(-\frac{(x+Cn+D)^2}{Bt}\right) \tag{B.2.1}$$

$$\frac{|U_{n+1}|}{|U_n|} = |z|\ exp\left(-\frac{(x+C(n+1)+D)^2 - (x+Cn+D)^2}{Bt}\right) \tag{B.2.2}$$

$$\frac{|U_{n+1}|}{|U_n|} = |z|\ exp\left(-\frac{2xC+C^2+2DC}{Bt}\right) exp\left(\frac{-2C^2 n}{Bt}\right) \tag{B.2.3}$$

If $C = 0$, then the series converges for $|z| < 1$ and $B, t > 0$; $x, A, D\epsilon\mathbb{R}$, $h(t,x) = \frac{A}{\sqrt{t}} \frac{1}{1-z} exp\left(-\frac{(x+D)^2}{Bt}\right)$. This case occurs if the distance between two interfaces ($|x_{1:2} - x_{2:3}|$) goes to zero (we may dismiss this case here).

Otherwise, if $C \neq 0$, then $\frac{|U_{n+1}|}{|U_n|} \underset{n\to+\infty}{\to} 0$. By the d'Alembert Ratio test, the series h converges $\forall z \epsilon \mathbb{C}$; $\forall B > 0, \forall t > 0$; $\forall x, A, C, D \epsilon \mathbb{R}$.

In conclusion, the series $h(x,t)$ and the analytical concentrations solutions (Eq.3.3.21 and 3.3.22) converge pointwise in all cases of interest.

B.2.2 Uniform convergence

Theorem 2. *[Rudin, 1976]*

Assume (f_n) is a sequence of functions defined on E, and assume $|f_n(x)| \leq M_n$ $(x \epsilon E, n = 1, 2, 3, ...)$. Then $\sum f_n$ converges uniformly on E if $\sum M_n$ converges.

The infinite series $h(x,t)$ is of the form:

$$h(x,t) = \sum_{n=0}^{+\infty} Az^n exp\left(-\frac{Bt\,ln(t) + 2(x + Cn + D)^2}{2Bt}\right) \tag{B.2.4}$$

Let us define $g_n(x,t)$ as:

$$g_n(x,t) = -\frac{Bt\,ln(t) + 2(x + Cn + D)^2}{2Bt} \tag{B.2.5}$$

For $t \geq 1$ we have $g_n \leq 0$. Thus,

$$\left|Az^n exp\left(-\frac{Bt\,ln(t) + 2(x + Cn + D)^2}{2Bt}\right)\right| \leq |A|\,|z|^n \tag{B.2.6}$$

Since the series $\sum_{n=0}^{+\infty} |A|\,|z|^n$ converges for $|z| < 1$, h is uniformly convergent on $\mathbb{R} \times [1; +\infty[$.

For $0 < t \leq 1$ we have $\frac{-B}{e} \leq Bt\,ln(t) \leq 0$.

- First, if $C > 0$ and for a fixed $x_0 \epsilon \mathbb{R}$; $\exists n_1 / \forall n \geq n_1; \forall x \geq x_0; Bt\,ln(t) + 2(x + Cn + D)^2 \geq Bt\,ln(t) + 2(x_0 + Cn + D)^2 \geq 0$. Hence, the series h converges uniformly on $[x_0; +\infty[\times]0; 1]$.

- Secondly, if $C < 0$ and for a fixed $x_0 \epsilon \mathbb{R}; \exists n_2 / \forall n \geq n_2; \forall x \leq x_0; Bt\, ln\,(t) + 2\,(-x - Cn - D)^2 \geq Bt\, ln\,(t) + 2\,(-x_0 - Cn - D)^2 \geq 0$. The series h converges uniformly on $]0;1] \times]-\infty; x_0]$.

Theorem 3. *[Rudin, 1976]*

If (f_n) is a sequence of continuous functions on E, and if $f_n \to f$ uniformly on E, then f is continuous on E.

Consequence For $z \epsilon \mathbb{C}$ such that $|z| < 1$, h is continuous with respect to (x,t) on $\mathbb{R} \times]0;+\infty[$.

Conclusion In all cases of interest, the analytical infinite series concentration solutions (Eq.3.3.21 and 3.3.22) are pointwise convergent and continuous with respect to (x,t) on $\mathbb{R} \times]0;+\infty[$.

Appendix C

Convergence and continuity of the series h for diffusion with multiple zero flux conditions

In this appendix, we study the convergence of the infinite series $h(x,t)$ (C.0.1) Eq5.2.14 which has the form of the solutions found in subsection 5.2.2. This solution (concentration $C(x,t)$) was used to induce the Random Walk Particle Tracking model proposed in this study for diffusion with multiple zero flux conditions.

The infinite series $h(x,t)$ corresponding to Eq.5.2.14 in addition to subsequent equations of subsection 5.2.2. $h(x,t)$ is of the form:

$$h(x,t) = \sum_{n=1}^{+\infty} Aexp\left(-\frac{Bt\,ln(t) + 2(x+Cn+D)^2}{2Bt}\right) \tag{C.0.1}$$

For $n \geq 1$, let us define $g_n(x,t)$ as, $\forall t \epsilon\,]0;+\infty[\,; \forall x \epsilon\, [x_{12};x_{23}]\,;$

$$g_n(x,t) = exp\left(-\frac{Bt\,ln(t) + 2(x+Cn+D)^2}{2Bt}\right) \tag{C.0.2}$$

For $t \geq 1$ we have

$$exp\left(-\frac{Bt\,ln(t)}{2Bt}\right) = exp\left(-\frac{1}{2}ln(t)\right) \leq 1 \tag{C.0.3}$$

Thus,

$$g_n(x,t) \leq exp\left(-\frac{(x+Cn+D)^2}{Bt}\right) = exp\left(-\frac{n^2\left(\frac{x}{n}+C+\frac{D}{n}\right)^2}{Bt}\right) \tag{C.0.4}$$

On the other hand the interval $[x_{12};x_{23}]$ is compact (closed and bounded) and the function $x \to \left(\frac{x}{n}+C+\frac{D}{n}\right)^2$ is continuous. Therefore,

$$\exists x_{0,n} \epsilon\, [x_{12};x_{23}]\,; \underset{x\epsilon[x_{12};x_{23}]}{Min}\left(\frac{x}{n}+C+\frac{D}{n}\right)^2 = \left(\frac{x_{0,n}}{n}+C+\frac{D}{n}\right)^2 \tag{C.0.5}$$

and

$$\underset{n\to+\infty}{lim}\left(\frac{x_{0,n}}{n}+C+\frac{D}{n}\right)^2 = C^2 \tag{C.0.6}$$

$$\forall \varepsilon > 0; \exists N \epsilon \mathbb{N}; \forall n \geq N; \left|\left(\frac{x_{0,n}}{n}+C+\frac{D}{n}\right)^2 - C^2\right| < \varepsilon \tag{C.0.7}$$

$$\forall \varepsilon > 0; \exists N \epsilon \mathbb{N}; \forall n \geq N; -\varepsilon < \left(\frac{x_{0,n}}{n}+C+\frac{D}{n}\right)^2 - C^2 < \varepsilon \tag{C.0.8}$$

For $\varepsilon = \frac{C^2}{2} > 0; \exists N_C \epsilon \mathbb{N}; \forall n \geq N_C;$

$$0 < \frac{C^2}{2} < \left(\frac{x_{0,n}}{n} + C + \frac{D}{n} \right)^2 \tag{C.0.9}$$

Therefore, $\forall x \epsilon \left[x_{12}; x_{23} \right];$

$$\frac{n^2 C^2}{2Bt} < \frac{n^2}{Bt} \left(\frac{x_{0,n}}{n} + C + \frac{D}{n} \right)^2 \leq \frac{n^2}{Bt} \left(\frac{x}{n} + C + \frac{D}{n} \right)^2 \tag{C.0.10}$$

For fixed $t_0 \geq 1$, we have $\forall t \epsilon \left[1; t_0 \right]$

$$\forall n \geq N_C; -\frac{n^2}{Bt} \left(\frac{x}{n} + C + \frac{D}{n} \right)^2 < -\frac{n^2 C^2}{2Bt} \leq -\frac{n^2 C^2}{2Bt_0} \tag{C.0.11}$$

$$g_n \left(x, t \right) \leq exp \left(-\frac{n^2 \left(\frac{x}{n} + C + \frac{D}{n} \right)^2}{Bt} \right) < exp \left(-\frac{C^2}{2Bt} \right)^{n^2} \tag{C.0.12}$$

and

$$exp \left(-\frac{C^2}{2Bt} \right)^{n^2} \leq exp \left(-\frac{C^2}{2Bt_0} \right)^{n^2} < 1 \tag{C.0.13}$$

Since the series $\sum_{n=0}^{+\infty} |A| \left| z \right|^{n^2}$ converges for $|z| < 1$ and $exp \left(-\frac{C^2}{2Bt_0} \right) < 1$, the series h is uniformly convergent on $[x_{12}; x_{23}] \times [1; t_0]$. Hence, h is continuous on $[x_{12}; x_{23}] \times [1; +\infty[$.

For $0 < t \leq 1$, and for a fixed $t_0 \epsilon \,]0, 1]$ we have $\forall t \epsilon \left[t_0, 1 \right]$

$$exp \left(-\frac{1}{2} ln \left(t \right) \right) \leq exp \left(-\frac{1}{2} ln \left(t_0 \right) \right) \tag{C.0.14}$$

and $\forall x \epsilon \left[x_{12}; x_{23} \right];$

$$g_n \left(x, t \right) = exp \left(-\frac{1}{2} ln \left(t \right) \right) exp \left(-\frac{n^2 \left(\frac{x}{n} + C + \frac{D}{n} \right)^2}{Bt} \right) \tag{C.0.15}$$

$$g_n \left(x, t \right) \leq exp \left(-\frac{1}{2} ln \left(t_0 \right) \right) exp \left(-\frac{n^2 \left(\frac{x}{n} + C + \frac{D}{n} \right)^2}{Bt} \right) \tag{C.0.16}$$

Using Eq.C.0.10, we have

$$g_n \left(x, t \right) \leq exp \left(-\frac{1}{2} ln \left(t_0 \right) \right) exp \left(-\frac{n^2 C^2}{2Bt} \right) \tag{C.0.17}$$

On the other hand,

$$t \leq 1 \Rightarrow -\frac{n^2C^2}{2Bt} \leq -\frac{n^2C^2}{2B} \tag{C.0.18}$$

Therefore, $\forall t\epsilon\,[t_0, 1]\,; \forall x\epsilon\,[x_{12}; x_{23}]\,;$

$$0 \leq g_n\,(x,t) \leq exp\left(-\frac{1}{2}ln\,(t_0)\right) exp\left(-\frac{n^2C^2}{2Bt}\right) \leq M_0 exp\left(-\frac{C^2}{2B}\right)^{n^2} \tag{C.0.19}$$

Since the series $\sum M_0 exp\left(-\frac{C^2}{2B}\right)^{n^2}$ converges, then the series h is uniformly convergent on $[x_{12}; x_{23}] \times [t_0; 1]$. Hence, h is continuous on $[x_{12}; x_{23}] \times\,]0; 1]$.

Theorem [Rudin, 1976] If (f_n) is a sequence of continuous functions on E, and if f_n converges to f uniformly on E, then f is continuous on E.

Conclusion In all cases of interest, the analytical infinite series concentration solutions shown in this study are pointwise convergent and continuous with respect to (x, t) on $\mathbb{R} \times\,]0; +\infty[$.

Bibliography

[Ackerer, 1985] Ackerer P.,(1985). Propagation d'un fluide en aquifère poreux saturé en eau. Prise en compte et localisation des hétérogénéités par outils théoriques et expérimentaux, Ph.D. thesis, Univ. Louis Pasteur de Strasbourg, Strasbourg, France.

[Ackerer & Mose, 2000] Ackerer P., and R. Mose (2000), Comment on "Diffusion theory for transport in porous media: Transition-probability densities of diffusion processes corresponding to advection-dispersion equations" by Eric M. LaBolle et al., Water Resour. Res., 36(3), 819–821, doi:10.1029/1999WR900326.

[Arnold, 1974] Arnold, L. (1974). Stochastic differential equations. New York.

[Bagtzoglou et al., 1992] Bagtzoglou A. C., A. F. B. Tompson, and D. E. Dougherty, (1992), Projection functions for particle grid methods, Numer. Methods Partial Differential Equations, 8, 325-340.

[Bechtold et al., 2011] Bechtold M., J. Vanderborght, O. Ippisch, and H. Vereecken, (2011), Efficient random walk particle tracking algorithm for advective-dispersive transport in media with discontinuous dispersion coefficients and water contents, Water Resour. Res., 47, W10526, doi:10.1029/2010WR010267.

[Bodin, 2015] Bodin, J. (2015), From analytical solutions of solute transport equations to multidimensional time-domain random walk (TDRW) algorithms, Water Resour. Res., 51, 1860–1871, doi:10.1002/2014WR015910.

[Carslaw & Jaeger, 1959] Carslaw, H. S., and J. C. Jaeger, Conduction of Heat in Solids, pp.363-365, Clarendon, Oxford, 1959.

[Chandrasekhar, 1943] CHANDRASEKHAR, S., (1943), Stochastic Problems in Physics and Astronomy, REVIEWS OF MODERN PHYSICS VOLUME 15, NUMBER 1.

[Cordes et al., 1991] Cordes, C., H. Daniels, and G. Rouve´ (1991), A new very efficient algorithm for particle tracking in layered aquifers, in Computer Methods in Water Resources II, Groundwater Modelling and Pressure Flow, vol. 1, pp. 41–55, edited by D. B. Sari et al., Springer, Germany.

[Delay & Bodin, 2001] Delay, F., & Bodin, J. (2001). Time domain random walk method to simulate transport by advection-dispersion and matrix diffusion in fracture networks. Geophysical Research Letters, 28(21), 4051-4054.

[Delay et al., 2005] Delay, F., P. Ackerer, and C. Danquigny (2005), Simulating solute transport in porous or fractured formations using random walk particle tracking: A review, Vadose Zone J., 4(2), 360–379, doi:10.2136/vzj2004.0125.

[Dirac, 1928] Dirac, P. A. M., (1928), The Quantum Theory of the Electron, Proc. R. Soc. Lond. A 1928 117 610-624; DOI: 10.1098/rspa.1928.0023. Published 1 February.

[Dirac, 1934] Dirac, P. A. M. (1934). "Discussion of the infinite distribution of electrons in the theory of the positron". Cambridge Phil. Soc. Cambridge Philosophical Society. 30 (2): 150–163

[Evans, 2010] Evans, L. C. (2010). Partial differential equations.

[Feller, 1957] Feller, W., An Introduction to Probability theory and its applications, John Wiley, New York, 1957.

[Gardiner, 1985] Gardiner, C. W.. Handbook of stochastic methods. Berlin: springer (1985).

[Gillespie, 1992] Gillespie, D.T.: Markov Processes: An Introduction for Physical Scientists. Academic press (1992).

[Gillespie & Seitaridou, 2013] Gillespie, D.T., Seitaridou, E.: Simple Brownian Diffusion. Oxford University Press (2013)

[Hoteit et al., 2002] Hoteit, H., R. Mose, A. Younes, F. Lehmann, and P. Ackerer (2002), Three-dimensional modeling of mass transfer in porous media using the mixed hybrid finite elements and the random-walk methods, Math. Geol., 34(4), 435–456, doi:10.1023/A:1015083111971

[Kang et al., 2015] Kang, P. K., T. Le Borgne, M. Dentz, O. Bour, and R. Juanes (2015), Impact of velocity correlation and distribution on transport in fractured media: Field evidence and theoretical model, Water Resour. Res. , 51 , 940–959, doi:10.1002/2014WR015799.

[Khamehchi et al., 2017] Khamehchi, M. A., Khalid Hossain, M. E. Mossman, Yongping Zhang, Th. Busch, Michael McNeil Forbes, and P. Engels (2017), Negative-Mass Hydrodynamics in a Spin-Orbit-Coupled Bose-Einstein Condensate, Phys. Rev. Lett. 118, 155301.

[Labolle et al., 1996] LaBolle, E. M., G. E. Fogg, and A. F. B. Tompson (1996), Random-walk simulation of transport in heterogeneous porous media: Local

mass-conservation problem and implementation methods, Water Resour. Res., 32(3), 583–593, doi:10.1029/95WR03528.

[Labolle et al., 1998] LaBolle, E. M., J. Quastel, and G. E. Fogg (1998), Diffusion theory for transport in porous media: Transition-probability densities of diffusion processes corresponding to advection-dispersion equations, Water Resour. Res., 34(7), 1685–1693, doi:10.1029/98WR00319.

[Labolle et al., 2000] LaBolle, E. M., J. Quastel, G. E. Fogg, and J. Gravner (2000), Diffusion processes in composite porous media and their numerical integration by random walks: Generalized stochastic differential equations with discontinuous coefficients, Water Resour. Res., 36(3), 651–662, doi:10.1029/ 1999WR900224.

[Lejay & Pichot, 2012] Lejay, A., and G., Pichot (2012), Simulating diffusion processes in discontinuous media: A numerical scheme with constant time steps, Journal of Computational Physics 231, 7299-7314, http://dx.doi.org/10.1016/j.jcp.2012.07.011.

[Lejay & Pichot, 2016] Lejay, A., and G., Pichot (2016), Simulating diffusion processes in discontinuous media: Benchmark tests. Journal of Computational Physics, Elsevier, 2016, 314, pp.384 - 413.<10.1016/j.jcp.2016.03.003>

[Lim, 2006] Lim, D. H. (2006), Numerical study of nuclide migration in a nonuniform horizontal flow field of a high-level radioactive waste repository with multiple canisters, Nucl. Technol., 156(2), 222–245.

[Luttinger, 1951] Luttinger, J. M. (1951). "On "Negative" mass in the theory of gravitation". Awards for Essays on Gravitation. Gravity Research Foundation

[Noetinger et al., 2016] Noetinger B., D. Roubinet, J De Dreuzy, A. Russian, P. Gouze, T. Le Borgne, M. Dentz, and F. Delay, (2016), Random Walk Methods for Modeling Hydrodynamic Transport in Porous and Fractured Media from Pore to Reservoir Scale, Transport in Porous Media, Springer Verlag, 115 (2), pp.345 – 385. <10.1007/s1142-016-0693-z>. <hal-014449131>

[Oukili et al., 2019] Oukili, H., R. Ababou, G. Debenest, B. Noetinger (2019), Random Walks with negative particles for discontinuous diffusion and porosity, Journal of Computational Physics, Volume 396, 2019, Pages 687-701, ISSN 0021-9991, https://doi.org/10.1016/j.jcp.2019.07.006.

[Papoulis, 1991] Papoulis, A.: Probability, Random Variables, and Stochastic Processes. McGraw-Hill, Inc. (1991).

[Peskin & Schroeder, 1995] Peskin, M.E., Schroeder, D.V. (1995). An Introduction to Quantum Field Theory, Westview Press, ISBN 0-201-50397-2, p. 80.

[Raviart, 1983] Raviart P.A 1983a 'Particle approximation of linear hyperbolic equation of the first order' Chap I 'Num Methods in Fluids Dynamics' Lectures Notes in Math., Springer Verlag

[Rudin, 1976] Rudin, W. (1976): Principles of Mathematical Analysis. New York: McGraw-Hill Book Company.

[Risken, 1996] Risken, H.: The Fokker-Planck Equation. Springer, Heidelberg New York (1996)

[Sahimi, 1993] Sahimi, M. Transp Porous Med (1993) 13: 3. https://doi.org/10.1007/BF00613269

[Hunt & Sahimi, 2017] Hunt, A. G., & Sahimi, M. (2017), Flow, Transport, and Reaction in Porous Media: Percolation Scaling, Critical-Path Analysis, and Effective Medium Approximation, Reviews of Geophysics, 55, 993–1078. https://doi.org/10.1002/2017RG000558

[Salamon et al., 2006] Salamon, P., D. Fernandez-Garcia, and J. J. Gomez-Hernandez (2006), A review and numerical assessment of the random walk particle

tracking method, J. Contam. Hydrol., 87(3–4), 277–305, doi:10.1016/j.jconhyd. 2006.05.005.

[Sbai, 2018] Sbai, A.(2018), A Practical Grid-based Alternative Method to Advective Particle Tracking, Ground Water, DOI: 10.1111/gwat.12646

[Semra et al., 1993] Semra, K., P. Ackerer, and R. Mose (1993), Three dimensional Groundwater Quality Modeling in Heterogeneous Media, in Water Pollution II : Modelling, Measuring and Prediction, edited by L. C. Wrobel and C. A. Brebbia, pp. 3–11, Southampton, U. K.

[Schwartz, 1951] Schwartz, L.: Théorie des distributions, Hermann, 2 volumes, 1950/1951, nouvelle édition 1966.

[Spiller et al., 2000] Spiller, M., R. Ababou and J. Koengeter (2000), Alternative approach to simulate transport based on the master equation, Tracers and Modelling in Hydrogeology (Proceedings of the TraM'2000 Conference held at Liège, Belgium, May 2000), IAHS Publ. no.262, 2000.

[Spiller et al., 2002] Spiller, M.; Ababou, R.; Becker, T.; Fadili, A.; Köngeter, J. (2002): Mass Transport with Heterogeneous Diffusion: Interpolation Schemes for Random Walks. IAMG 2002: 8th Annual Conference of the International Association for Mathematical Geology, Berlin, Germany, 15-20

September 2002. Berlin: Selbstverlag der Alfred-Wegner-Stiftung (Terra Nostra: Schriften der Alfred-Wegener-Stiftung; 4,2), pp. 305-310.

[Spiller, 2004] Spiller, M. (2004).Physical and numerical modeling of flow and transport in heterogeneous fractured media: high Reynolds flow and reactive particle transport.Doctoral thesis. IMFT Institut National Polytechnique de Toulouse (France) & IWW RWTH University of Aachen (Germany), 25 Nov. 2004.

[Tompson & Gelhar, 1990] Tompson, A. F. B., and L. W. Gelhar (1990), Numerical-simulation of solute transport in 3-dimensional, randomly heterogeneous porous-media, Water Resour. Res., 26(10), 2541–2562, doi:10.1029/WR026i010p02541.

[Uffink, 1985] Uffink, G. J. M. (1985), A random-walk method for the simulation of macrodispersion in a stratified aquifer, IAHS symposia, IUGG 18th general assembly, 65, 26–34.

[Van Kampen, 2007] Van Kampen, N.G.: Stochastic Processes in Physics and Chemistry. A volume in North-Holland Personal Library Book 3rd Edition (2007).

[Yong et al., 2014] Yumei Yong, Xiaojun Lou, Sha Li, Chao Yang, Xiaolong Yin, Direct simulation of the influence of the pore structure on the diffu-

sion process in porous media, Computers & Mathematics with Applications, Volume 67, Issue 2, 2014, Pages 412-423, ISSN 0898-1221, https://doi.org/10.1016/j.camwa.2013.08.032.